

# UNIVERSITY OF CINCINNATI

Date: 5/22/2009

I, Rachel Elizabeth Agnew,

hereby submit this original work as part of the requirements for the degree of:  
Master of Science

in Environmental Engineering

It is entitled:

The Characterization and Size Distribution of Engineered Carbon  
Nanomaterials

Student Signature: Rachel Agnew

This work and its defense approved by:

Committee Chair: Mingming Lu

Eileen Birch

Tim Keener

George Sorial

Jagjit Yadav

Approval of the electronic document:

I have reviewed the Thesis/Dissertation in its final electronic format and certify that it is an accurate copy of the document reviewed and approved by the committee.

Committee Chair signature: Mingming Lu

*The Characterization and Size Distribution of Engineered Carbon*

*Nanomaterials*

A thesis proposal submitted to the  
Division of Research and Advanced Studies of the University of Cincinnati

In partial fulfillment of the requirement for the degree of

**Master of Science**

In the Department of Civil and Environmental Engineering of the College of  
Engineering

May 2009

By

Rachel Elizabeth Agnew

Bachelor of Science in Civil & Environmental Engineering, University of Cincinnati  
2007

Committee

Dr. Mingming Lu (Chair)

Dr. Eileen Birch

Dr. Tim Keener

Dr. George Sorial

Dr. Jagjit Yadav

## **I. Abstract**

Carbon nanofibers (CNFs) and carbon nanotubes (CNTs) have become wonder products for industrial use because of their unique characteristics such as thermal and electrical conductivity, heat distortion resistance, mechanical reinforcement, and high surface area. As a result, engineered carbon nanomaterials are being produced at a rapid rate for use in the aerospace, automotive, environmental, computer, and recreational industries. However, certain characteristics of carbon nanomaterials make them a cause for concern. CNFs and CNTs are tiny, cylindrical or cone-shaped, manufactured forms of carbon and their structure can be similar to that of asbestos. The effects of asbestos exposure include severe lung fibrosis or scarring, lung cancer, including cancer of the lining of the lungs, or pleura, called mesothelioma.

In this study, five samples of carbon nanomaterials are aerosolized and sampled through a cascade impactor to determine their size distribution and geometric mean diameter (GMD). The samples are evaluated using a scanning electron microscope with energy dispersive x-ray analysis (SEM/EDS) to determine their morphology and metal content. Seven samples, including three CNFs and four CNTs of different lengths and diameters, are tested for PAH concentration using gas chromatography/mass spectrometry (GC/MS). The carbon nanomaterials used in this study are produced via chemical vapor deposition (CVD), which uses metal catalysts such as Fe, Co, and/or Ni. Inductively coupled plasma atomic emission spectroscopy (ICP-AES) is used to quantify trace metals in the carbon nanomaterials.



## Table of Contents

I. Objective.....	7
II. Introduction.....	7
III. Carbon Nanomaterials.....	19
IV. Experimental Design and Method.....	23
A. Size Distribution and Geometric Mean Diameter.....	23
1) Size Selective Sampling	
2) Analysis	
3) Results	
B. Scanning Electron Microscopy with Energy Dispersive X-Ray Microanalysis (SEM/EDS) Study for Morphology and Metal Content .....	46
1) Carbon Nanomaterial Collection	
2) Filter Preparation	
3) SEM/EDS Description	
4) Results	
i. Trace Metals	
ii. Morphology	
C. Determination of Trace Metals by Inductively Coupled Plasma Atomic Emission Spectroscopy (ICP-AES).....	61
1) Method	
2) Results	

D. Determination of Polycyclic Aromatic Hydrocarbons (PAHs) by Gas Chromatography/Mass Spectrometry (GC/MS).....	69
1) Method	
2) Results	
V. Conclusions and Recommendations.....	77
VI. References.....	81
VII. Appendix A – Cheap Tubes Inc. – Information about their SWCNTs and MWCNTs.....	84
VIII. Appendix B – SEM/EDS Results for Samples #21, #22, #28, #38, and the Final Product.....	89
IX. Appendix C – TEM Images of Sample #28.....	127

**List of Figures**

1. Number of Patents Containing the Prefix "Nano."
2. Global Market Growth and Forecasts for Nanomaterials
3. The London Smog Episode
4. Simulated Structure of a SWCNT
5. Simulated Structure of a SWCNT
6. TEM Micrograph of CNFs
7. Micrograph of a Cluster of Asbestos Fibers
8. Standardized Curve for Particle Penetration Probability into the Respiratory System as a Function of Diameter
9. Human Respiratory System
10. Particle Classification by Size ( $\mu\text{m}$ )
11. Photo: CNT Sample #38
12. Photo: Reactor A Bulk Material
13. Photo: Reactor B Bulk Material
14. Photo: Final Product Bulk Material
15. Schematic of the TSI Small Scale Particle Disperser

16. Small-Scale Particle Disperser (SSPD) and Chamber Setup
17. SSPD Turntable Loaded with CNTs
18. Marple Personal Cascade Impactor with a Quartz Filter
19. Sunset Instruments OC-EC Thermal-Optical Analyzer
20. Quartz filter Loaded with CNTs after Aerosolization
21. OC/EC Thermal-Optical Analyzer Thermogram- Sample #21 Marple Impactor Stage 5
22. OC/EC Thermal-Optical Analyzer Thermogram- Final Product Bulk Material
23. Sample #21 Size Distribution Chart
24. Sample #21 Differential Particle Size Distribution
25. Sample #22 Size Distribution Chart
26. Sample #22 Differential Particle Size Distribution
27. Sample #28 Size Distribution Chart
28. Sample #28 Differential Particle Size Distribution
29. Sample #38 Size Distribution Chart
30. Sample #38 Differential Particle Size Distribution
31. Final Product Size Distribution Chart
32. Final Product Differential Particle Size Distribution
33. Sioutas Cascade Impactor
34. Scanning Electron Microscope (FEI/Phillips XL30 ESEM-FEG) at the University of Cincinnati
35. SEM Micrograph of #28 on Stage A
36. SEM Micrograph of #28 on Stage D
37. SEM Micrograph of #38 on Stage A
38. SEM Micrograph of #38 on Stage D
39. SEM Micrograph of #38 on the Final Filter
40. SEM Micrograph of #21 on Stage A
41. SEM Micrograph of #21 on Stage D
42. SEM Micrograph of #21 on the Final Filter
43. SEM Micrograph of #22 on Stage A
44. SEM Micrograph of #22 on Stage D
45. SEM Micrograph of #22 on the Final Filter
46. SEM Micrograph of Final Product on Stage A
47. SEM Micrograph of Final Product on Stage D
48. SEM Micrograph of Final Product on the Final Filter

49. Structure and Numbering of Selected PAHs
50. GC/MS Located at NIOSH Cincinnati
51. PAHs Present in Reactor A CNFs
52. PAHs Present in Reactor B CNFs
53. PAHs Present in Final Product CNFs

#### **List of Tables**

1. CNT Physical Properties
2. Marple Cascade Impactor Cutpoints
3. Sample #21 Cumulative Mass Present Less than  $D_p$
4. Sample #22 Cumulative Mass Present Less than  $D_p$
5. Sample #28 Cumulative Mass Present Less than  $D_p$
6. Sample #38 Cumulative Mass Present Less than  $D_p$
7. Final Product Cumulative Mass Percent Less than  $D_p$
8. Approximate Mass Percentages in the Respirable Range
9. Sioutas Cascade Impactor Cutpoints
10. ICP-AES Results
11. Top Metal Mass Percentages Determined by ICP-AES
12. USEPA 16 Priority PAHs
13. GC/MS Sample Preparation Concentrations

## I. Objective

The focus of this work is to develop a better understanding of the aerodynamic behavior and composition of engineered carbon nanomaterials. With this information, policymakers will have a wider knowledge base for future regulation.

## II. Introduction

In 1986, K. Eric Drexler wrote "Engines of Creation" and introduced the term "nanotechnology" [1]. Since then, scientific research has expanded greatly and inventors and corporations are not far behind. Today, more than 13,000 patents registered with the United States Patent Office contain the prefix "nano" (see Figure 1). Nanostructured materials, including nanometer-diameter particles or nanoparticles, are defined as particles having at least one dimension less than 100 nanometers ( $10^{-9}$  m).

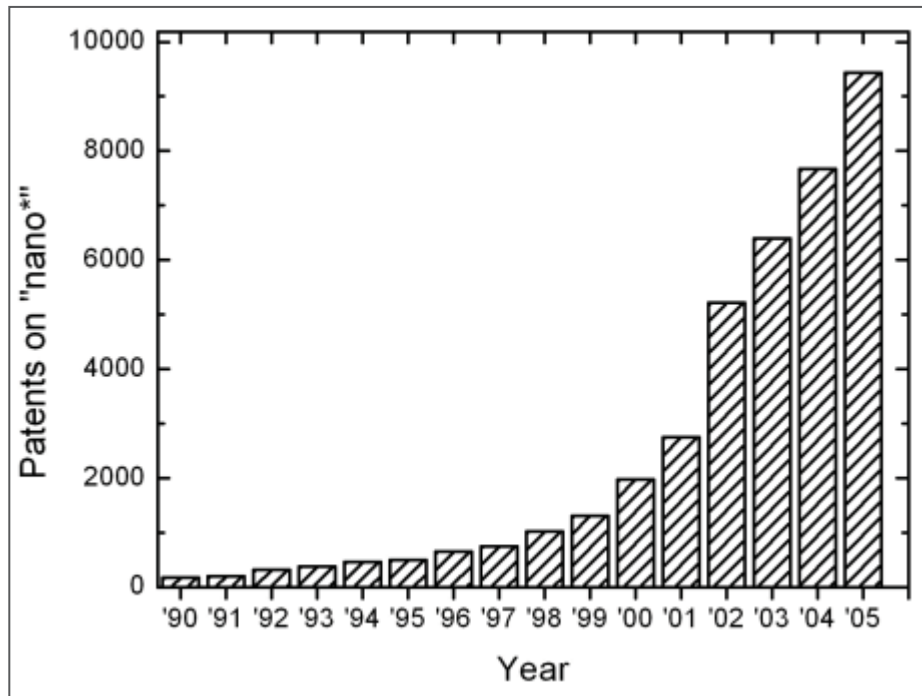


Figure 1: Number of patents containing the prefix "nano."  
Source: [www.metacel.ugent.be/whatisnano.html](http://www.metacel.ugent.be/whatisnano.html)

In 1959, Dr. Richard P. Feynman, a Nobel Prize laureate, performed a speech titled “There's Plenty of Room at the Bottom.” In this speech Feynman discussed the problem of manipulating and controlling things on a small scale. He hypothesized that if this can be accomplished, (controlling things on a small scale) that it might tell us much of great interest about the strange phenomena that occur in complex situations. Furthermore, a point that is most important is that it would have an enormous number of technical applications [2]. Later in the talk Feynman discussed the rearranging of atoms. He stated that “when we have some *control* of the arrangement of things on a small scale we will get an enormously greater range of possible properties that substances can have, and of different things that we can do.” Feynman concluded his talk with the statement “the principles of physics, as far as I can see, do not speak against the possibility of maneuvering things atom by atom. It is not an attempt to violate any laws; it is something, in principle, that can be done; but in practice, it has not been done because we are too big” [2].

Now in 2009, we have the capability to manipulate and rearrange things on a small scale by means of nanotechnology. Nanotechnology refers to the development and application of materials, devices and systems with fundamentally new properties and functions because of their structures in the range of about 1–100 nanometers. It involves the manipulation and/or creation of material structures at the nano-scale, in the atomic, molecular and supramolecular realm [3]. Nanotechnology is rapidly becoming an interdisciplinary field. It is expected that the number of US dollars invested in nanomaterials will have nearly tripled from its value in 2004 by the year 2010; a nearly

200% increase in just six years (Figure 2). In 2000, the US National Science Foundation (NSF) estimated that \$1 trillion worth of products worldwide would incorporate nanotechnology in key functional components by the year 2015 [4]. Biologists, chemists, physicists and engineers are all involved in the study of substances at the nano-scale. According to the National Nanotechnology Initiative, carbon is the second most prevalent nanomaterial used in consumer products. The nano-structural diversity of carbon gives rise to nanomaterials with various properties such as hydrogen-storage, field emission, high mechanical strength, high surface area, and high electrical conductivity. It is thus possible to synthesize tailored nanostructured carbon corresponding to a certain application.

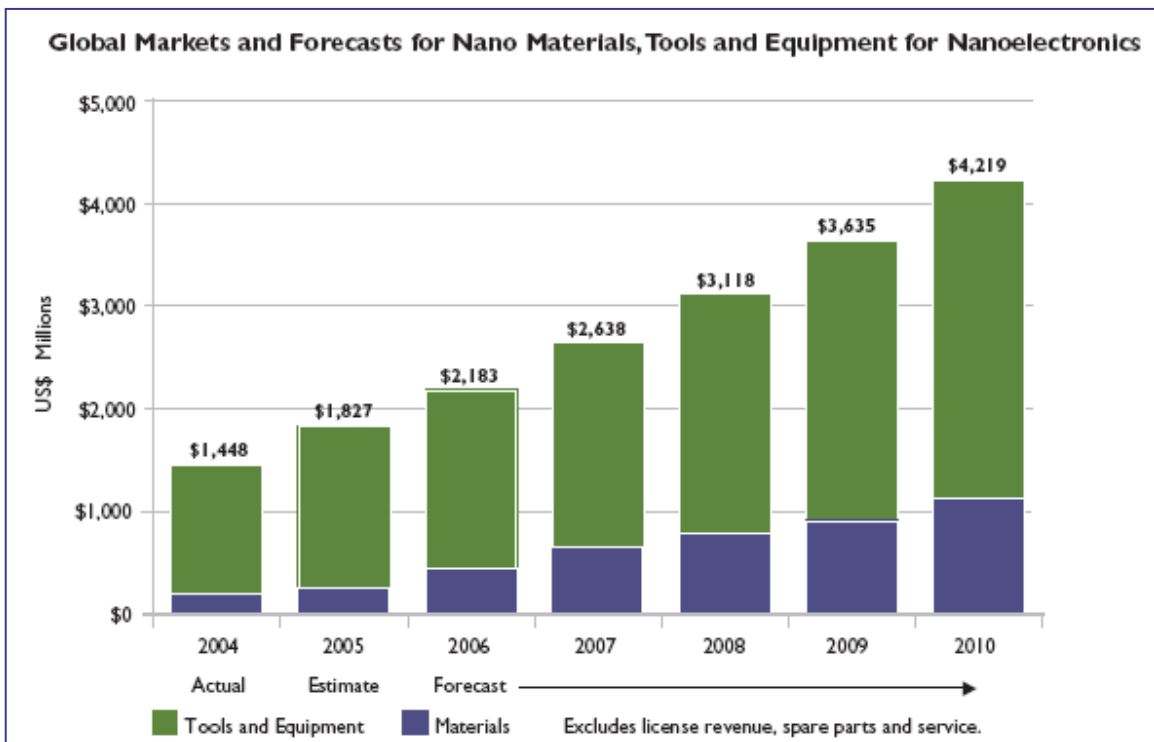


Figure 2: Global Market Growth and Forecasts for Nano Materials  
 Source: <http://www.electronics.ca>

A potential hurdle in the nanotechnology field is the potential for occupational safety and health risks. According to a 2009 NIOSH report, “Approaches to Safe Nanotechnology,” nanotechnology is an emerging field. As such, there are many uncertainties as to whether the unique properties of engineered nanomaterials (which underpin their commercial and scientific potential) also pose occupational health risks [5]. Roco and Renn stated that the main deficit for the future generations of nanoproducts (including active nanodevices, nano-bio applications, and nanosystems) is the uncertain/unknown evolution of the technology and human health effects (for example health, changes at birth, brain understanding and cognitive issues and human evolution), as well as a framework through which organizations and policies can address such uncertainties [3]. Airborne particles from natural and anthropogenic sources have long been recognized as a potential health risk at sufficiently high concentrations and durations of exposure. But there is limited published information on the potential adverse health effects of engineered nanomaterials [6].

The 1952 London Smog Episode (Figure 3) was one of the first occurrences demonstrating the potentially severe health impacts of inhaling fine particulate matter (PM). The incident had major impacts on science, public awareness of air pollution, and government guidelines. In December of 1952, Londoners began to burn more coal than usual. As a result, an inversion layer was formed, whereby cold dense air settled over the city. Concentrations of pollutants, mainly coal smoke, built up significantly. The smoke laden fog that shrouded the city brought the premature death of an estimated 12,000 people and illness to many others. Events such as this one have led to federal

regulations on airborne PM, namely, PM10 and PM2.5, which refer to particles with an aerodynamic diameter smaller than 10  $\mu\text{m}$  and 2.5  $\mu\text{m}$ , respectively.



Figure 3: The London Smog Episode

The Occupational Safety and Health Administration (OSHA) established permissible inhalation exposure limits for graphite of  $15 \text{ mg/m}^3$  and  $5 \text{ mg/m}^3$ , for total dust and respirable fraction, respectively. These values are sometimes listed as the PELs for CNTs. In 2005, the National Institute for Occupational Safety and Health (NIOSH) determined that these values may not be suitable for CNTs based on the effects seen in laboratory studies [7]. Further studies are needed to determine exposure limits for CNTs.

Carbon nanotubes can be: 1. produced and/or cleaned using one of several different methods; 2. produced using one of several different metal catalysts; 3. single or multi-

walled; 4. of various lengths; and 5. subjected to numerous surface modifications [8]. The result of these permutations is that a vast number of unique carbon nanotubes can be derived, all of which fall under one broad category, namely the carbon nanotube.

Figure 4 shows a representation of a single-walled carbon nanotube (SWCNT), which can be thought of as a single roll of graphite. Figure 5 shows a representation of a multi-walled carbon nanotube, referred to as a MWCNT. Nanotubes are members of the fullerene structural family, which also includes the spherical buckyball. The bonding in carbon nanotubes is  $sp^2$ , with each atom joined to three neighbors, as in graphite. The strength of the  $sp^2$  carbon-carbon bonds provides for the amazing mechanical properties of CNTs.

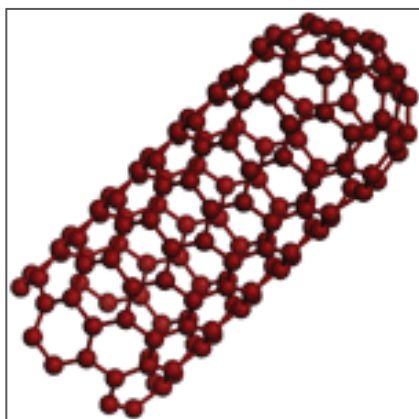


Figure 4: Simulated Structure of a SWCNT.

Source:

[www.brl.ntt.co.jp/people/fmaeda/top\\_e.html](http://www.brl.ntt.co.jp/people/fmaeda/top_e.html)

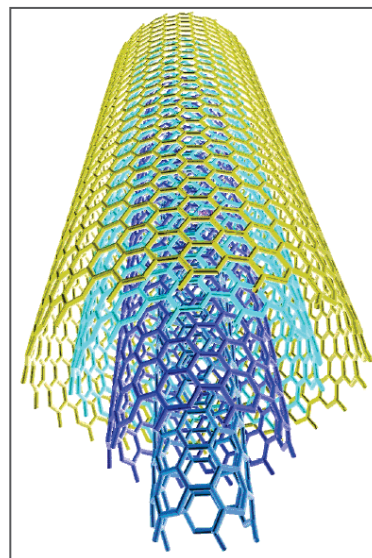


Figure 5: Simulated Structure of a MWCNT. Source:

[www.cancer2blog.com/](http://www.cancer2blog.com/)

Despite many benefits, there are several potential health hazards related to CNT and CNF exposure including. The hazards may depend on particle properties such as:

particle size (lung deposition), morphology, and trace metal content. This research examines the physical and chemical properties of these materials that may predict recommendations/legislation to reduce health risks.

CNTs in particular are being compared to asbestos for several reasons. Several studies have shown similar effects in animals as those caused by asbestos exposure [7, 9, 10, 11]. Some varieties of CNTs are similar in shape to asbestos fibers, and like asbestos, some varieties of CNTs have been shown in laboratory studies to persist in the lungs of laboratory animals [7]. A 2008 study titled “Carbon Nanotubes Introduced into the Abdominal Cavity of Mice Show Asbestos-like Pathogenicity in a Pilot Study,” by Poland et al. found that long, thin multi-walled carbon nanotubes that look like asbestos fibers also behave like asbestos fibers [9]. Asbestos fibers are harmful because they are thin enough to penetrate deep into the lungs, but sufficiently long to confound the lungs’ built-in clearance mechanisms for getting rid of particles. A significant finding in the Poland study was the uniqueness of the mesothelial response to long CNT fibers. It was observed that long MWCNTs produced inflammation, foreign body giant cells (FBGCs) and granulomas (lesions) that were qualitatively and quantitatively similar to the foreign body inflammatory response caused by long asbestos. This foreign body response is the normal reaction to indigestible or non-degradable material that macrophages cannot eliminate [9].

Figure 6 shows a micrograph taken of group of CNFs created by electron cyclotron resonance chemical vapor deposition (ECR-CVD). Figure 7 shows a micrograph of a cluster of asbestos fibers. The similarities in structure are apparent.

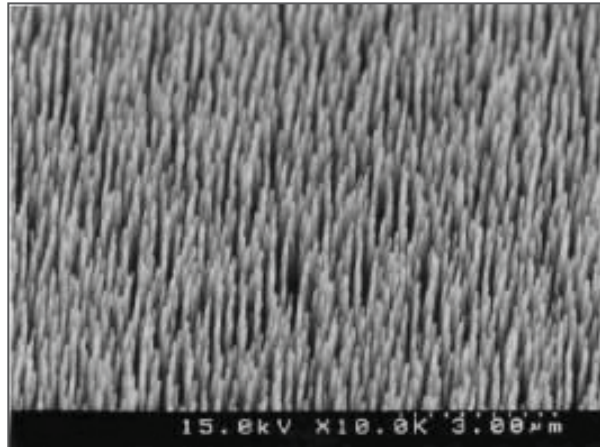


Figure 6: TEM Micrograph of CNFs  
Source: [www.eng.auburn.edu/.../ADCFCTabstract](http://www.eng.auburn.edu/.../ADCFCTabstract)



Figure 7: Cluster of asbestos fibers  
Source: [http://www.asbestos-laboratory.com/asbest\\_bild\\_Antofyllit.jpg](http://www.asbestos-laboratory.com/asbest_bild_Antofyllit.jpg)

On June 21, 1984, NIOSH testified at the Occupational Safety and Health Administration (OSHA) public hearing on occupational exposure to asbestos and

presented supporting evidence that there is no safe airborne concentration of fibers for any asbestos mineral [12]. With striking similarities to asbestos, it is essential to understand the physical/chemical characteristics of CNTs and CNFs being manufactured today.

Past industrial experience with asbestos has called attention to the potential hazards associated with small diameter fibers [13]. Based on animal studies, discrete nanoparticles may enter the bloodstream from the lungs and translocate to other organs [14]. Previous work has demonstrated that the inflammatory response to purified SWCNT included recruitment and activation of macrophages in the lung of exposed animals [15]. A recent review of engineered nanomaterial toxicity tests emphasized the need to fully characterize airborne CNTs in the submicrometer size range [16]. CNFs can vary widely in diameter, length, and structure. They may agglomerate, which can affect their potential for deposition in the lungs if inhaled, their ability to penetrate the body's membranes, and their interaction with cells and tissue [7]. For external wind speeds of a few meters per second and lower, the probability of a particle entering the mouth or nose (inhalable particles) may be generalized as being around 100% for particles with aerodynamic diameters of a few micrometers ( $\mu\text{m}$ ) and below, reducing to around 50% at 100  $\mu\text{m}$  aerodynamic diameter [17]. Figure 8 shows the standardized curve for particle penetration as a function of diameter. The probability of penetration for a particle smaller than one micron in diameter is nearly 100 percent.

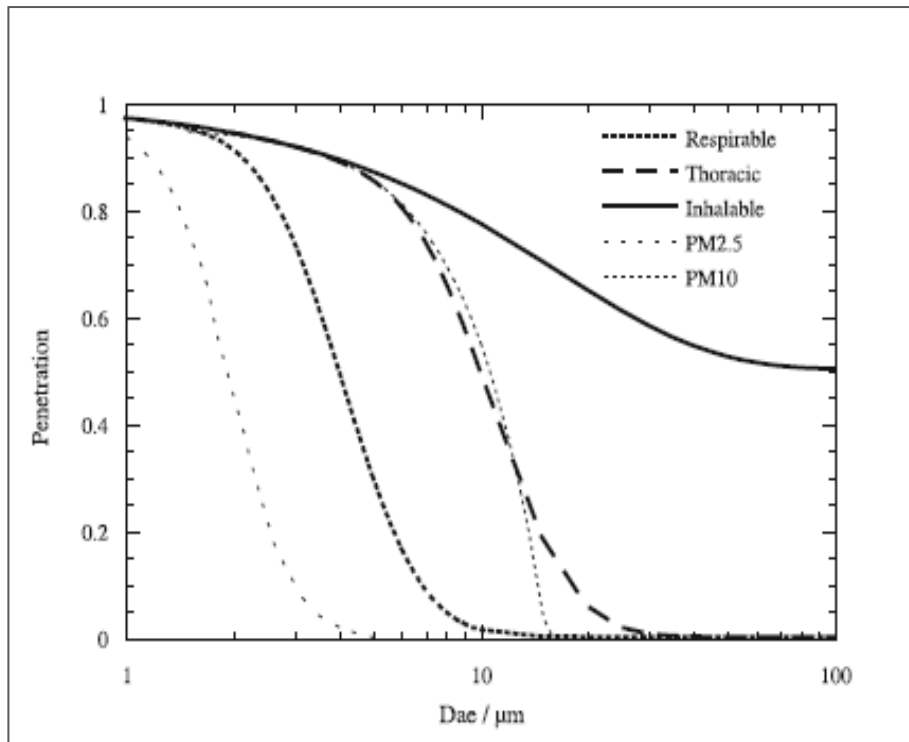


Figure 8: Standardized curve for particle penetration probability into the respiratory system as a function of diameter.

The respiratory system is the primary indicator of air pollution effects in humans (See Figure 9). The major organs of the respiratory system include the nose, pharynx, larynx, trachea, bronchi, and lungs. The bronchi and the lungs make up the lower respiratory tract (LRT). The remaining organs make up the upper respiratory tract (URT). The respiratory system has defense mechanisms to help prevent airborne particles from entering the lungs and causing harm. As we breathe, the air becomes moist and makes numerous twists and turns through the nasal passages and branching airways. Particles 100  $\mu\text{m}$  or larger are not typically drawn into the body by inhalation due to their large size. Particles in the size of range of 10 to 100  $\mu\text{m}$  are unable to make

the turns and therefore impact on the nasal hairs, nasal mucosa, or mucus-covered ciliated epithelium in the bronchi and bronchioles. Particles less than 10  $\mu\text{m}$  in size are generally able to travel into the pulmonary part of the lungs (Figure 10); the respiratory bronchioles, alveolar ducts, and alveolar sacs [18]. Particles ranging from 1-2  $\mu\text{m}$  are most likely to penetrate to the alveoli. These particles sizes are large enough that their settling velocity allows them to deposit where they can do the most damage [19].

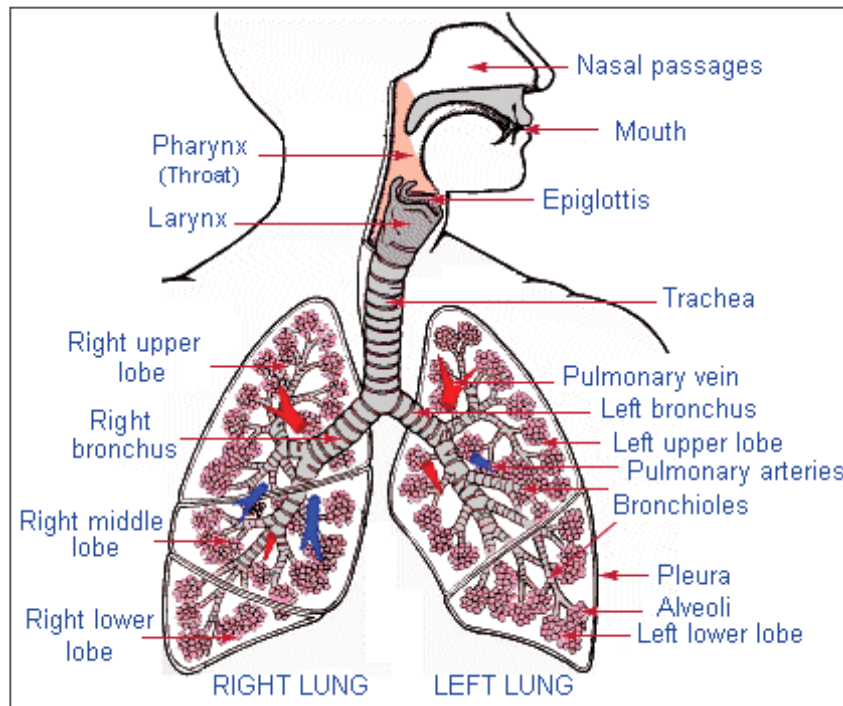


Figure 9: Human Respiratory System

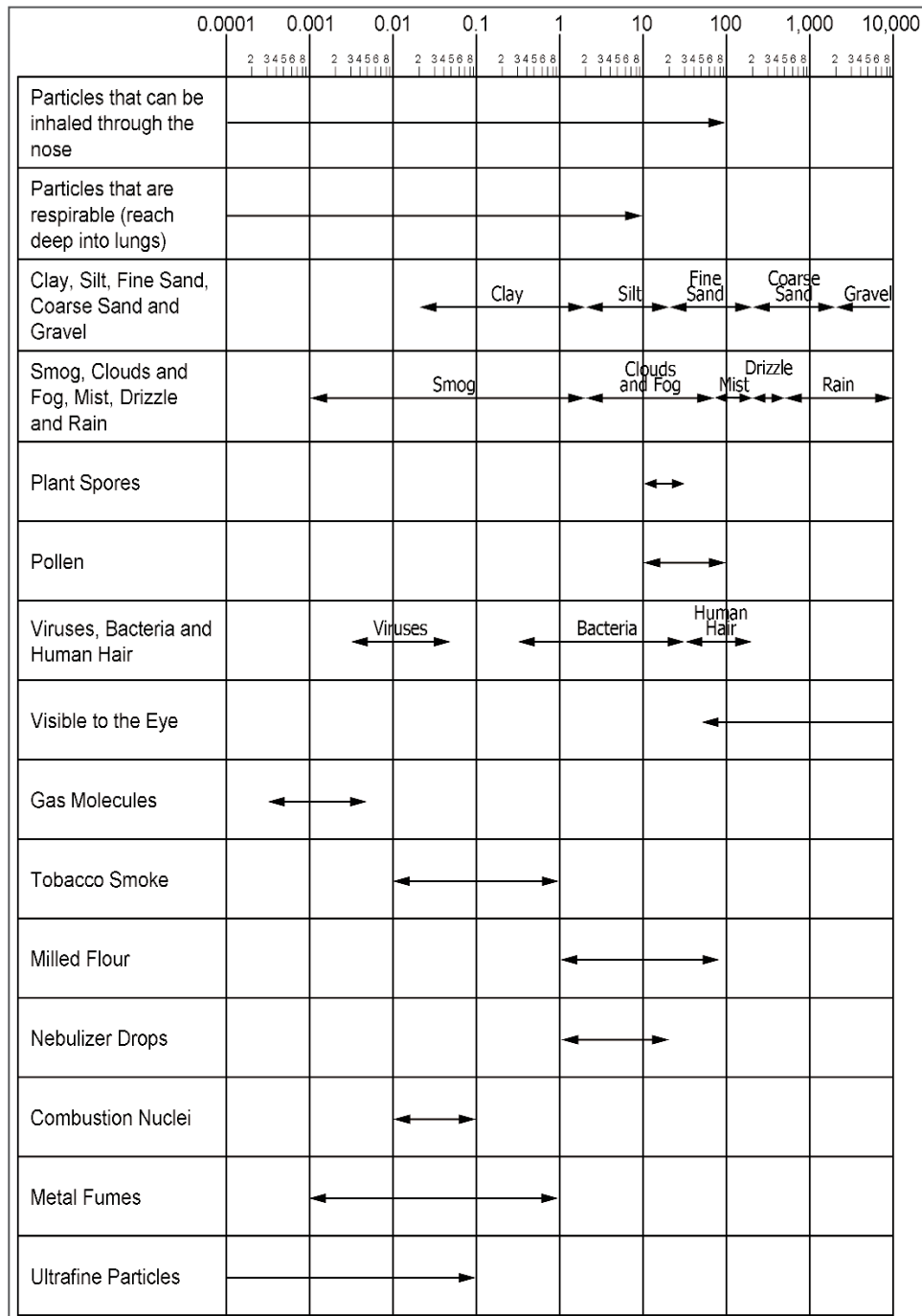


Figure 10: Particle Classification by Size (µm)

### III. Carbon Nanomaterials

In this experiment, four CNT samples are analyzed along with three CNF samples. The CNTs were purchased from Cheap Tubes Inc., a leading distributor of high quality, low cost CNTs for research and industry. Cheap Tubes Inc. offers SWCNTs, MWCNTs, short CNTs, OH functionalized CNTs, COOH functionalized CNTs, and industrial grade CNTs for industrial scale applications. Functionalization, a process by which molecules or atoms are bound to the carbon atoms of a SWNT, is necessary to mix or blend SWNTs into materials such as composites [20]. The samples used in this experiment are referred to as #21, #22, #28, and #38 and their physical characteristics are shown in Table 1. Two SWCNTs and two MWCNTs were chosen to be analyzed. The SWCNTs (#22 and #28) have the same outer diameter (1-2nm) but have differing lengths, 0.5-2.0 and 5-30  $\mu\text{m}$ , respectively. Similarly, the two MWCNTs (#21 and #38) have the same outer diameter (20-30nm) but have differing lengths, 0.5-2.0 and 10-30  $\mu\text{m}$ , respectively.

The CNTs are produced by the chemical vapor deposition method (CVD). Chemical vapor deposition of hydrocarbons over a metal catalyst is a classical method that has been used to produce various carbon materials such as carbon fibers and filaments. Large amounts of CNTs can be formed by catalytic CVD of acetylene over cobalt and iron catalysts supported on silica or zeolite [20]. CVD is a chemical process commonly used to create high-purity, high-performance solid materials. CVD results from the chemical reaction of gaseous precursors (such as halides, hydrides or metal organic

compounds) at a heated substrate to yield a fully dense deposit. The catalyst consists of nano-sized particles of metal, usually Fe, Co, or Ni. These particles catalyze the breakdown of the gaseous molecules into carbon, which results in a CNT with a metal end [21]. A cobalt-nickel catalyst helps the growth of the nanotubes, presumably because it prevents the ends from being "capped" during synthesis, and about 70-90% of the carbon target can be converted to single-wall nanotubes. According to the vendor, Co is the catalyst used in the production of the SWCNTs (#22 and #28) and Fe or Ni is the chosen catalyst for the MWCNTs (#21 and #38). During purification, dilute nitric acid is used to dissolve the catalyst in the CNTs. The CNTs are separated by filtration. The filtrate is recycled to prepare new catalyst material. The CNTs which have a reported purity of 95% by weight (#21 and #38) receive air oxidation first, and then receive the acid purification process, while the 60% by weight CNTs (#22 and #28) only receive the acid purification process. The CNT ends/caps are removed during the air oxidation and acid purification processes. The SWCNTs with a 60% purity may contain <3.0% ash by weight, >30% MWNT content by weight, and <5.0% amorphous carbon content [20]. Each of the materials is in the form of a fine black powder. A photo of sample #38 is shown in Figure 11. Further information on the characteristics of SWCNTs and MWCNTs from Cheap Tubes Inc. can be found in Appendix A.

**Table 1: CNT Physical Properties**

<b>Number</b>	<b>Type</b>	<b>Length</b>	<b>Outer Diameter</b>	<b>Density at 20°C</b>	<b>Purity</b>
21	MWCNT	0.5-2.0 $\mu$ m	20-30nm	$\sim$ 2.1g/cm <sup>3</sup>	95 % (wgt)
22	SWCNT	0.5-2.0 $\mu$ m	1-2nm	$\sim$ 2.1g/cm <sup>3</sup>	60 % (wgt)
28	SWCNT	5-30 $\mu$ m	1-2nm	$\sim$ 2.1g/cm <sup>3</sup>	60 % (wgt)
38	MWCNT	10-30 $\mu$ m	20-30nm	$\sim$ 2.1g/cm <sup>3</sup>	95 % (wgt)

The three CNFs samples were produced by a commercial manufacturer, whose name must remain anonymous. These materials will be referred to as “Reactor A,” “Reactor B,” and “Final Product.” The CNF samples are produced via CVD, as discussed above. The materials from Reactors A and B are raw products that have not passed through any purification process. The Final Product, as the name implies, is ready to be distributed. Reactors A and B are functionally the same, but Reactor B is newer. Here, the catalyst used in the CVD method is iron (Fe). The Final Product has been heated to about 750°C to remove organics and catalyst particles. Photos of Reactor A, Reactor B, and Final Product are shown on Figures 12, 13, and 14, respectively.



Figure 11: CNT Sample #38



Figure 12: Reactor A Bulk Material



Figure 13: Reactor B Bulk Material



Figure 14: Final Product Bulk Material

## **IV. Experimental Design and Method**

### **A. Size Distribution and Geometric Mean Diameter**

#### *1) Size Selective Sampling*

The focus of this part of the study is to aerosolize the carbon nanomaterials within a chamber to simulate what an exposed worker might experience in the event of airborne exposure. In the workplace, bulk materials can become airborne due to gusts of air, spills, transfer of materials from one location to another or any number of accidents. Adding to the potential hazard is the fact that CNTs are extremely light. The slightest movement of air may cause these materials to become airborne.

A TSI Model 3433 Small-Scale Powder Disperser (SSPD) was used to aerosolize and direct the carbon nanomaterial samples into a chamber. A schematic of the SSPD is shown in Figure 15. For this part of the experiment, all of the CNTs (#21, #22, #28, and #38) are analyzed as well as the Final Product. The samples from Reactors A and B are too large to be aerosolized using this method. The SSPD is designed to efficiently disperse small quantities of dry powder. The powder is removed from a turntable by means of a venturi aspirator and capillary delivery tube. The powder is then released into a rectangular Plexiglas chamber measuring 12" x 12" x 30.5". The powder travels through three feet Tygon tubing before entering the center of the top of the chamber. A Plexiglas plate is placed inside the chamber approximately 2.5 inches from the top to catch large particles. The plate acts as a pre-separator, and is commonly used in particulate matter collection [22]. A photo of the SSPD and Plexiglas chamber is

shown in Figure 16. A detailed view of the turntable containing a sample of CNTs is shown in Figure 17.

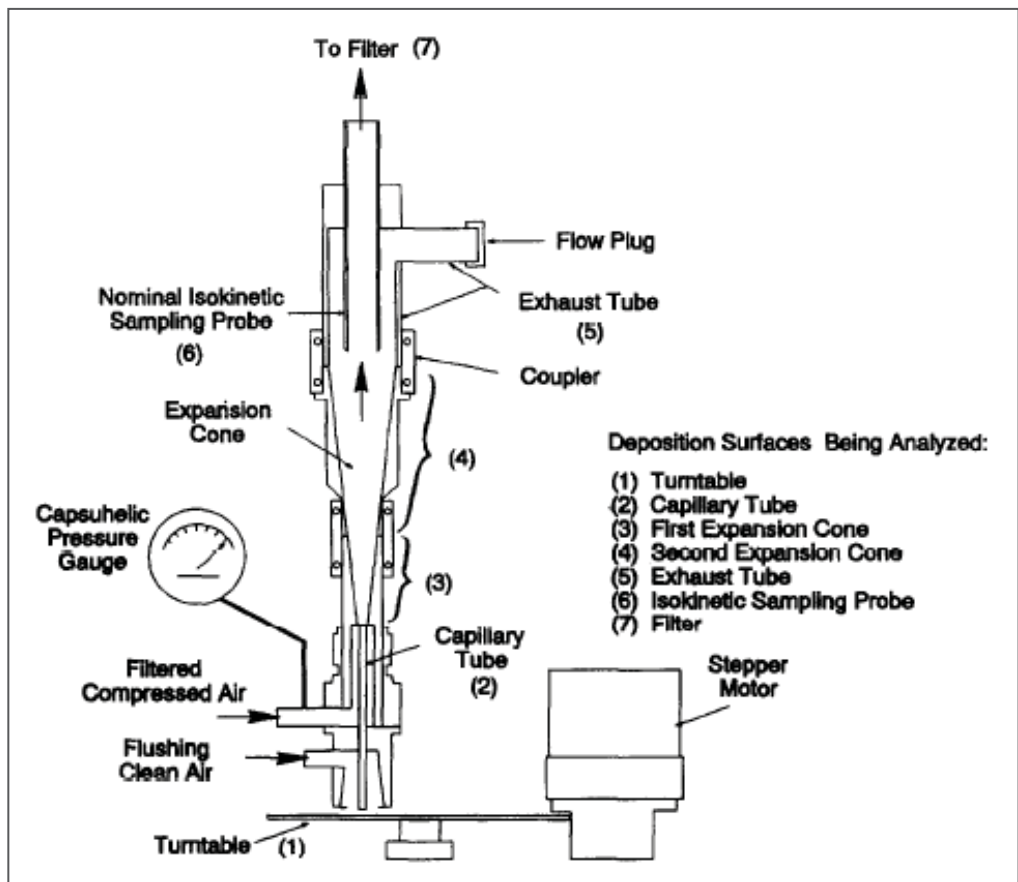


Figure 15: Schematic of the TSI Small Scale Particle Dispenser

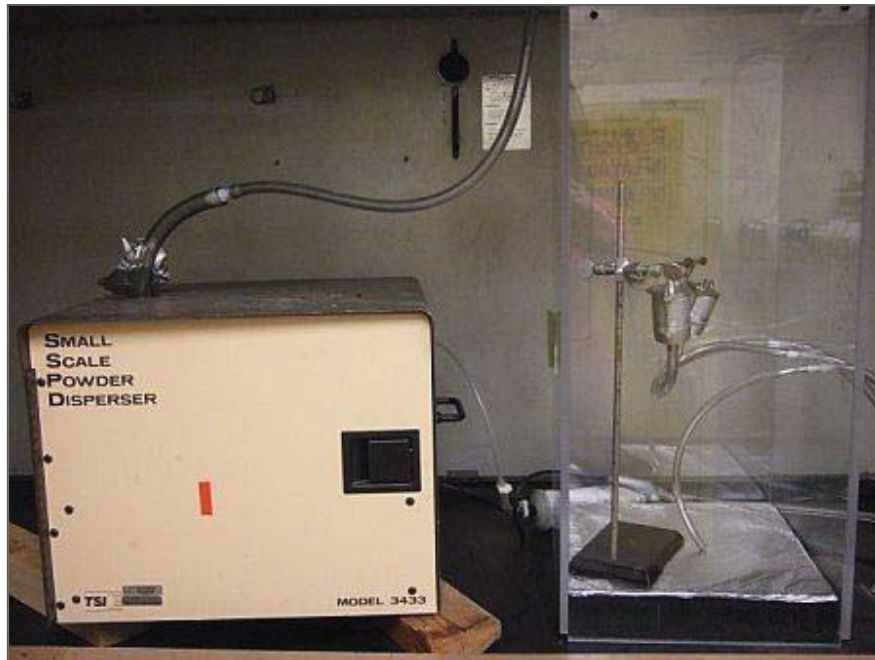


Figure 16: SSPD and Chamber Setup

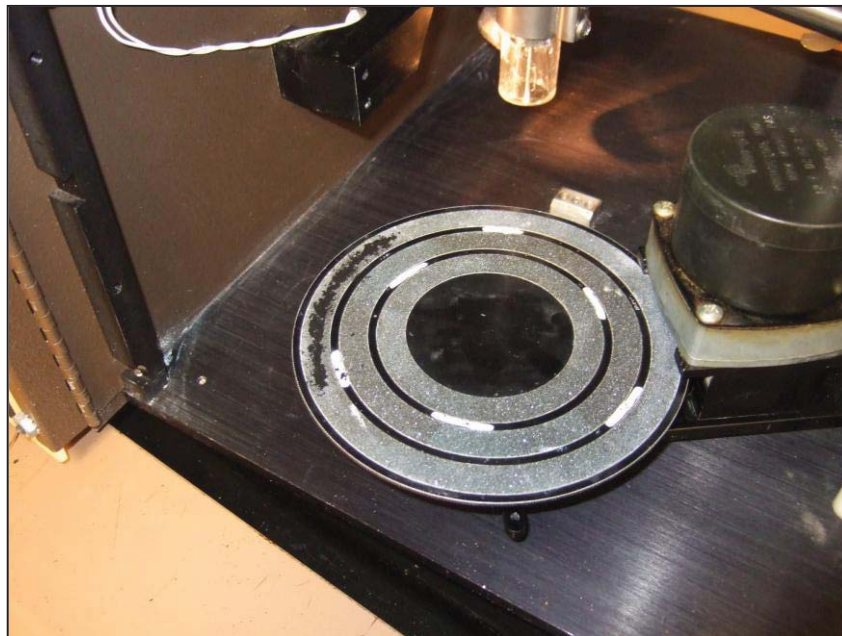


Figure 17: SSPD Turntable Loaded with CNTs

A Marple Personal Cascade Impactor, model 290 (Figure 18) is placed inside the chamber to size classify the aerosolized particles. Cascade impactors classify particles by means of inertial impaction, also referred to as impingement, which occurs as the air-stream passes through a series of stacked stages. Some particles will impact onto the filter medium and be caught due to their inertia. The smaller particles that do not impact will flow to the subsequent stage. Marple impactors have eight stages and a final filter. The cutpoints are shown in Table 2. The Marple impactor is connected to an SKC personal sampling pump calibrated to 2 Liters per minute (Lpm). SKC Type R-100 quartz filters measuring 34 mm in diameter with radial slits (380  $\mu\text{m}$  thick) are placed on each stage for collection of particles.

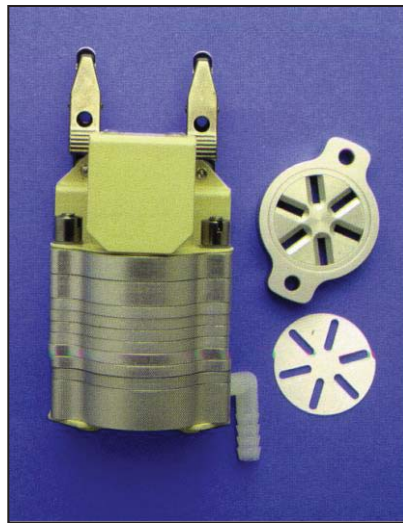


Figure 18: Marple Personal Cascade Impactor shown with a Quartz Filter

**Table 2: Marple Impactor Cutpoints**

Stage	Cutpoint
1	21.3 $\mu\text{m}$
2	14.8 $\mu\text{m}$
3	9.8 $\mu\text{m}$
4	6.0 $\mu\text{m}$
5	3.5 $\mu\text{m}$
6	1.55 $\mu\text{m}$
7	0.93 $\mu\text{m}$
8	0.52 $\mu\text{m}$
Final	<0.52 $\mu\text{m}$

During each run, a pressure gauge on the SSPD was set to 200 inches H<sub>2</sub>O. This pressure drop corresponds to a flow rate of 18.3 Lpm, which was kept constant throughout each run. The materials to be dispersed were placed on the surface of the turntable and were removed by venturi aspiration via a capillary delivery tube. The feed rate, or the rate at which the turntable rotates, was held constant for each sample run. The sheathe air flow rate was set at 3.5 lpm. The Marple Impactor is placed at the center of the chamber horizontally and 12” from the bottom during each run. After each run, the SSPD and chamber were cleaned with a high efficiency vacuum followed by isopropanol. The Tygon tubing connecting the SSPD and chamber was also cleaned with isopropanol. The mass of carbon nanomaterials placed in the SSPD was determined by trial and error so as to collect a sufficient amount of material on the filters, and to prevent overloading of the filters and carbon analyzer. The mass loadings for samples #21, #22, #28, #38, and the Final Product are 26mg, 37mg, 70mg, 40mg,

and 23mg, respectively. The sampling times are dependent on the mass and ranged from 22 to 90 minutes.

## 2) *Analysis*

After sampling, the cascade impactor was removed from the chamber and the quartz filters were analyzed for elemental carbon (EC) content using a Sunset Laboratory OC-EC thermal-optical analyzer, shown in Figure 19. This instrument is the basis for the NIOSH Manual of Analytical Methods (NMAM) Method 5040 for the measurement of organic and elemental carbon (OC-EC) on quartz filters. The method is based on a thermal-optical analysis technique for particulate carbon. A section of quartz filter measuring either 1 cm<sup>2</sup> or 1.5 cm<sup>2</sup> is used for analysis. The filter sections are directly inserted into a quartz oven. Once the oven is purged with Helium (He), a stepped temperature ramp increases the oven temperature to 870°C, thermally desorbing organic compounds and pyrolysis products into a manganese dioxide oven (MnO<sub>2</sub>) oxidizing oven. The carbon fragments are quantitatively converted to CO<sub>2</sub>, which is swept out of the oxidizing oven in the helium stream and mixed with hydrogen gas. This mixture then flows through a heated nickel catalyst where it is quantitatively converted to methane, which is measured using a flame ionization detector (FID). The oven is then cooled to 600°C and the flow stream is switched to an oxidizing He/O<sub>2</sub> carrier gas mixture. A second temperature ramp is initiated in the oxidizing gas stream and any EC is oxidized off the filter into the oxidizing oven. The EC is then detected in the same manner as the OC [23]. Results are given in mass of carbon (µg), both organic and elemental, per square centimeter of filter deposit, and the total OC-EC on the filter is

determined by multiplying the result by the deposit area. Analysis time is about 13 minutes.



Figure 19: Sunset Laboratory OC-EC Thermal-Optical Analyzer

Because the impactor substrates have six radial slits, they were divided into six sections and each section was analyzed. The total mass on the filter is the sum of the masses on all six sections. A photo of a quartz filter (with three sections removed) loaded with CNTs is shown in Figure 20. A comparison of EC on all six sections determined that the dust was evenly distributed over the impaction substrate. Figure 21 shows a resulting thermogram (Sample #21- Marple Impactor Stage 5) which provides the mass of OC, EC, TC, and the EC/TC ratio. As described above, the area of the initial peaks (before the temperature is ramped a second time) is proportional to the mass of OC, and the area of the peak after the second temperature ramp is proportional to the mass of EC

in the sample. Figure 22 shows a thermogram for a bulk material, in this case Final Product, placed directly on a section of quartz filter and analyzed, rather than impaction via chamber sampling. Figure 21 shows that the amount of OC in the bulk product is negligible, which is expected because the bulk materials do not contain OC. In contrast, the aerosolized samples show some OC contamination from the aerosolization system.

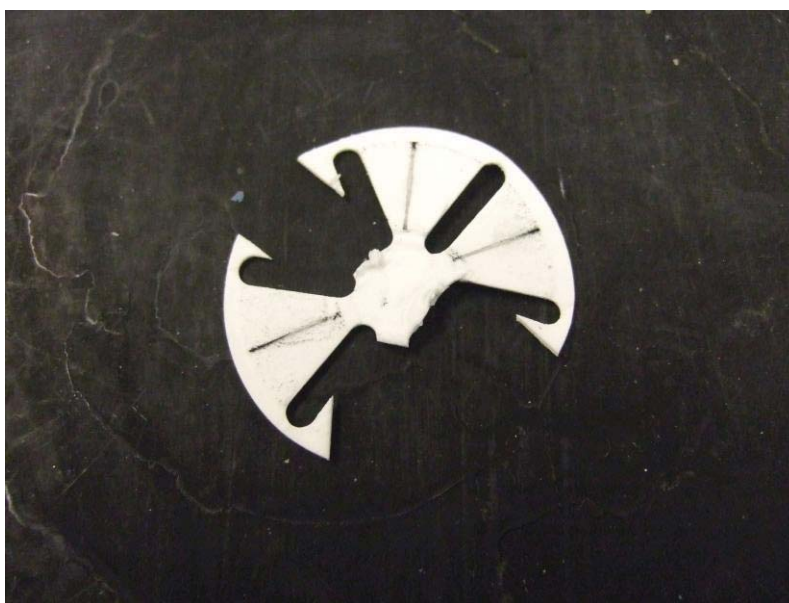


Figure 20: Quartz Filter Loaded with CNTs after Aerosolization

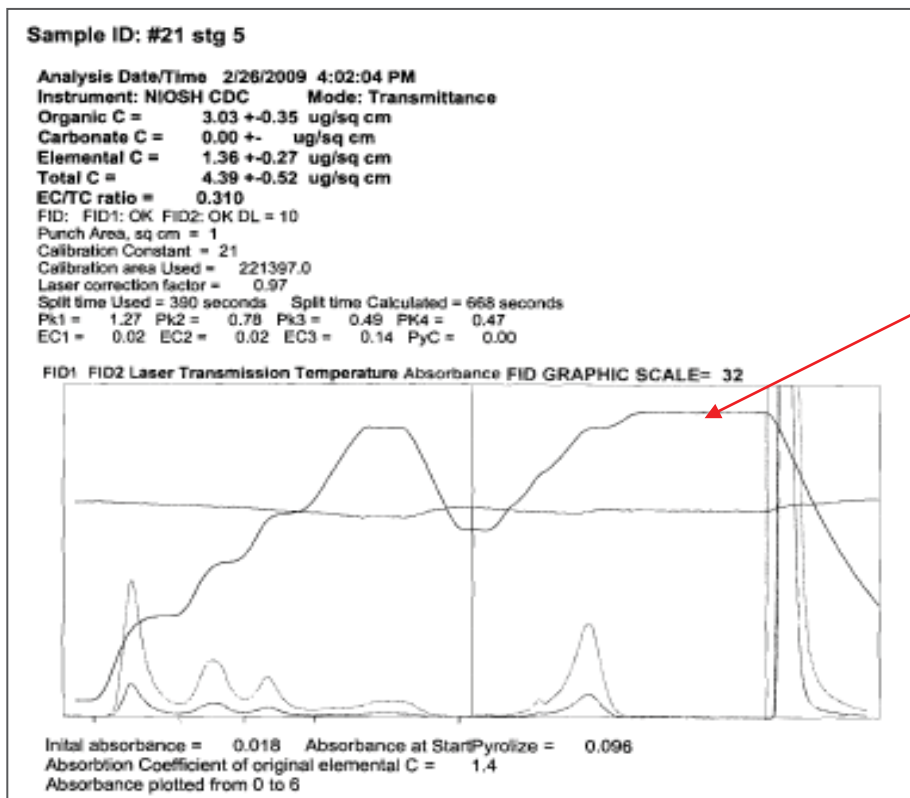


Figure 21: Thermogram of Sample #21 Impactor Stage 5

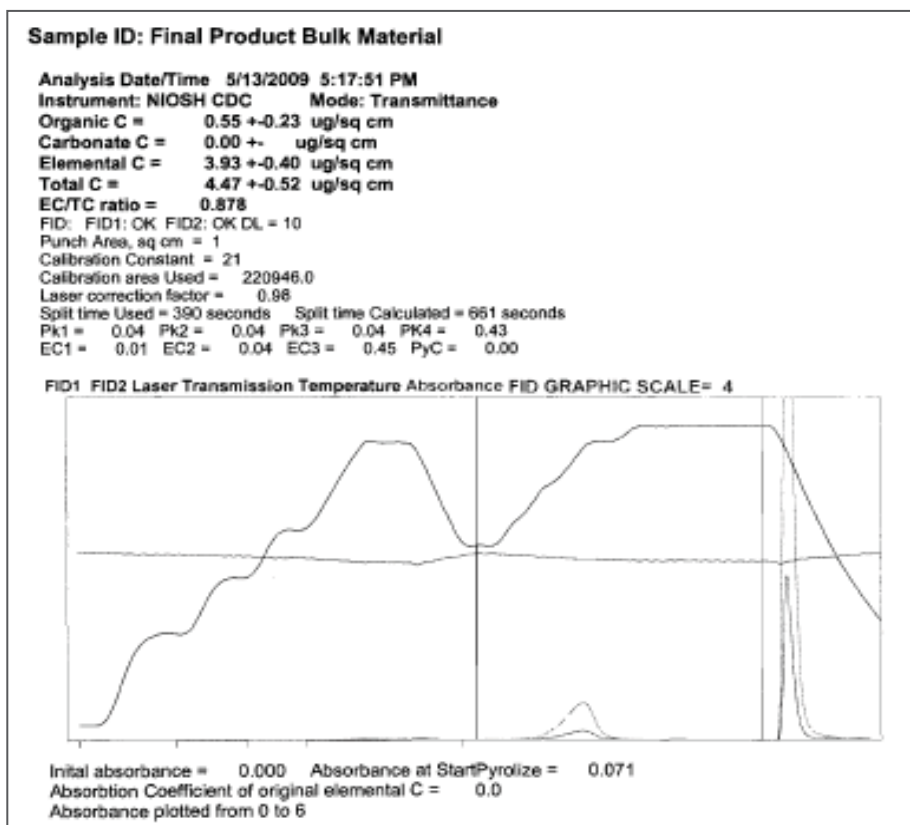


Figure 22: Thermogram of Final Product Bulk Material

### 3) *Results*

For each of the carbon nanomaterials aerosolized (#21, #22, #28, #38, and the Final Product), a size distribution chart and differential particle size distribution plot is developed. The size distribution plot is a bar chart with cutpoint diameter on the x-axis and mass ( $\mu\text{g}$ ) on the y-axis. The differential particle size distribution, a plot of geometric mass mean diameter (GMD) vs.  $dC/d\log D_p$ , gives the details, or "fine" structure, of the particle size distribution [24]. The GMD is the diameter of a particle that has the logarithmic mean for the size distribution. A table is developed for each carbon nanomaterial showing the stage, cutpoint, mass collected on the filter, concentration (C), GMD, weight percent, and percent less than  $D_p$ , where  $D_p$  is the cutpoint diameter in micrometers. The particulate weight (as EC) is determined by the OC-EC thermal-optical analyzer in micrograms ( $\mu\text{g}$ ). The EC concentration for different size ranges is measured as the mass on each substrate stage divided by the volume of air sampled through the impactor ( $2.0\text{Lpm}\cdot\text{time}$ ). The total EC concentration is determined as the sum of the mass on all stages divided by the air volume sampled. GMD is calculated using the following formula:

$$\text{GMD}_i = \sqrt{D_{pi} \times D_{pi-1}},$$

where  $D_{po}$  is the largest particle size sampled. By convention, 50 microns is used if this value is not known. Next, the weight percent is calculated for each stage. This is calculated by dividing the weight on the stage by the total weight. For example, the weight percent on stage six of sample #21 is calculated as follows:

$$19.13\mu\text{g} / 45.4\mu\text{g} \times 100 = 42.2\%$$

Finally, the %<D<sub>p</sub> is calculated as 100 minus the sum of the weight percentages on the upper stages. For example, the %<D<sub>p</sub> on stage 4 of sample #21 is calculated as follows:

$$100 - \sum 2.6 + 2.1 + 1.7 = 93.6\%$$

The cumulative mass percent less than D<sub>p</sub> for samples #21, #22, #28, and #38, and Final Product are shown in Tables 3, 4, 5, 6, and 7, respectively. The size distribution plots are shown on Figures 23, 25, 27, 29, and 31, respectively. The differential particle size distribution curves are shown in Figures 24, 26, 28, 30, and 32, respectively.

**Table 3: Sample #21: Cumulative Mass Percent Less than Dp**

Stage #	Cutpoint (Dp) (μm)	Mass Collected (μg)	Concentration (mg/m <sup>3</sup> )	GMD (μm)	W/W <sub>total</sub> (%)	%<Dp
Final	0.26	1.37	0.017	0.37	3.0	3.0
8	0.52	1.51	0.018	0.70	3.3	6.4
7	0.93	10.04	0.122	1.20	22.1	28.5
6	1.55	19.13	0.233	2.33	42.2	70.7
5	3.50	7.45	0.091	4.58	16.4	87.1
4	6.00	2.94	0.036	7.67	6.5	93.6
3	9.80	1.20	0.015	12.04	2.6	96.2
2	14.80	0.94	0.011	17.75	2.1	98.3
1	21.30	0.78	0.010	32.63	1.7	100

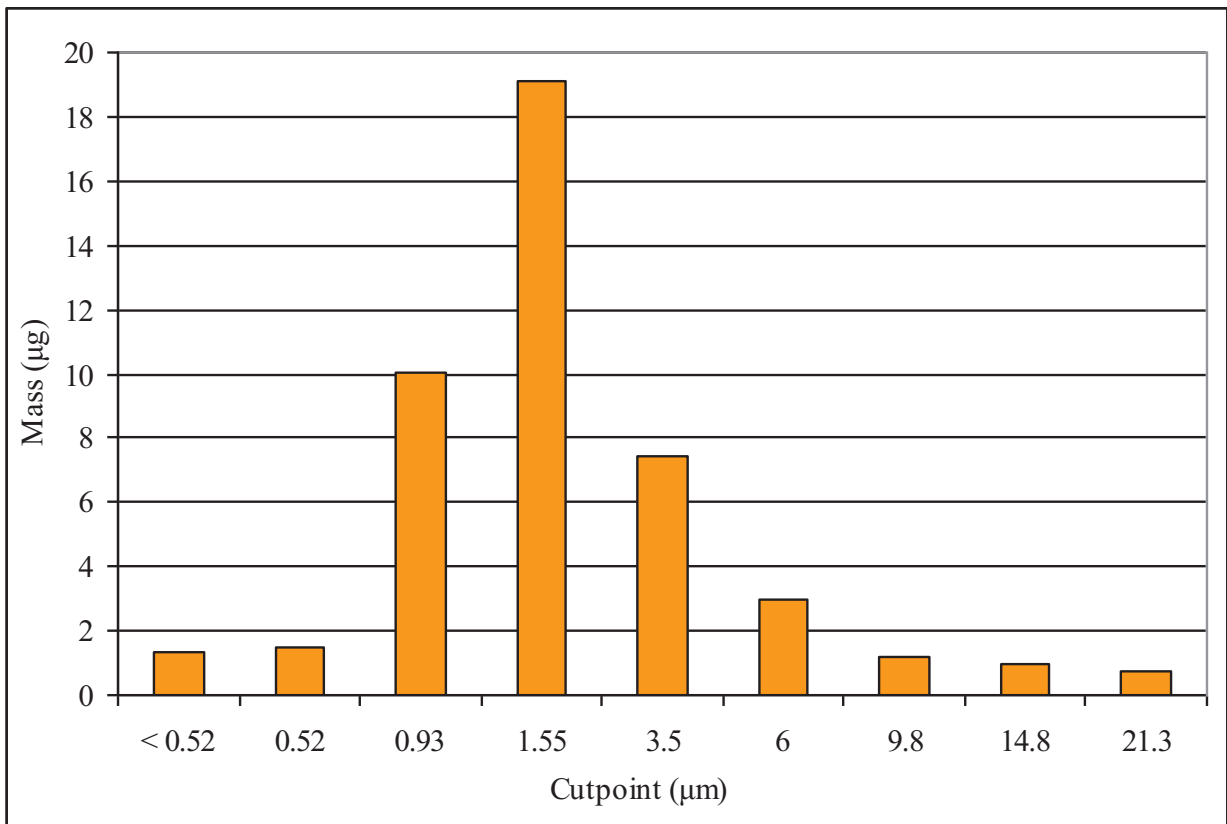


Figure 23: Sample #21 Size Distribution Chart

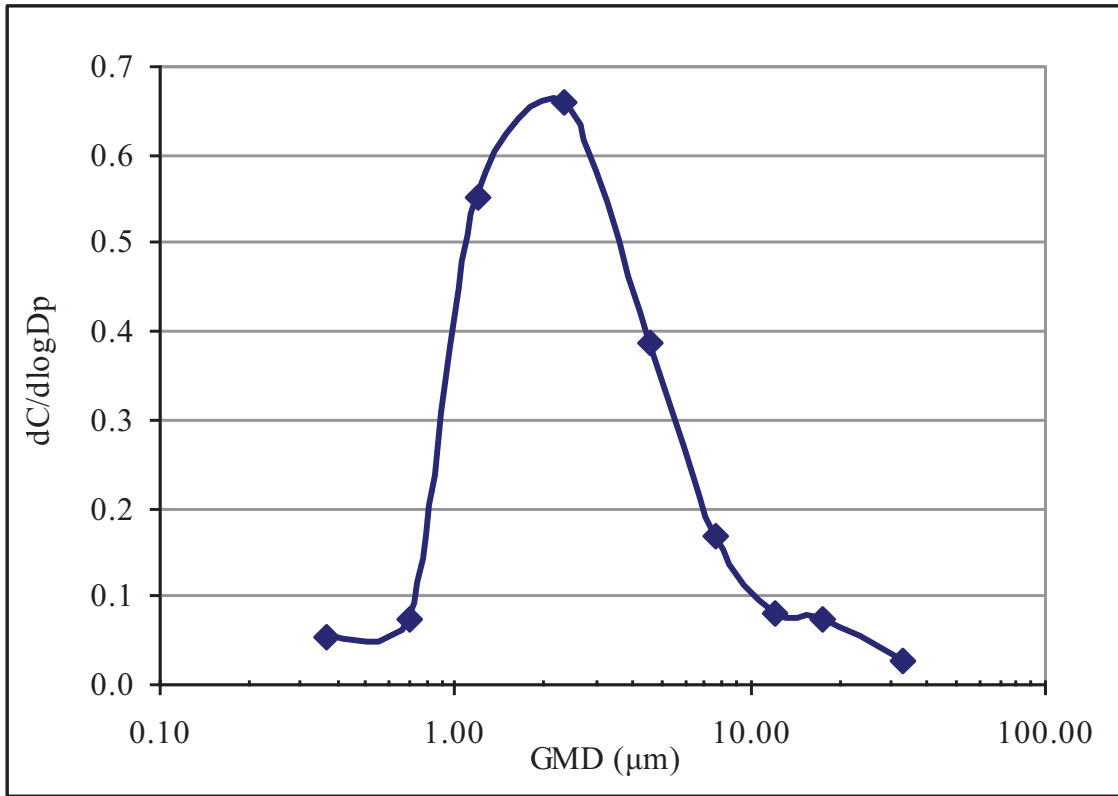


Figure 24: Sample #21 Differential Particle Size Distribution

**Table 4: Sample #22: Cumulative Mass Percent Less than D<sub>p</sub>**

Stage #	Cutpoint (D <sub>p</sub> ) (μm)	Mass Collected (μg)	Concentration (mg/ m <sup>3</sup> )	GMD (μm)	W/W <sub>total</sub> (%)	%<D <sub>p</sub>
Final	0.26	0.72	0.016	0.37	4.4	4.4
8	0.52	0.87	0.020	0.70	5.3	9.7
7	0.93	3.70	0.084	1.20	22.5	32.1
6	1.55	5.76	0.131	2.33	35.0	67.1
5	3.50	2.04	0.046	4.58	12.4	79.5
4	6.00	1.48	0.034	7.67	9.0	88.5
3	9.80	0.50	0.011	12.04	3.0	91.6
2	14.80	0.51	0.012	17.75	3.1	94.7
1	21.30	0.88	0.020	32.63	5.3	100

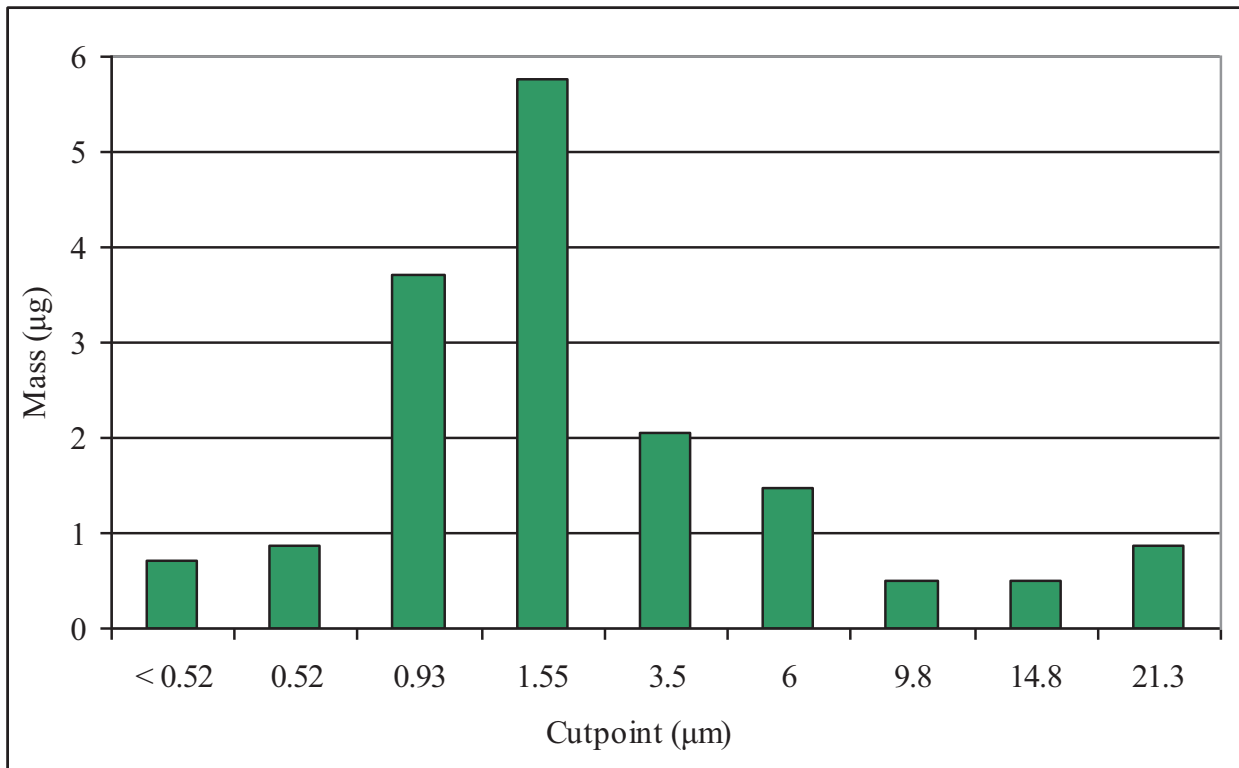


Figure 25: Sample #22 Size Distribution Chart

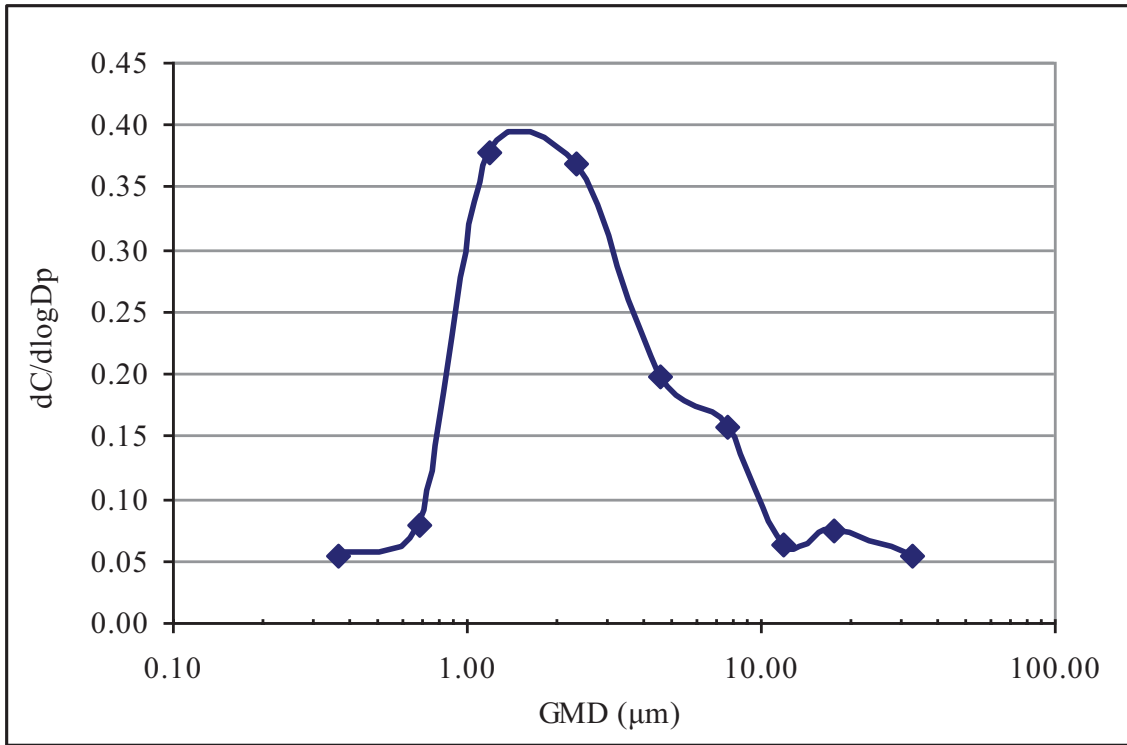


Figure 26: Sample #22 Differential Particle Size Distribution

**Table 5: Sample #28: Cumulative Mass Percent Less than Dp**

Stage #	Cutpoint (Dp) (µm)	Mass Collected (µg)	Concentration (mg/ m <sup>3</sup> )	GMD (µm)	W/W <sub>total</sub> (%)	%<Dp
Final	0.26	1.11	0.017	0.37	6.0	6.0
8	0.52	0.84	0.013	0.70	4.5	10.5
7	0.93	2.01	0.030	1.20	10.8	21.3
6	1.55	7.74	0.117	2.33	41.6	62.9
5	3.50	3.27	0.050	4.58	17.6	80.5
4	6.00	2.07	0.031	7.67	11.1	91.6
3	9.80	0.48	0.007	12.04	2.6	94.2
2	14.80	0.24	0.004	17.75	1.3	95.5
1	21.30	0.84	0.013	32.63	4.5	100

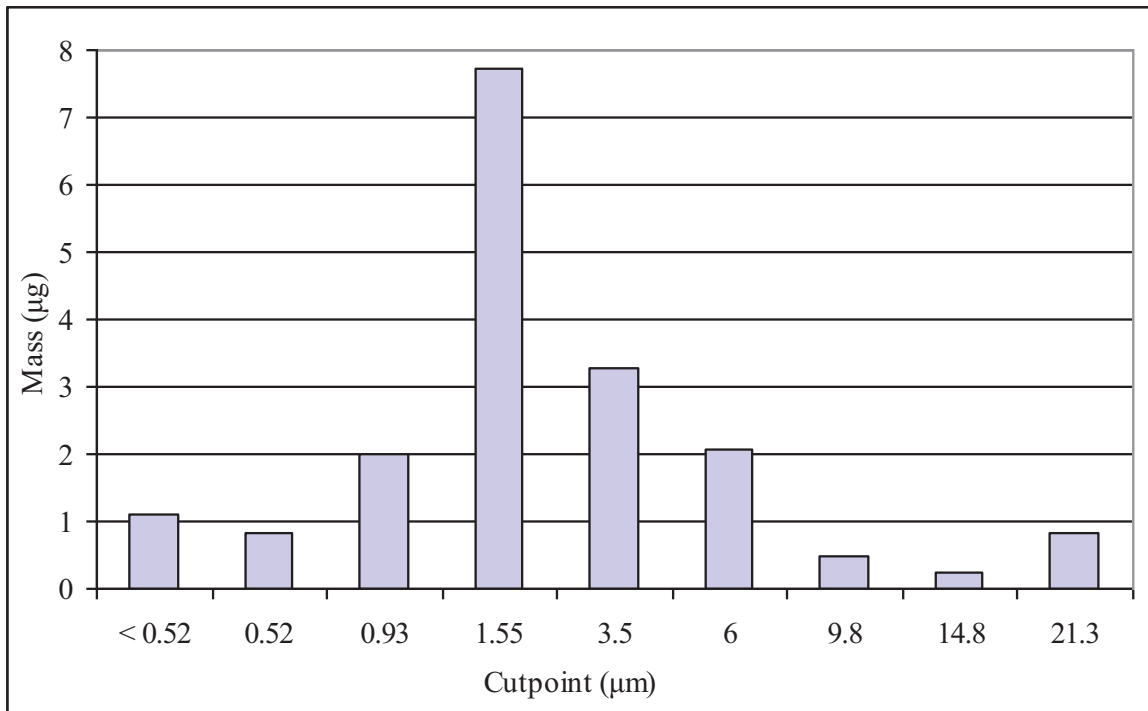


Figure 27: Sample #28 Size Distribution Chart

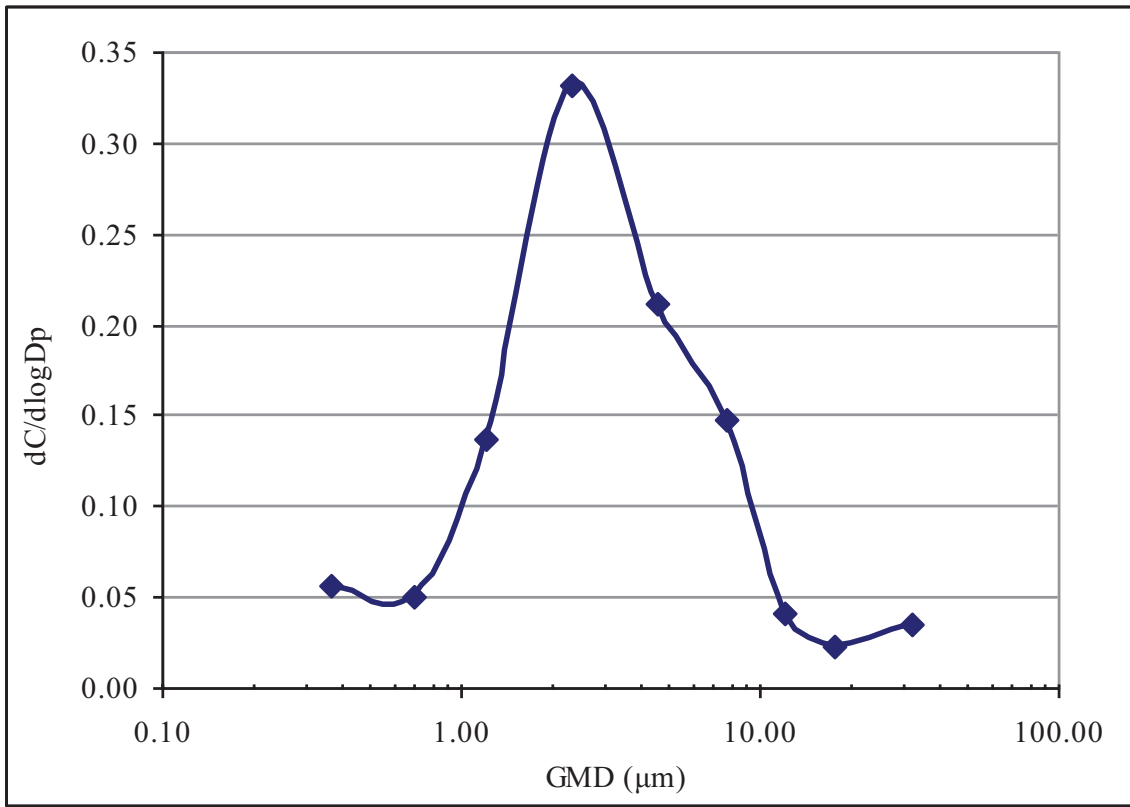


Figure 28: Sample #28 Differential Particle Size Distribution

**Table 6: Sample #38: Cumulative Mass Percent Less than Dp**

Stage #	Cutpoint (Dp) (µm)	Mass Collected (µg)	Concentration (mg/ m <sup>3</sup> )	GMD (µm)	W/Wtotal (%)	%<Dp
Final	0.26	0.96	0.005	0.37	3.9	3.9
8	0.52	1.06	0.006	0.70	4.3	8.2
7	0.93	2.25	0.013	1.20	9.1	17.3
6	1.55	6.76	0.038	2.33	27.4	44.8
5	3.50	6.37	0.035	4.58	25.9	70.6
4	6.00	3.10	0.017	7.67	12.6	83.2
3	9.80	1.31	0.007	12.04	5.3	88.5
2	14.80	1.45	0.008	17.75	5.9	94.4
1	21.30	1.38	0.008	32.63	5.6	100

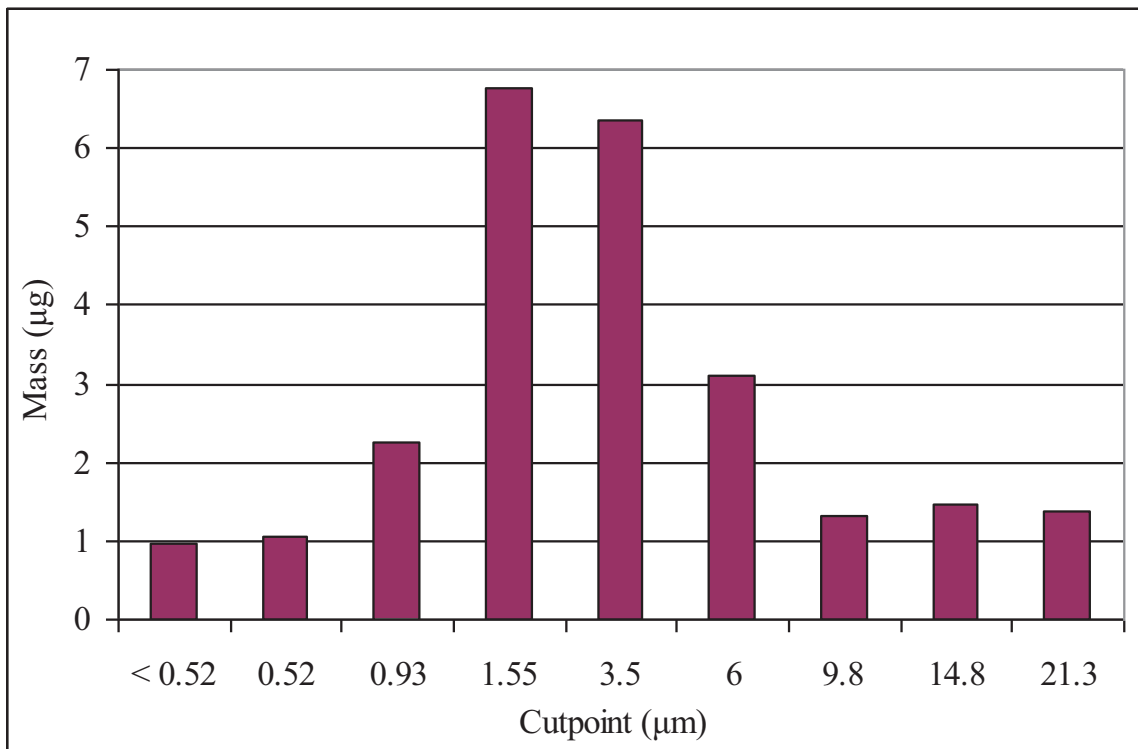


Figure 29: Sample #38 Size Distribution Chart

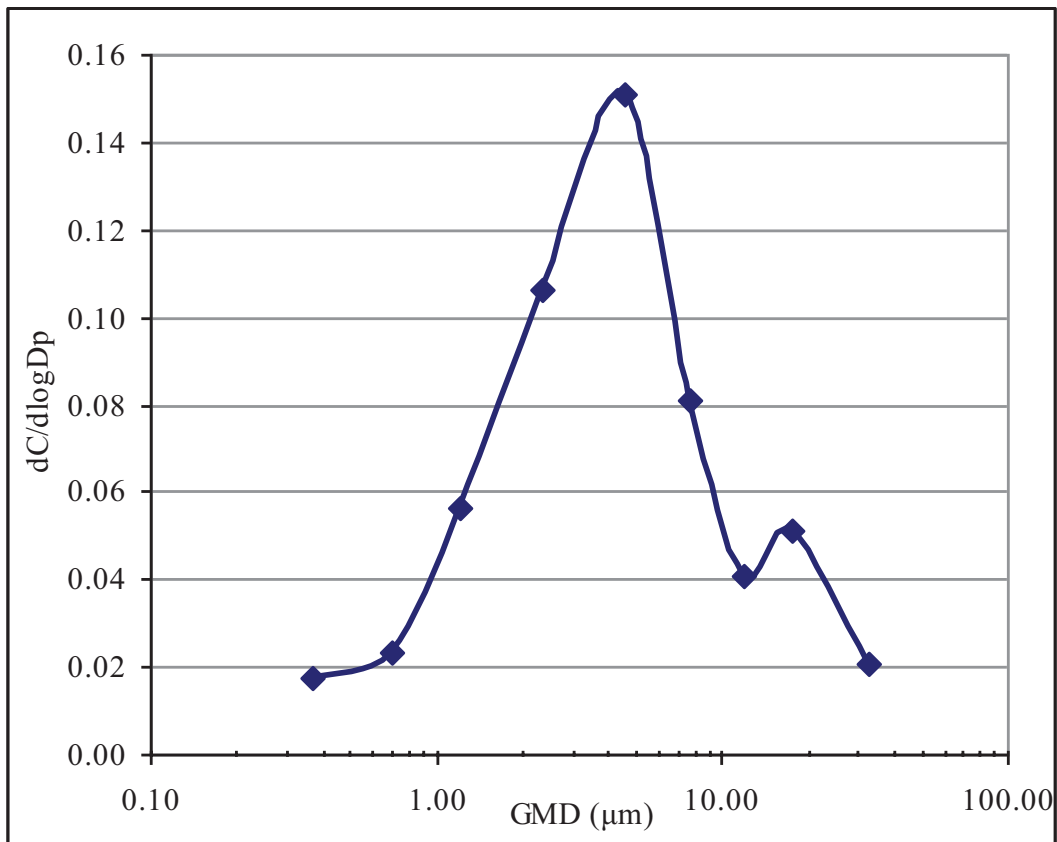


Figure 30: Sample #38 Differential Particle Size Distribution

**Table 7: Final Product: Cumulative Mass Percent Less than Dp**

Stage #	Cutpoint (Dp) (µm)	Mass Collected (µg)	Concentration (mg/m <sup>3</sup> )	GMD (µm)	W/Wtotal (%)	%<Dp
Final	0.26	0.72	0.014	0.37	1.6	1.6
8	0.52	1.02	0.020	0.70	2.3	3.9
7	0.93	8.61	0.166	1.20	19.3	23.2
6	1.55	17.58	0.338	2.33	39.4	62.6
5	3.50	8.55	0.164	4.58	19.2	81.8
4	6.00	5.37	0.103	7.67	12.0	93.8
3	9.80	1.11	0.021	12.04	2.5	96.3
2	14.80	0.90	0.017	17.75	2.0	98.3
1	21.30	0.76	0.015	32.63	1.7	100

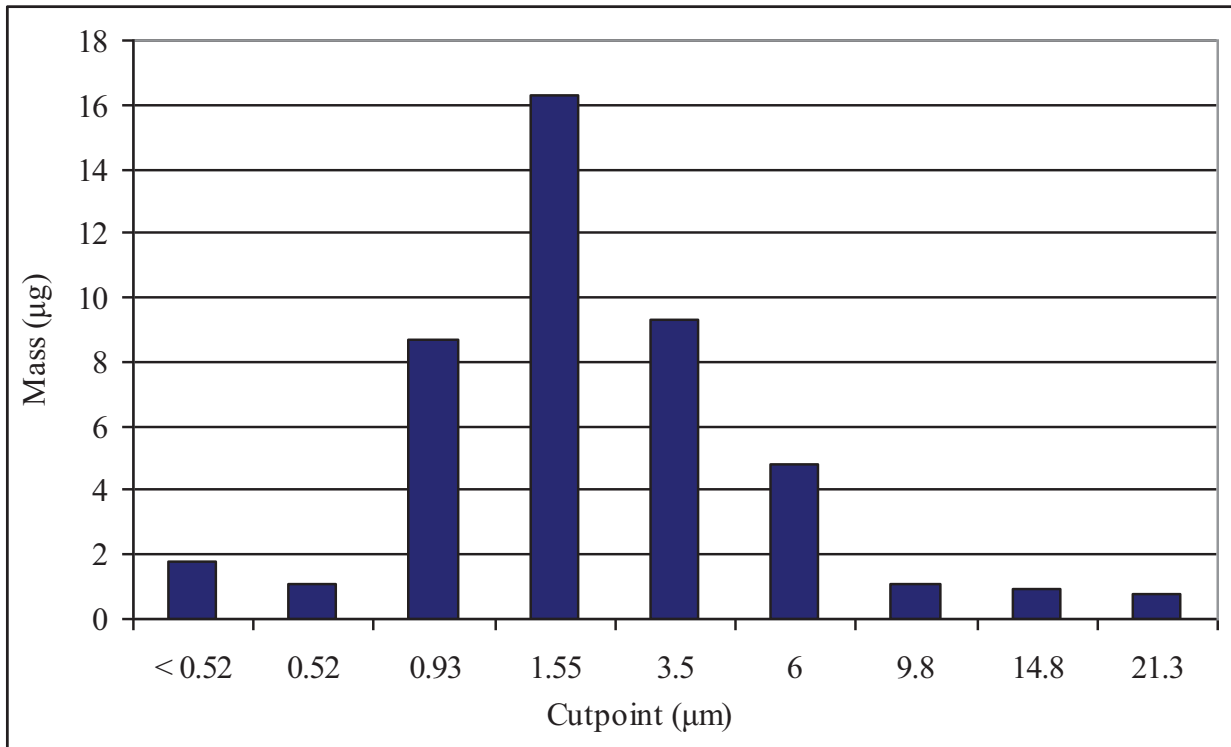


Figure 31: Final Product Size Distribution Chart

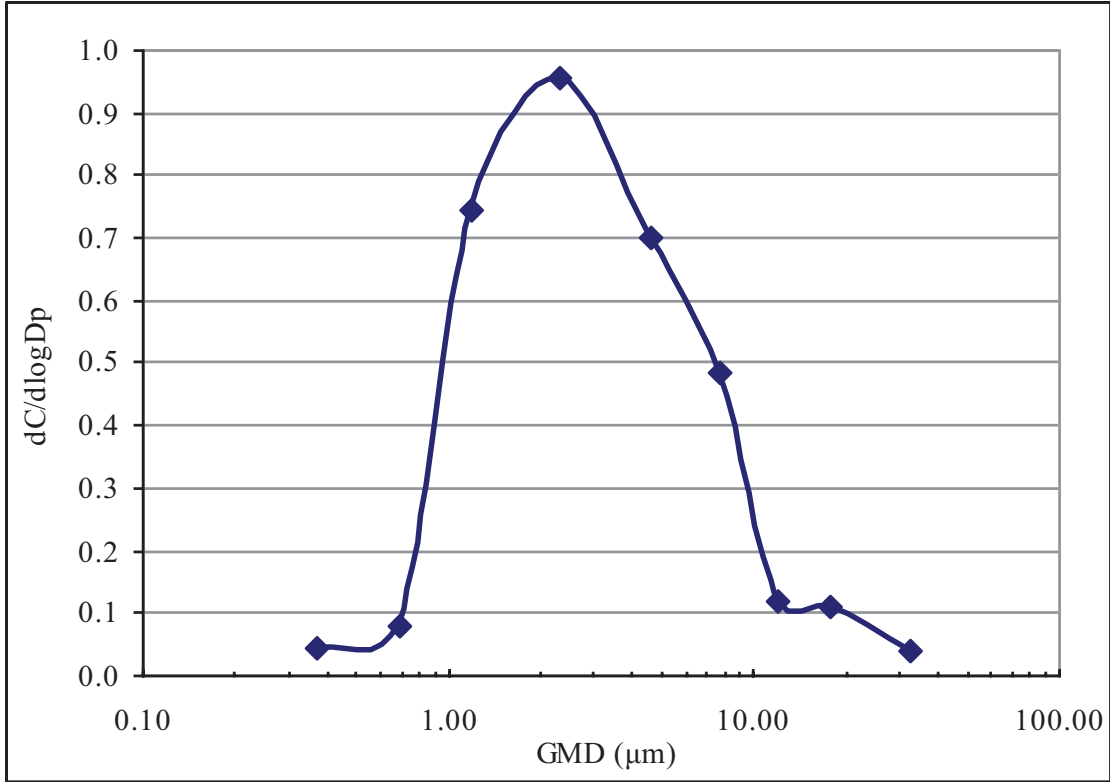


Figure 32: Final Product Differential Particle Size Distribution

The size distribution bar charts indicate that the most prevalent size range of particles is from 1.55  $\mu\text{m}$  to 3.5  $\mu\text{m}$ . The weight percentages in this size range for samples #21, #22, #28, #38, and Final Product are 42.2%, 35.0%, 41.6%, 27.4%, and 28.5%, respectively. According to the size classification chart in Figure 10, particles that are respirable (capable of reaching the deepest part of the lung) range in size from 0.0001 to 10 microns. Particles with an aerodynamic diameter less than 10  $\mu\text{m}$  are generally able to travel into the pulmonary part of the lungs (the respiratory bronchioles, alveolar ducts, and alveolar sacs [18]. Particles ranging from 1-2  $\mu\text{m}$  are most likely to penetrate to the alveoli. These particle sizes are large enough that their settling velocity allows them to deposit where they can do the most damage [19]. In Table 8, the mass percentages of particles between 1  $\mu\text{m}$  and 2  $\mu\text{m}$ , and the mass percentages of particles less than 10  $\mu\text{m}$  are shown. The mass percentages for samples #21 and #22 between 1  $\mu\text{m}$  and 2  $\mu\text{m}$  are 32% and 31%, respectively. The mass percentages of samples #28 and #38 between 1  $\mu\text{m}$  and 2  $\mu\text{m}$  are about 50 to 60% of that in samples #21 and #22. This may be explained by the shorter length of samples #21 and #22.

**Table 8: Approximate Mass Percentages in the Respirable Range**

<b>Sample</b>	<b>Mass (%) between 1<math>\mu\text{m}</math> and 2<math>\mu\text{m}</math></b>	<b>Mass (%) less than 10<math>\mu\text{m}</math></b>
21	32	96
22	31	92
28	20	94
38	15	89
Final Product	23	96

The GMD curves present a mean diameter mode for each of the samples analyzed. The GMD mode for samples #21, #22, #28, #38, and Final Product are approximately 2.0 $\mu\text{m}$ , 1.5 $\mu\text{m}$ , 2.5 $\mu\text{m}$ , 4.5 $\mu\text{m}$ , and 2.3 $\mu\text{m}$ , respectively. Sample #38 has the largest GMD (4.5 $\mu\text{m}$ ), which is expected due to its comparatively larger dimensions (length=10-30 $\mu\text{m}$ , OD=20-30nm). Sample #22 has the smallest GMD (1.5 $\mu\text{m}$ ), which is caused by its smaller dimensions (length=0.5-2.0 $\mu\text{m}$ , OD=1-2nm).

## **B. Scanning Electron Microscopy with Energy Dispersive X-Ray Microanalysis (SEM/EDS) Study for Morphology and Metal Content**

A scanning electron microscope is used to get a visual picture of the aerosolized carbon nanomaterial particles. Micrographs give an indication of the size of the particles and agglomerates collected on the substrate. The micrographs also show a more detailed view of the structures of these nanomaterials. Energy dispersive x-ray microanalysis is a technology which provides rapid qualitative analysis of the elemental composition of a particular material. In this experiment, EDS was used as a tool for detecting metals present in the carbon nanomaterials. A quantitative method for detection of trace metals is discussed in Section 3: “Determination of Trace Metals by Inductively Coupled Plasma Atomic Emission Spectroscopy (ICP-AES).”

### *1) Carbon Nanomaterial Collection*

The sample collection method is the same as that in the “Size Distribution” section with two exceptions:

1. A Sioutas Cascade Impactor was used rather than a Marple Impactor
2. Mixed Cellulose Ester (MCE) filters were used rather than quartz filters. Quartz filters are undesirable because they have a cross-hatched background when viewed under the SEM, making it difficult to distinguish between the filter medium and the CNTs.

The Sioutas Cascade Impactor is a personal sampling device with four impaction stages and a final filter that allows the separation and collection of airborne particles in five size ranges [25]. The Sioutas Cascade Impactor was used with a Leland Legacy Sample Pump (SKC Cat. No. 100-3000), which was calibrated to 9 lpm. The Sioutas Cascade Impactor cutpoints are shown on Table 9 and a photo of the impactor is shown on Figure 33. The Sioutas Cascade Impactor was placed at the center of the chamber horizontally and 12” from the bottom vertically. As stated in the previous section, the materials from Reactors A and B are too large for use in the SSPD. The results shown in this section are for samples #21, #22, #28, #38, and the Final Product. The MCE filters placed on stages A and D, which collect the largest ( $>2.5\mu\text{m}$ ) and the smallest ( $0.25\text{-}0.50\mu\text{m}$ ) particles, respectively, were analyzed for their elemental composition.

**Table 9: Sioutas Cascade Impactor Cutpoints**

<b>Stage</b>	<b>Cutpoint</b>
A	$2.5\mu\text{m}$
B	$1.0\mu\text{m}$
C	$0.50\mu\text{m}$
D	$0.25\mu\text{m}$
Final	$<0.25\mu\text{m}$



Figure 33: Sioutas Cascade Impactor

## 2) *Filter Preparation*

After a ten minute sampling time, the Sioutas impactor is removed from the chamber. The MCE filters are removed from the Sioutas Impactor, placed in a filter cassette, and transported to the University of Cincinnati's Advanced Materials Characterization Center. The filters are then cut to a slightly smaller size and mounted on a specimen holder called a specimen stub. Specimens must be electrically conductive on the surface and electrically grounded to prevent the accumulation of electrostatic charge at the surface. Nonconductive specimens tend to charge when scanned by the electron beam, and are therefore coated with a gold/palladium (Au/Pd) alloy.

## 3) *SEM/EDS Description*

The Advanced Materials Characterization Center at the University of Cincinnati is home to the Scanning Electron Microscope (FEI/Phillips XL30 ESEM-FEG), equipped with an energy dispersive x-ray microanalysis system (Figure 34). During SEM

analysis, an electron beam is scanned across the surface of a sample. When the electrons hit the sample, the detection of specific signals produces an image. Secondary electrons are emitted from the atoms occupying the top surface and produce a readily interpretable image of the surface. The contrast in the image is determined by the sample morphology. A high resolution image can be obtained because of the small diameter of the primary electron beam. Interaction of the primary beam with atoms in the sample causes shell transitions which result in the emission of an x-ray. The emitted x-ray has an energy characteristic of the parent element. Detection and measurement of the energy permits elemental analysis [26].



Figure 34: Scanning Electron Microscope (FEI/Phillips XL30 ESEM-FEG) at the University of Cincinnati

#### 4) *Results*

The resulting micrographs and EDS results are shown in Appendix B. The smaller light-colored box on the micrograph depicts the area which was analyzed by EDS. For each sample, five to seven different areas of the filter deposit were analyzed to ensure a representative analysis of the particles. Note that the two largest peaks at approximately 2.2KeV and 3KeV are the peaks of gold and palladium. These peaks are caused by the Au/Pd coating and may be ignored.

##### **i. Trace Metals**

Sample number 28 is composed of long SWCNTs (length 5-30 $\mu$ m, diameter 1-2nm).

According to the vendor (Cheap Tubes Inc.), cobalt is the catalyst used in the CVD method for making SWCNTs. The results show a small amount of Co in each of the areas analyzed with EDS. The percentages by weight range from 0.66% to 1.59%.

These values are qualitative and may not necessarily be actual weight percentages. But they indicate that a small amount of Co remains in the CNTs after purification.

Chromium was detected in two of the sampled areas, both from the stage D filter. The weight percents were 0.85% and 0.92%. According to the SEM/EDS supervisor at the University of Cincinnati Advanced Materials Characterization Center, percentages less than 1.00 % are not considered accurate. Based upon the low percentages of Cr detected, it was determined that chromium may not actually be present in the sample.

No metals were found in the CNTs collected on the final filter.

Sample number 38 is composed of long MWCNTs (length 10-30 $\mu$ m, diameter 20-30nm). According to the vendor, iron or nickel is the catalyst used in the production of MWCNTs. However, neither Fe nor Ni was detected in any of the sample areas. Chromium was detected on both stages A and D. The percentage by weight detected on stage A ranged from 0.44% to 0.79%. The percentage by weight detected on stage D ranged from 1.69% to 2.57%. The amount of Cr detected on stage A is less than 1.00% and therefore it cannot be confirmed that Cr is actually present in the sample area. The mass percentages on stage D indicate that Cr may be present in small amounts in various areas of the sample. The elevated percentages of Cr on stage D, and the detection of Co on stage D in sample #28, may indicate that the metals left over from the manufacturing process are concentrated on the smaller CNTs. However, no metals were found in the CNTs collected on the final filter.

The Final Product is composed of CNFs which have been heated to about 750°C to remove organics and catalyst. The catalyst used in the manufacturing process is iron. However, Fe was not detected in any of the areas sampled with EDS.

Sample number 21 is composed of short MWCNTs (length 0.5-2.0 $\mu$ m, diameter 20-30nm). According to the vendor, iron or nickel is the catalyst used in the production method. However, neither Fe nor Ni was detected in any of the sample areas.

Sample number 22 is composed of short SWCNTs (length 0.5-2.0 $\mu$ m, diameter 1-2nm). According to the manufacturer, cobalt is the catalyst used in the manufacturing process.

Cobalt was detected in the deposits on stage A, ranging in weight percent from 2.16% to 2.49%. Cobalt was also detected in the deposits from stage D, ranging from 2.72 to 8.75%. Cobalt was not detected in the CNTs collected on the final filter.

Cobalt was detected in varying amounts from samples #22 and #28, which is expected because Co is the catalyst of choice as stated by the vendor. While the results are not quantitative, they indicate that some residual Co is likely to be left over in the CNTs due to the manufacturing process. The varying amounts of Co may be attributed to their sporadic occurrences.

## **ii. Morphology**

Sample number 28 is composed of long SWCNTs. Figure 35 and Figure 36 show the morphology of the CNTs collected on stages A and D, respectively. Recall stage A collects dust which is greater than 2.5  $\mu\text{m}$  in size, and stage D collects dust between 0.25 $\mu\text{m}$  and 0.50 $\mu\text{m}$ . Figure 35 shows a large agglomerate measuring approximately 5 $\mu\text{m}$  in size. The SEM images indicate that the CNT particles on stage A tend to be micrometer-size rather than forming individual fibers. Varying lengths of individual fibers are seen jutting out from the agglomerates in some areas. On stage D, fiber agglomerates also are seen, but smaller particles are expected on stage D given its lower cutpoint. The micrograph of the stage D particles shows the long fibrous structure of the tubes. Micrographs of sample #28 collected on the final filter can be found in Appendix B. The micrographs do not give a clear indication of the morphology of the particles collected on the final filter.

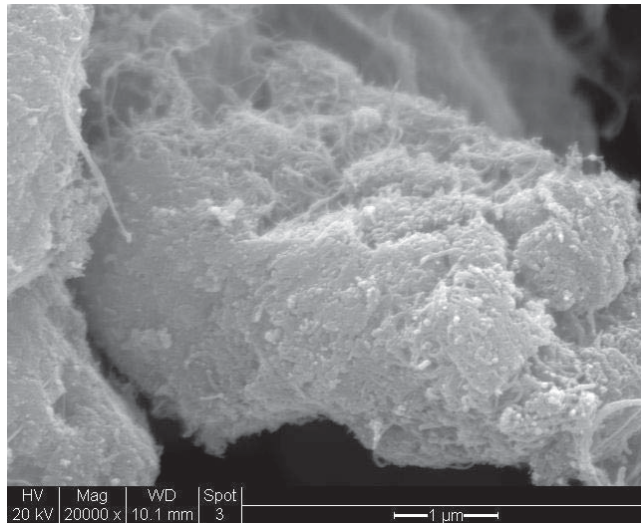


Figure 35: SEM Micrograph of #28 on Stage A

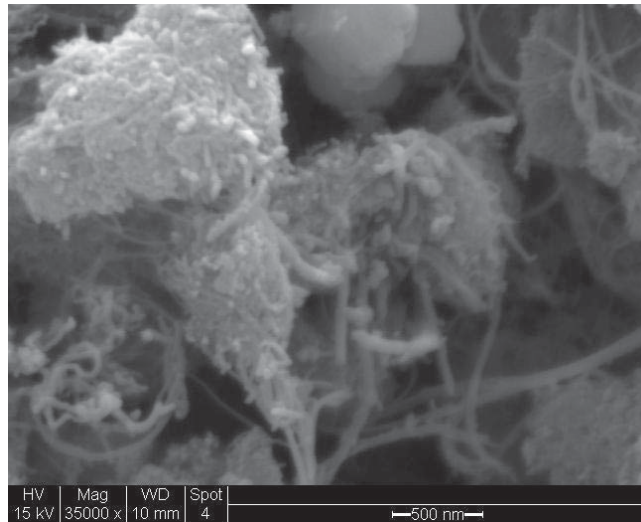


Figure 36: SEM Micrograph of #28 on Stage D

Sample number 38 is composed of long MWCNTs. Figures 37, 38, and 39 show the morphology of the CNTs on stages A, D, and the final filter, respectively. Figure 37 indicates that the particles collected on stage A are agglomerates rather than individual fibers. But the fibrous structure is still apparent: long fibers can be seen extending from the surface of the bundles. The agglomerates on stage D are similar in structure to those seen on stage A, but smaller. The bundles on stage D are less dense than those on stage

A. The high magnification shows how the fibers intertwine with each other. Sample #38 has a more fibrous structure than any of the CNTs analyzed in this study.

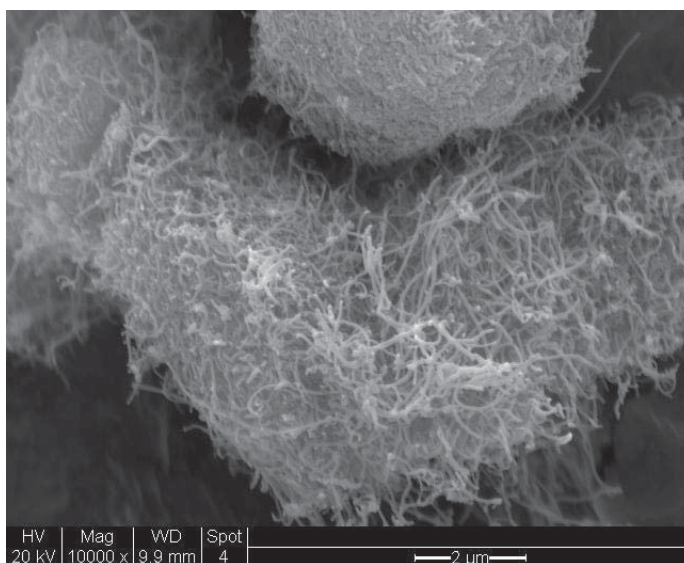


Figure 37: SEM Micrograph of #38 on Stage A

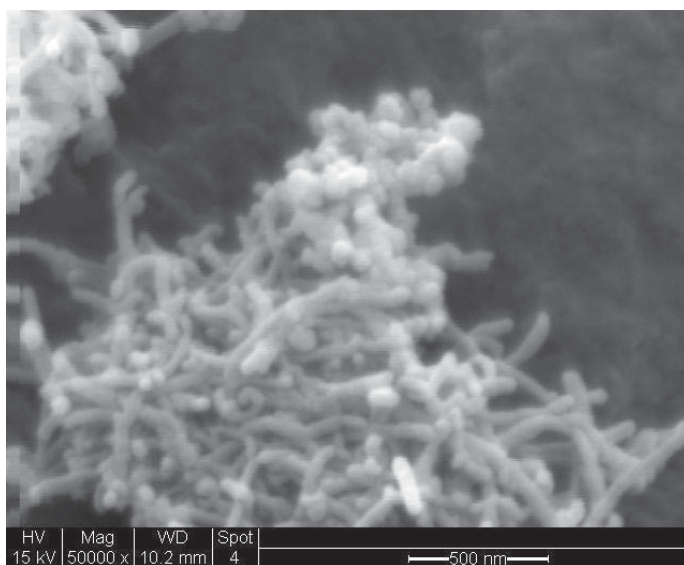


Figure 38: SEM Micrograph of #38 on Stage D

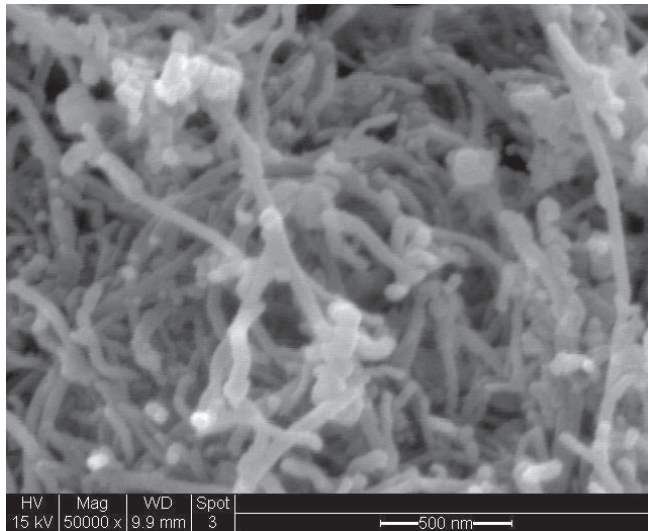


Figure 39: SEM Micrograph of #38 on the Final Filter

Sample number 21 is composed of short MWCNTs. Figures 40, 41 and 42 below show the morphology of the CNTs on stages A, D, and the final filter, respectively. Figure 40 depicts the CNTs as agglomerates ranging in width from about 3 to 6  $\mu\text{m}$ . The CNTs appear as bundles with short fibers only showing on their surfaces. Figure 41 shows the CNTs on stage D of the impactor. This figure more clearly indicates fibrous structure, but the tendency to agglomerate is still apparent. The agglomerate sizes range from about 1 to 2  $\mu\text{m}$  in width. The tubes in Figures 40- 42 are smaller than those seen in samples #28 and #38, which may relate to the shorter length (0.5-2.0  $\mu\text{m}$ ) reported for sample #21. This sample appears to be less fibrous than any of the samples from Cheap Tubes Inc.

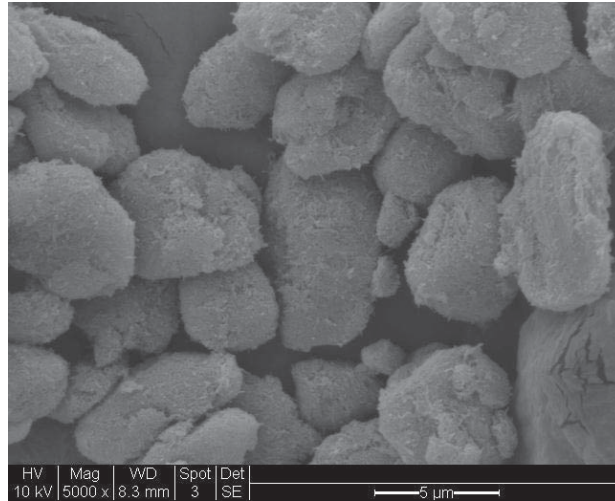


Figure 40: SEM Micrograph of #21 on Stage A

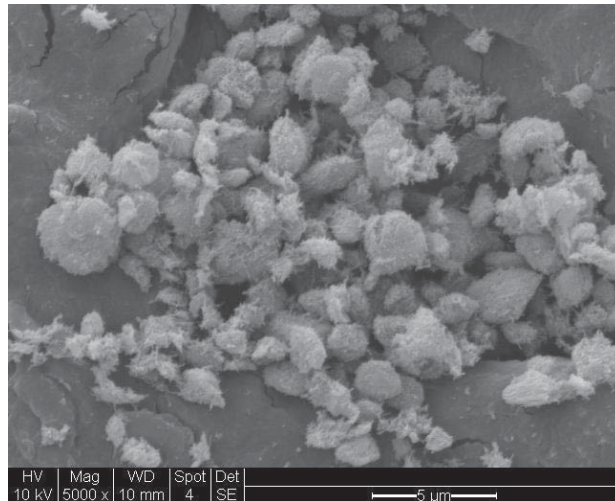


Figure 41: SEM Micrograph of #21 on Stage D

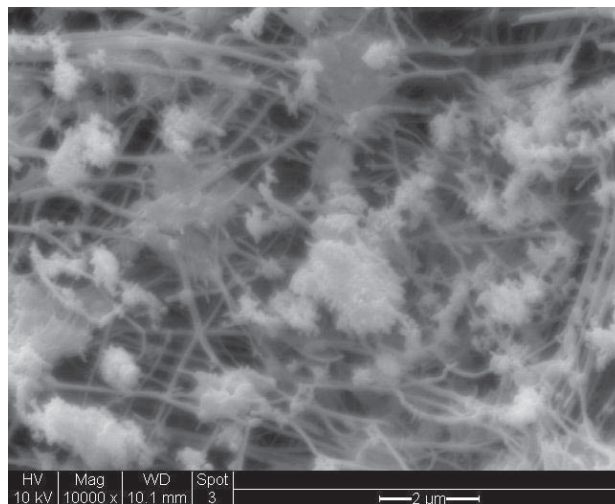


Figure 42: SEM Micrograph of #21 on the Final Filter

Sample number 22 is composed of short SWCNTs. Figures 43, 44, and 45 show the morphology of the CNTs collected on stages A, D, and the final filter, respectively. Figure 43 depicts the CNTs as agglomerates which, similar to sample number 28, seem to only have fibers extending from the surface of the bundle. Both samples 28 and 22 are SWCNTs, but the CNTs from sample number 28 are longer, 5-30  $\mu\text{m}$  versus 0.5-2  $\mu\text{m}$  for sample number 22. Figure 44 shows the CNTs on stage D of the impactor. This figure is similar to that of Figure 43, but the CNT agglomerates are much smaller. A close look at the bundles indicates fibers emerging from the surface. The micrograph of the final filter shows very small agglomerates. The image is not quite clear enough to tell if individual tubes are present.

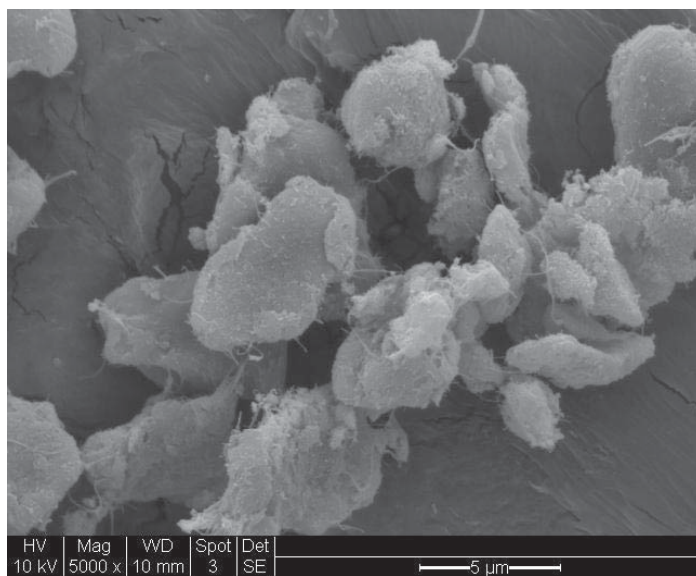


Figure 43: SEM Micrograph of #22 on Stage A

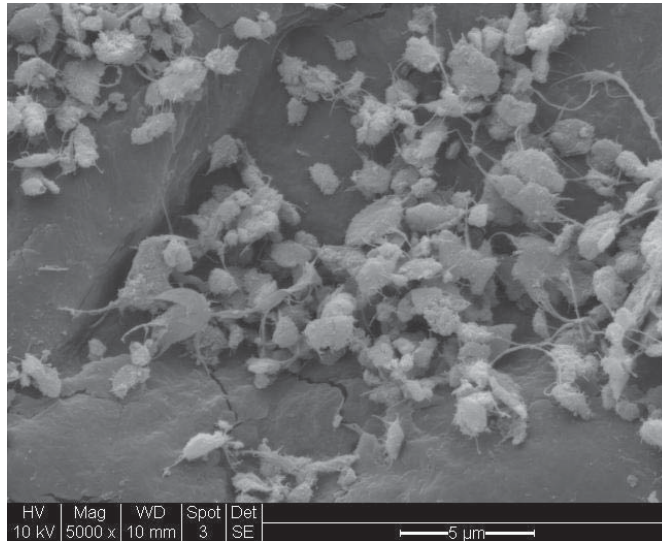


Figure 44: SEM Micrograph of #22 on Stage D

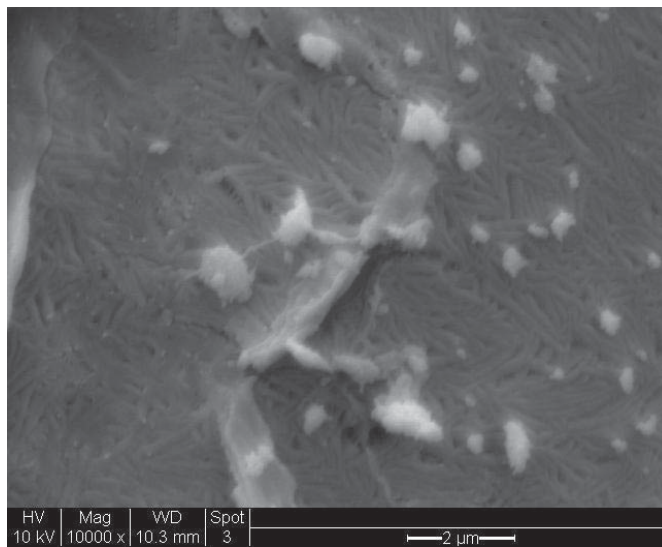


Figure 45: SEM Micrograph of #22 on the Final Filter

The Final Product micrographs from stages A, D, and the final filter are presented in Figures 46, 47, and 48, respectively. These images clearly indicate long fibers intertwined with each other. Again in Figure 46, we see that the particle fibers are tightly bound. The Final Product material most resembles sample #38 (long MWCNT),

but has longer fibers. Figure 47 shows the CNFs on stage D of the impactor. The sample appears to be a vast array of fibers layered on top of one another. Figure 48 shows the fibers collected on the final filter ( $<0.25\mu\text{m}$ ). Here, the first freestanding fibers can be seen. These micrographs indicate that particles in the Final Product aerosol are more likely to have a fibrous structure than any of the CNT materials examined.

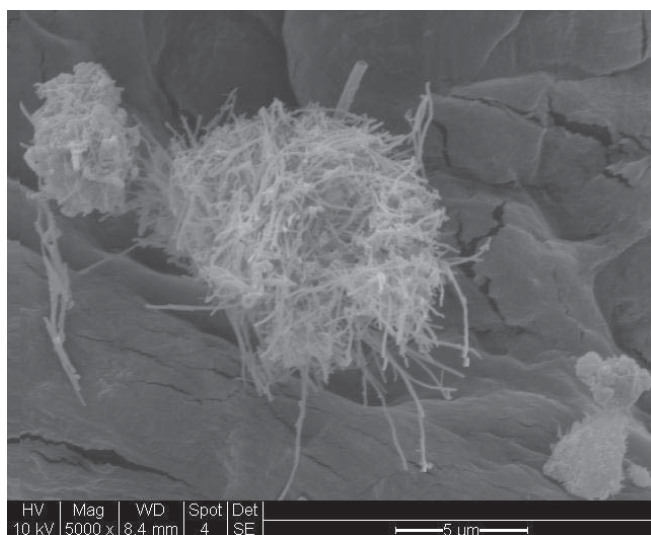


Figure 46: SEM Micrograph of the Final Product on Stage A

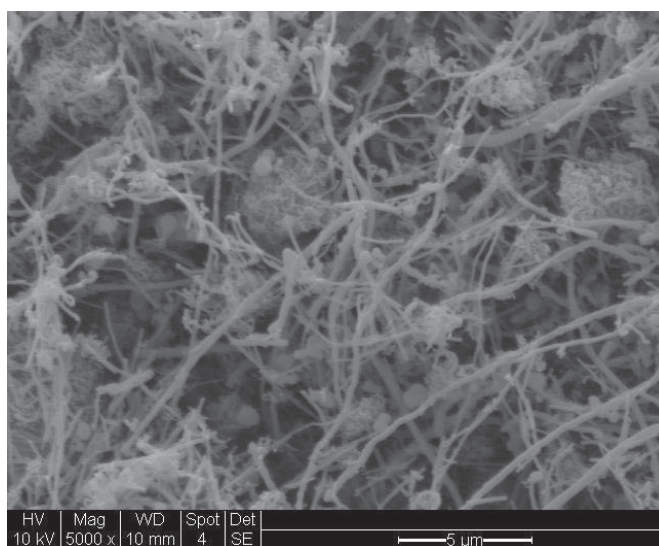


Figure 47: SEM Micrograph of the Final Product on Stage D

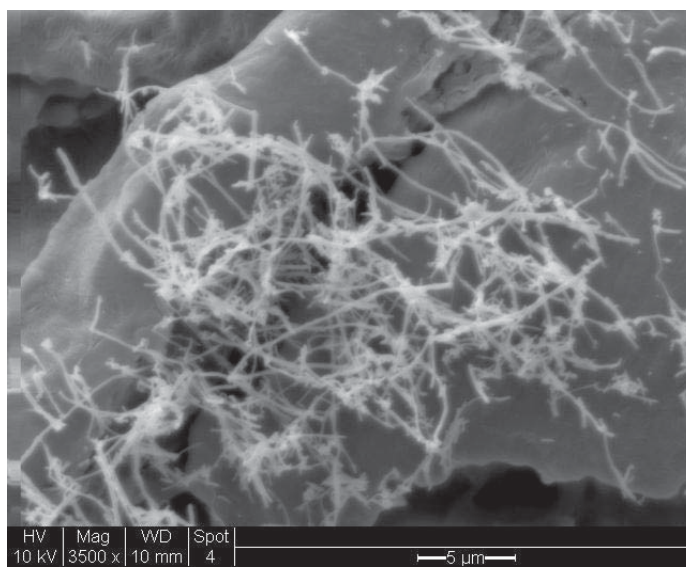


Figure 48: SEM Micrograph of the Final Product on the Final Filter

### **C) Determination of Trace Metals by Inductively Coupled Plasma Atomic Emission Spectroscopy (ICP-AES)**

ICP-AES is an analytical technique used for the detection of trace metals. It is a type of emission spectroscopy that uses the inductively coupled plasma to produce excited atoms and ions that emit electromagnetic radiation at wavelengths characteristic of a particular element [27]. The intensity of this emission is indicative of the concentration of the element within the sample.

In the occupational environment, exposure to metals may cause diseases of the lung. The exposure situation in the occupational environment as well as in the general environment is usually complex and includes many pollutants, and it is generally difficult to decide whether a certain disease is caused by a single metal or a combination of metals and other pollutants [28].

According to Renn and Roco, fibers such as carbon nanotubes could cause adverse health effects, not only due to their shape and dimension, but also because of their potential to be combined with iron or other metals. The addition of metals could cause catalytic effects having free-radical-releasing pro-inflammatory properties [3].

Laboratory studies of animals have also shown negative health implications after exposure. Animal studies on nano-sized particles such as titanium dioxide, metallic cobalt, and metallic nickel found that metallic nickel demonstrated a statistically significant greater inflammation response than either cobalt or titanium dioxide, and that cobalt was more inflammogenic than titanium dioxide. Nickel and cobalt caused

lipid peroxidation [3]. A study by A.R. Murray et al. suggests that SWCNT may be toxic to the skin and that SWCNT toxicity may be dependent upon the metal (particularly iron) content of SWCNT via the metal's ability to interact with the skin, initiate oxidative stress, and induce redox-sensitive transcription factors thereby affecting/leading to inflammation [29]. For these reasons, metals were determined in the bulk nanomaterials.

### 1) *Method*

All samples (Reactor A, Reactor B, Final Product, and samples 21, 22, 28, and 38) were weighed and placed into small vials. The masses are shown in Table 10 (at the bottom). Next, the samples were transferred to 125 mL beakers and analyzed according to NIOSH Manual of Analytical Methods (NMAM) 7300 modified for bulk carbon nanotubes. For sample digestion, 4 mL of concentrated nitric acid and 11 mL of concentrated perchloric acid were added to each sample. The samples were covered with a watch glass and refluxed at 200°C until complete dissolution occurred (~3 days). The watchglass covers were then removed and the samples heated at 150°C until they had reached near-dryness. The sample residues were dissolved in a dilute solution (4%/1%) of nitric acid/perchloric acid and then analyzed for trace metals by ICP-AES. The samples were filtered with 0.45 micron filters prior to analysis, if needed.

### 2) *Results*

The results have been corrected for the reagent blank and are reported as µg/sample. The limits of detection (LOD) and quantitation (LOQ) are based upon a final volume of

10mL. Due to the varying range of supplied weights, the LOD and LOQ values have not been corrected for sample weight. The values reported in brackets are between the LOD and LOQ. Due to poor recoveries of analyst samples, the Cr results are not quantitative and for informational purposes only. Table 10 shows the metals and corresponding mass per sample ( $\mu\text{g}$  metal/sample). The bulk material mass is listed in the bottom row.

**Table 9: ICP-AES Results**

<b>Sample</b>	<b><u>1</u></b>	<b><u>2</u></b>	<b><u>3</u></b>	<b><u>21</u></b>	<b><u>22</u></b>
<b>Ag</b>	n.d.	n.d.	n.d.	[0.085]	n.d.
<b>Al</b>	2.35	2.46	1.67	2.52	14.3
<b>As</b>	n.d.	n.d.	n.d.	0.446	[0.14]
<b>Ba</b>	0.0165	[0.0024]	0.0412	0.924	0.167
<b>Be</b>	n.d.	n.d.	n.d.	n.d.	n.d.
<b>Ca</b>	1.15	1.33	23.0	14.2	7.67
<b>Cd</b>	0.0191	0.0450	0.0426	0.0429	n.d.
<b>Co</b>	[0.0084]	n.d.	[0.0079]	23.7	1480
<b>Cr</b>	0.983	1.09	1.64	6.07	18.0
<b>Cu</b>	n.d.	n.d.	n.d.	0.359	0.444
<b>Fe</b>	205	419	451	431	42.5
<b>K</b>	0.633	[0.13]	1.50	0.809	5.34
<b>La</b>	n.d.	n.d.	n.d.	10.2	1.47
<b>Li</b>	[0.0020]	n.d.	n.d.	0.00350	[0.0033]
<b>Mg</b>	0.198	[0.057]	10.3	3.29	2.92
<b>Mn</b>	0.00590	0.0185	0.0801	0.434	2.83
<b>Mo</b>	n.d.	n.d.	[0.0098]	7.97	234
<b>Na</b>	[6.1]	[4.6]	[15.]	n.d.	[8.9]
<b>Ni</b>	0.0611	[0.038]	0.276	1670	13.13
<b>P</b>	n.d.	0.193	0.200	n.d.	n.d.
<b>Pb</b>	n.d.	n.d.	[0.036]	0.466	0.351
<b>Sb</b>	n.d.	[0.36]	[0.31]	n.d.	1.30
<b>Se</b>	n.d.	n.d.	n.d.	n.d.	n.d.
<b>Sr</b>	0.00540	[0.0010]	0.108	0.106	0.0525
<b>Te</b>	n.d.	n.d.	n.d.	n.d.	n.d.
<b>Ti</b>	0.356	0.369	0.113	0.652	0.807
<b>Tl</b>	n.d.	n.d.	n.d.	n.d.	2.77
<b>V</b>	n.d.	n.d.	n.d.	0.0477	0.151
<b>Y</b>	n.d.	n.d.	n.d.	n.d.	n.d.
<b>Zn</b>	0.819	0.889	0.353	8.61	0.939
<b>Zr</b>	[0.0052]	n.d.	[0.033]	n.d.	[0.031]
<b>weight (g)</b>	0.0207	0.0429	0.0421	0.1008	0.0731

**Table 9: ICP-AES Results cont'd**

<b>Sample</b>	<b>28</b>	<b>38</b>	<b>LOD</b>	<b>LOQ</b>
<b>Ag</b>	[0.070]	n.d.	0.034	0.115
<b>Al</b>	5.99	0.952	0.026	0.0866
<b>As</b>	[0.21]	[0.32]	0.10	0.333
<b>Ba</b>	0.169	1.01	0.0012	0.00395
<b>Be</b>	n.d.	n.d.	0.0029	0.00970
<b>Ca</b>	173	7.87	0.28	0.919
<b>Cd</b>	n.d.	[0.012]	0.0050	0.0167
<b>Co</b>	1380	380	0.0058	0.0192
<b>Cr</b>	11.1	4.25	0.0087	0.0291
<b>Cu</b>	1.44	1.88	0.048	0.161
<b>Fe</b>	316	221	0.10	0.333
<b>K</b>	4.69	1.52	0.044	0.147
<b>La</b>	0.727	6.35	0.024	0.0813
<b>Li</b>	0.0396	0.00400	0.0010	0.00333
<b>Mg</b>	39.2	1.84	0.046	0.155
<b>Mn</b>	5.08	0.231	0.0010	0.00333
<b>Mo</b>	229	3.05	0.0089	0.0297
<b>Na</b>	638	n.d.	8.09	27.0
<b>Ni</b>	5.39	477	0.014	0.0470
<b>P</b>	0.691	[0.12]	0.050	0.167
<b>Pb</b>	0.562	0.174	0.028	0.0946
<b>Sb</b>	[0.62]	n.d.	0.26	0.877
<b>Se</b>	n.d.	n.d.	0.086	0.285
<b>Sr</b>	1.08	0.0849	0.0010	0.00333
<b>Te</b>	n.d.	n.d.	0.064	0.214
<b>Ti</b>	0.204	0.691	0.027	0.0908
<b>Tl</b>	2.68	1.16	0.036	0.121
<b>V</b>	0.0491	[0.016]	0.0093	0.0311
<b>Y</b>	n.d.	n.d.	0.010	0.0333
<b>Zn</b>	2.10	2.65	0.086	0.286
<b>Zr</b>	[0.043]	n.d.	0.025	0.0833
<b>weight (g)</b>	0.0963	0.0523		

Table 11 shows the mass percentages of those metals which had a percentage greater than 1.0% in at least one of the samples. The metals which have the highest percentages in the bulk samples are the metals used as catalysts in the CVD method. Iron is the catalyst used in the production of materials: Reactor A, Reactor B, and Final Product. The mass percentages of Fe in Reactor A, Reactor B, and Final Product are 0.99%, 0.98%, and 1.07%.

**Table 11: Top Metal Mass Percentages Determined by ICP-AES**

<b>Element</b>	<b>Reactor A</b>	<b>Reactor B</b>	<b>Final Product</b>	<b>Sample #21</b>	<b>Sample #22</b>	<b>Sample #28</b>	<b>Sample #38</b>
Co	-	-	-	-	2.02%	1.43%	0.73%
Fe	0.99%	0.98%	1.07%	0.43%	-	0.33%	0.42%
Ni	-	-	-	1.66%	-	-	0.91%

Cobalt has the highest mass percentages, 2.02% and 1.43%, in samples 22 and 28, respectively. According to the vendor, Co is the catalyst used in the production of these SWCNTs, so these results are expected. Cobalt is also present in sample 38 with a mass percentage of 0.73%.

Nickel has the highest mass percentages, 1.66% and 0.91%, in samples 21 and 38, respectively. According to the vendor, Ni (or Fe) is the chosen catalyst in the production of these MWCNTs, so these results are expected.

Iron is present in samples 21, 28, and 38, with percentages of 0.43%, 0.33%, and 0.42%, respectively. According to the vendor, Fe or Ni is used in the production of the

MWCNTs (samples #21 and #38) and Co is used in the production of the SWCNTs (samples #22 and #28). The presence of Fe in sample number 28 may indicate that an Fe/Co alloy was actually used as the catalyst in the manufacture of these materials. According to the vendor, large amounts of CNTs can be formed by catalytic CVD of acetylene over cobalt and iron catalysts supported on silica or zeolite[12]. The presence of Co, Fe, and Ni in sample #38 may also indicate that an alloy of these elements was used as the catalyst. According to Qian et al., the introduction of Fe to Ni may increase the activity and stability of the iron-based catalyst and hence the yield of CNTs [30]. Iron/Cobalt catalysts have also been used to grow CNTs [31].

Appendix A provides information from the vendor's website about their SWCNTs and MWCNTs. The percentages of elemental components for SWCNTs (length 5-30  $\mu\text{m}$ ) are listed. The percentage of Co in these samples, similar to sample #28, is listed as 2.91%. Iron is not listed as a component. A similar table presents the elemental components for MWCNTs (length 10-20  $\mu\text{m}$ ), similar to sample #38. The percentages of Ni and Fe in these samples are reported as 0.94% and 0.26%, respectively. The analysis method listed on the website is energy dispersive x-ray spectroscopy (EDS). The ICP-AES analysis in this study found 1.43% Co in sample #28, and 0.91% Ni and 0.42% Fe in sample #38. There is some discrepancy between the percentages of elements found in these two different analysis techniques. This may be caused by the small sample size of EDS and the inhomogeneity of the samples (i.e. sporadic occurrences of catalysts). This study has indicated that the metal content of carbon nanomaterials as detected via EDS can vary widely as the area of analysis changes.

Whereas ICP-AES analysis detects trace metals in the bulk sample. For this reason, ICP-AES may be a more accurate method for the quantification of trace metals in carbon nanomaterials.

#### D. Determination of Polycyclic Aromatic Hydrocarbons (PAHs) by Gas Chromatography/ Mass Spectrometry (GC/MS)

Polycyclic aromatic hydrocarbons (PAHs, also known as polynuclear aromatic hydrocarbons) are composed of two or more aromatic, or benzene, rings which are fused together when a pair of carbon atoms is shared between them (see Figure 49) [32]. Physical and chemical characteristics of PAHs vary with molecular weight. The environmentally significant PAHs are those molecules which contain two (e.g., naphthalene) to seven benzene rings (e.g., coronene). The lower molecular weight PAHs (e.g., 2 to 3 ring group of PAHs such as naphthalenes, fluorenes, phenanthrenes, and anthracenes) have significant acute toxicity to aquatic organisms, whereas the high molecular weight PAHs, 4 to 7 rings (from chrysenes to coronenes) do not [32].

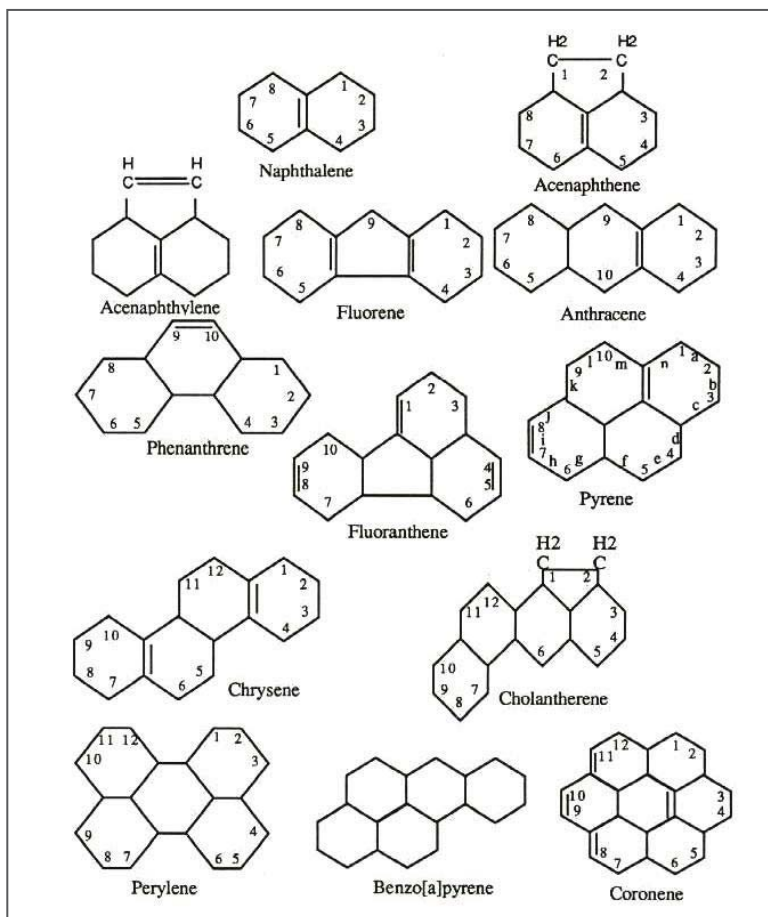


Figure 49: Structure and numbering of selected PAHs

Eight PAHs (Car-PAHs) typically considered as possible carcinogens include [33]:

- benzo(a)anthracene
- chrysene
- benzo(b)fluoranthene
- benzo(k)fluoranthene
- benzo(a)pyrene (B(a)P)
- dibenzo(a,h)anthracene
- indeno(1,2,3-cd)pyrene
- benzo(g,h,i)perylene

In particular, benzo(a)pyrene has been identified as being highly carcinogenic. The US Environmental Protection Agency (USEPA) has promulgated 16 unsubstituted PAHs (EPA-PAH) as priority pollutants (Table 12). PAHs are commonly associated with industrial processes in which carbonaceous materials such as coke, coal tar, coal tar pitch and asphalt oils are produced or used [34]. Thus, exposure assessments of PAHs in the workplace are a top priority.

Some people who have breathed or touched mixtures of PAHs and other chemicals for long periods of time have developed cancer. Several PAHs have caused cancer in laboratory animals when they breathed air containing them (lung cancer), ingested them in food (stomach cancer), or had them applied to their skin (skin cancer) [33].

**Table 12: USEPA 16 priority PAHs**

<b>Compound</b>	<b>Formula</b>	<b>Molecular Weight (g/gmol)</b>
Naphthalene	C <sub>10</sub> H <sub>8</sub>	128.17
Acenaphthylene	C <sub>12</sub> H <sub>8</sub>	152.19
Acenaphthene	C <sub>12</sub> H <sub>10</sub>	154.21
Fluorene	C <sub>13</sub> H <sub>10</sub>	166.22
Phenanthrene	C <sub>14</sub> H <sub>10</sub>	178.23
Anthracene	C <sub>14</sub> H <sub>10</sub>	178.23
Fluoranthene	C <sub>16</sub> H <sub>10</sub>	202.25
Pyrene	C <sub>16</sub> H <sub>10</sub>	202.25
Benzo(a)anthracene	C <sub>18</sub> H <sub>12</sub>	228.29
Chrysene	C <sub>18</sub> H <sub>12</sub>	228.29
Benzo(b)fluoranthene	C <sub>20</sub> H <sub>12</sub>	252.31
Benzo(k)fluoranthene	C <sub>20</sub> H <sub>12</sub>	252.31
Benzo(a)pyrene	C <sub>20</sub> H <sub>12</sub>	252.31
Indeno(1,2,3-cd)pyrene	C <sub>22</sub> H <sub>12</sub>	276.33
Dibenzo(a,h)anthracene	C <sub>22</sub> H <sub>14</sub>	278.35
Benzo(g,h,i)perylene	C <sub>22</sub> H <sub>12</sub>	276.33

1) *Method*

This method involves extraction using dichloromethane (DCM) and quantification by gas chromatography/mass spectrometry (GC/MS). The method is designed to determine the concentration of PAHs in micrograms per milligram of sample ( $\mu\text{g}/\text{mg}$ ). The GC system is an Agilent Technologies 6890N Network (Figure 50). The mass spectrometer is an Agilent 5973 Network Mass Selective Detector. The column used for the analysis is an Agilent HP-5MS (5% phenol methyl siloxane; length 30m; internal diameter 250 $\mu\text{m}$ ; film thickness 0.25  $\mu\text{m}$ ). Gas chromatography separates the

components of a mixture and mass spectroscopy characterizes each of the components individually.



Figure 50: GC/MS located at NIOSH Cincinnati

Samples are prepared by adding a known mass of CNT or CNF to a known volume of DCM. The mixture is shaken vigorously for at least three minutes. The resulting solution is then filtered with using a Whatman Anotop 25 disposable syringe filter (0.02  $\mu\text{m}$ ). Quantification is accomplished using a commercial 16 PAH standard.

To begin the analysis, 1.0  $\mu\text{L}$  of PAH standard solution (6.4ppm) is injected into the GC. The total sampling time is 44 minutes. The MS then provides a spectrum containing unique PAH peaks. The retention time and area of each PAH peak is recorded. Next, 1.0uL of the prepared DCM solution is injected into the GC. The resulting spectrum is analyzed for peaks having the same retention time as the standard peaks. A chemical compound library built into the GC/MS software is used to verify

the identity of the peaks. When peaks on the carbon nanomaterial sample spectrum match the retention time of the standard peaks, the areas are recorded. The peak areas are directly proportional to the concentration of PAHs in the sample. Using the initial concentration of carbon nanomaterial in DCM, the volume injected into the GC (1.0 $\mu$ L), and the spectra provided by the MS, the concentration of each PAH in the bulk sample is calculated. Table 13 shows the mass of each sample and volume of DCM added.

**Table 13: GC/MS Sample Preparation Concentrations**

<b>Sample Name</b>	<b>Mass (mg)</b>	<b>DCM (mL)</b>	<b>Concentration (mg/mL)</b>	<b>% Soluble</b>
Reactor A	24.1	3	8.0	13
Reactor B	84.1	3	28.0	4
Final	109.8	2	54.9	1
21	24.8	3	8.3	24
22	24.5	3	8.2	26
28	25.6	3	8.5	21
38	28.2	3	9.4	20

## 2) Results

Figures 51, 52, and 53 show the concentration of PAHs in Reactor A, Reactor B, and the Final Product, respectively. The PAHs are listed by molecular weight (See Table 11 for the corresponding PAH name). PAHs were not detected in any of the samples from Cheap Tubes Inc. Therefore results are not shown for samples #21, #22, #28, and #38.

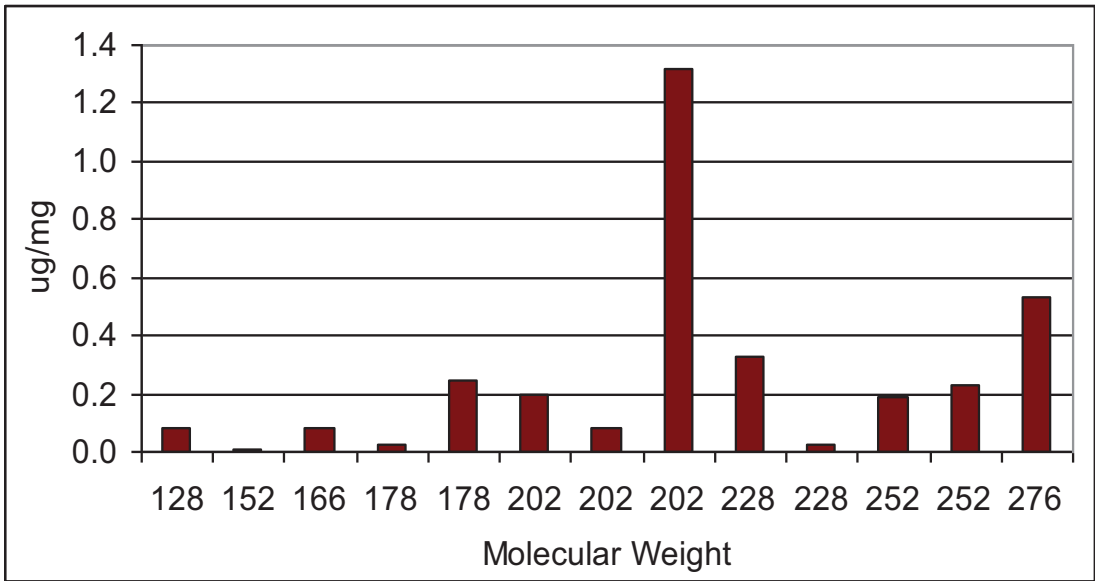


Figure 51: PAHs present in Reactor A

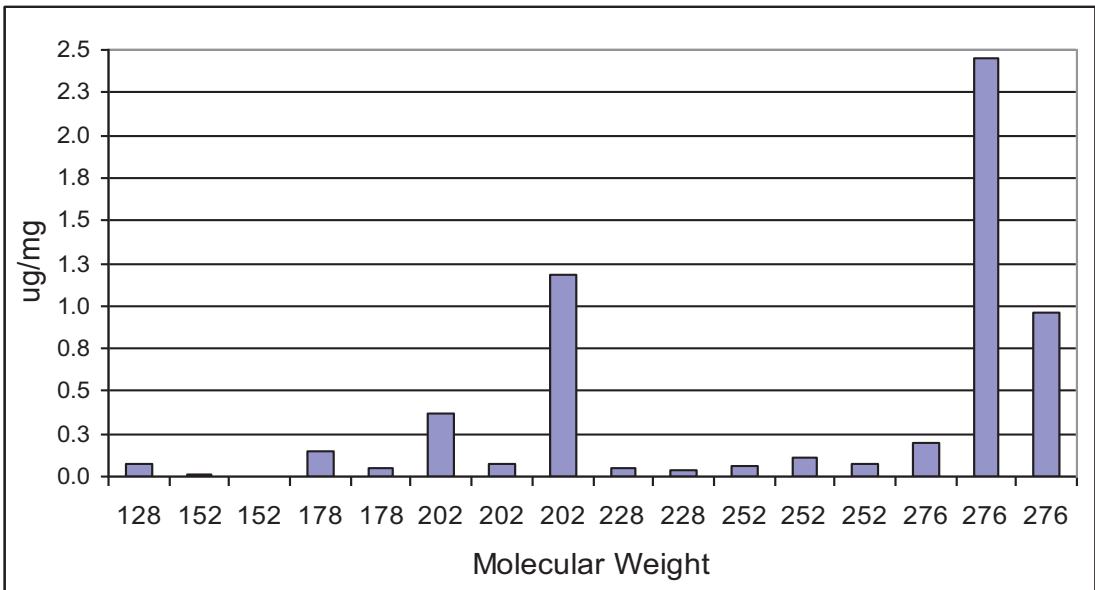


Figure 52: PAHs present in Reactor B

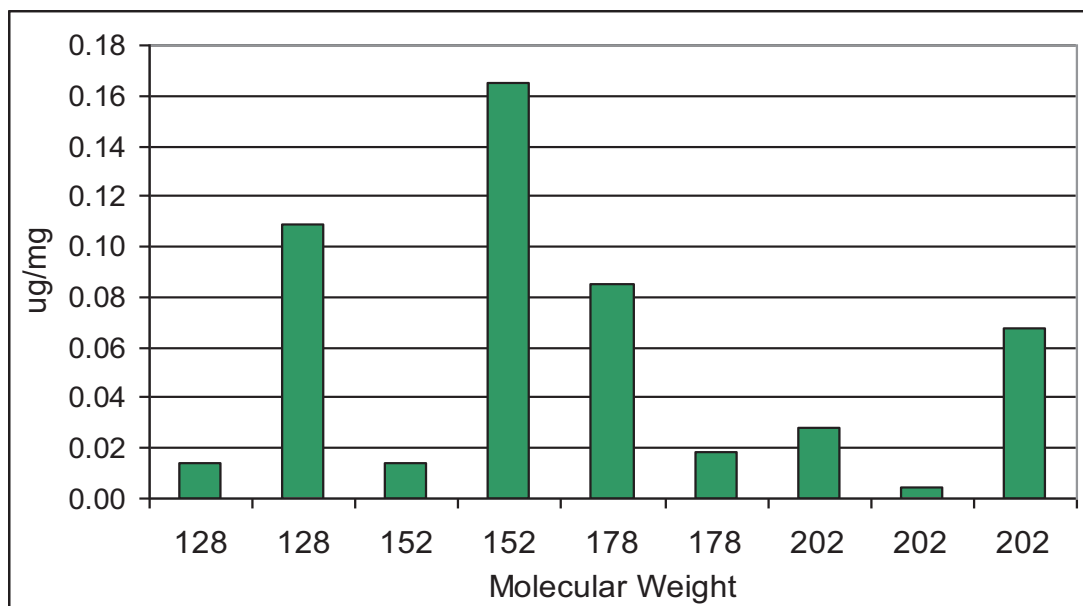


Figure 53: PAHs present in Final Product

Pyrene (mw=202g/gmol) and indeno(1,2,3-cd)pyrene (mw=276g/gmol) are the primary PAHs found in Reactor A with concentrations of 1.3 and 0.5  $\mu\text{g}/\text{mg}$ , respectively. The primary PAHs found in Reactor B are also pyrene and indeno(1,2,3-cd)pyrene at concentrations of 1.2 and 2.5  $\mu\text{g}/\text{mg}$ , respectively. The PAHs detected in the Final Product are those with fewer benzene rings (2-4). The primary PAHs detected are naphthalene (mw=128g/gmol), acenaphthylene (mw=152 g/gmol), phenanthrene (mw=178 g/gmol), and pyrene (mw = 202g/gmol) with concentrations of 0.11, 0.16, and 0.08, and 0.07  $\mu\text{g}/\text{mg}$ , respectively. These results indicate that the Final Product is more pure in terms of number and concentration of PAHs present, which was expected because it is processed to remove residual organic compounds.

Figures 51 and 52 show that the same PAHs are present in Reactors A and B with one exception: fluorene (mw=166g/gmol), which is only present in Reactor A. The concentrations of PAHs in both materials are generally comparable with the exception of indeno(1,2,3-cd)pyrene, which has a much higher concentration in Reactor B (2.5 µg/mg). All of the PAHs detected in the CNFs are listed as priority pollutants. Six of the eight possible carcinogens (Car-PAHs) are detected in the CNFs from Reactors A and B.

## **V. Conclusions and Recommendations**

The size distribution analysis has led to a significant finding that the particles analyzed in this study are highly respirable. Generally, particles ranging from 1-2  $\mu\text{m}$  are most likely to penetrate to the alveoli. These particles sizes are small enough to enter the respiratory system and large enough that their settling velocity allows them to deposit where they can do the most damage [19]. Inhalation of hazardous or toxic particles is detrimental to human health, as reported in numerous studies [3, 4, 6, 7, 15, 18, 28]. The results have shown that the highest percentage of particles examined in this study range in size from 1.55 to 3.5 microns. Dust particles less than 10  $\mu\text{m}$  in size are considered respirable. The results indicate that 89% to 96% of the samples analyzed in this study are less than 10 microns in size, and 15-32% of the samples are within the 1-2  $\mu\text{m}$  range, with the short CNTs having the highest percentages in the 1-2  $\mu\text{m}$  range. The highly respirable nature of these carbon nanomaterials, partnered with the ease with which they become airborne, is cause for concern.

The SEM results indicate that the carbon nanomaterials aerosolized in this study tend to contain agglomerates. This is especially apparent in samples #21 and #22, where the CNT bundles only vaguely resemble fibers. This is consistent with other studies involving carbon nanotubes [13, 16, 35, 36, 37, 38, 39]. Because of the high surface area to volume ratio, CNTs have the propensity to form agglomerates that are difficult to separate into individual nanotubes [35]. According to a study by Lam et. al., SWCNTs do not naturally exist as individual tubes; van der Waals forces between the molecules cause them to aggregate into microscopic bundles or ropes, which in turn

agglomerate loosely into small clumps [38]. A 2008 study by Bello et. al investigated airborne exposures to nanoscale particles and fibers generated during dry and wet abrasive machining of two three-phase advanced composite systems containing carbon nanotubes (CNTs), micron-diameter continuous fibers (carbon or alumina), and thermoset polymer matrices. TEM analysis indicated that no clearly identifiable individual CNT structures could be found in fibers or the particle agglomerates [39]. The SEM micrographs developed in this study show the tendency for airborne CNT and CNF particles to be present as agglomerates. The micrographs of samples #28, #38, and Final Product best show the fibrous structure of the carbon nanomaterials. A comparison of the micrographs of the Final Product with images of asbestos fibers indicates similarities in structure. This is consistent with Poland's finding that long, thin carbon nanomaterials may look and also behave like asbestos fibers [9].

CNTs are generally entangled in the form of curved agglomerates [40]. Dispersion of CNTs and CNFs continues to be a field which is highly researched. Several researchers have solved aggregation problems by using melt mixing, bulk polymerization, and sonication during the CNT dispersion process. However, aggregation problems of solvent-based CNT dispersion have not been fully addressed [39]. The vendor of the CNTs examined in this experiment (Cheap Tubes Inc) recommends using Sonics VCX750 ultrasonic equipment. The vendor also suggests adding a dispersing reagent (surfactant) into the solution to accelerate the dispersion effect and help to keep the CNTs well separated [12].

The determination of metal content by ICP-AES provided quantitative data on trace metals (except Cr) found in the bulk samples. The metals which had the highest concentrations in the samples were those used as catalysts in the CVD process; Ni, Fe, and Co, which is consistent with previous research [3, 28, 41]. According to Arepalli, all of the SWCNT and MWCNT products produced by CVD contain residual metals [40]. The mass percentages of Fe ranged from 0.98% to 1.07% in the CNF samples. Nickel, the catalyst used in making the MWCNTs in this study, had mass percentages of 1.66% and 0.91% in samples #21 and #38, respectively. Cobalt, the catalyst used in the production of the SWCNTs in this study, had mass percentages of 2.02% and 1.43% for samples #22 and #28, respectively. These results give a clearer image of the amount of residual catalyst present in carbon nanomaterials produced by the CVD manufacturing process. According to previous research, fibers such as carbon nanotubes could cause adverse health effects, not only due to their shape and dimension, but also because of their potential to be combined with metals. The presence of metals in these materials may have free-radical-releasing pro-inflammatory properties [5]. To address the location of catalysts, TEM/EDS analysis would be effective.

The presence of PAHs on the CNF samples (Reactor A, Reactor B, and Final Product) adds another layer of risk to occupational exposure. All of the PAHs detected in the CNFs are listed by the EPA as priority pollutants, and six of the eight PAHs detected in the CNFs from Reactors A and B, which have not been purified, are possible carcinogens [33]. According to Yang et al., CNTs have a high capacity for adsorption of toxic substances due to their large surface area [42]. The health hazards related to

PAHs, several of which are considered mutagenic and teratogenic, have been well established [33, 34, 42, 43, 44, 45, 46]. Future research on the influence of nanoparticle properties on the human body and the potential for adverse health effects is needed.

According to Renn and Roco, most of the assumptions on the potential adverse health impacts (of nanomaterial exposure) come from the emergence of evidence in air pollution, in the effects from the inhalation of welding fumes and extrapolation from the extensive body of knowledge on the health effects of existing micrometer sized and sub-micrometer particles. There are, however, a number of long-term studies underway which should clarify the current assumptions [3].

The SEM analysis provided images of the aerosolized carbon nanomaterials sampled using a cascade impactor. Due to the large size of the agglomerates, the SEM was sufficient to show the morphology of these materials. Future work, perhaps using a TEM, would give better insight into the structure of individual carbon nanomaterial particles.

Future studies involving the monitoring of dust in occupational settings, such as industry and academia, would be helpful to further characterize carbon nanomaterial exposure risks. Many students, scientists, and researchers work with and manipulate carbon nanomaterials for various applications. These individuals are potentially at risk of exposure and may not realize the potential dangers of working with these materials.

## VI. References

1. Drexler, Eric. Engines of Creation: The Coming Era of Nanotechnology. Anchor Books, 1986.
2. Feynman, Richard P. "There's Plenty of Room at the Bottom." An Invitation to Enter a New Field of Physics. Speech delivered Dec. 29, 1959.
3. O. Renn and M. C. Roco. "Nanotechnology and the need for risk governance." Journal of Nanoparticle Research 8 (2006) 153–191.
4. Roco M.C. "International strategy for nanotechnology research." Journal of Nanoparticle Research 3(5–6) (2001) 353–360.
5. DHHS, CDC, NIOSH. "Approaches to Safe Nanotechnology," DHHS (NIOSH) Publication No. 2009–125 March 2009.
6. Maynard, A.M., and E.D. Kuempel: "Airborne nanostructured particles and occupational health." Journal of Nanoparticle Research. 7 (2005): 587-614.
7. Vladimir V. Murashov, Ph.D. "Nanotechnology: Should carbon nanotubes be handled in the workplace like asbestos?" August 2008. Online Posting. Center for Disease Control, NIOSH. <[http://www.cdc.gov/niosh/blog/nsb052008\\_nano.html](http://www.cdc.gov/niosh/blog/nsb052008_nano.html)>
8. Jeffrey W. Card, Darryl C. Zeldin, James C. Bonner, and Earle R. Nestmann. "Pulmonary applications and toxicity of engineered nanoparticles." Am J Physiol Lung Cell Mol Physiol 295 (2008): 400–411.
9. Poland, Craig, A., et al. "Carbon nanotubes introduced into the abdominal cavity of mice show asbestos like pathogenicity in a pilot study." Nature Nanotechnology 3 (2008) 423 – 428.
10. Hirano, Seishiro; Kanno, Sanae; Furuyama, Akiko. "Multi-walled carbon nanotubes injure the plasma membrane of macrophages." Toxicology and Applied Pharmacology 232 (2008): 244-251.
11. Lavadie B, ed. "Definitions for asbestos and other health-related silicates: a symposium." ASTM Special Technical Publication 834 (1984). Philadelphia, PA: American Society for Testing and Materials, 1984.
12. US. Department of Health and Human Services, Public Health Service Centers for Disease Control and Prevention, NIOSH. "Comments of the National Institute for Occupational Safety and Health on the Mine Safety and Health Administration Advanced Notice of Proposed Rulemaking on Measuring and Controlling Asbestos Exposure." June 2002.
13. P.A. Baron, C.M. Sorensen, J.E. Brockman, "Nonspherical particle measurements: shape factors, fractals, and fibers." In: P.A. Baron, K. Willeke (Eds.), Aerosol Measurement: Principles, Techniques, and Applications, second ed., Wiley, New York, 2001: 705–749.
14. Takenaka S, et al. "Pulmonary and systemic distribution of inhaled ultrafine silver particles in rats." Environmental Health Perspectives 109 (2001) 547–551.
15. Shvedova, A.A. et al. "Unusual inflammatory and fibrogenic pulmonary responses to single walled carbon nanotubes in mice." Am. J. Physiol. Lung Cell Mol Physiol. 289 (2005): 698–708.
16. Ku, Bon Ki, Andrew D. Maynard, Paul A. Baron, Gregory J. Deye. "Observation and measurement of anomalous responses in a differential mobility analyzer caused

- by ultrafine fibrous carbon aerosols.” Journal of Electrostatics 65 (March, 2007): 542–548.
17. Vincent J.H., D. Mark, B.G., Miller, L. Armbruster & T.L. Ogden. “Aerosol inhalability at higher windspeeds.” Journal of Aerosol Science 21 (1990) 577–586.
  18. “Particles: Size Makes All the Difference” <ehponline.org/science-ed> P.A. Baron, C.M. Sorensen, J.E. Brockman, Nonspherical particle measurements: shape factors, fractals, and fibers, in: P.A. Baron, K. Willeke (Eds.), Aerosol Measurement: Principles, Techniques, and Applications, second ed., Wiley, New York, (2001) 705–749.
  19. Davis and Cornwell. Introduction to Environmental Engineering, 4th Edition, Graw-Hill Book Co., New York, NY, 2008.
  20. <Cheaptubes.com> Site visited: April 2009.
  21. Harris, Peter. “Carbon nanotube science and technology.” March 2007 <<http://www.personal.rdg.ac.uk/~scsharip/tubes.htm>>
  22. W. D. Griffiths. “The development of sampling methods for the assessment of indoor bioaerosols.” Journal of Aerosol Science 28 (1997) 437-457.
  23. Sunset Laboratory Inc. “Thermal/Optical Carbon Analyzer: guide to running and maintaining the sunset laboratory OCEC analyzer.” Version 5.0. January, 2000.
  24. Marple Style Personal Cascade Impactors 290 Series Operators Manual: 12/03
  25. SKC Inc. Sioutas Cascade Impactor. “Operating Instructions”
  26. Bush, Peter. South Campus Instrumentation Center University of Buffalo. “SEM/EDS: Scanning Electron Microscopy with X-ray microanalysis.” <<http://www.sdm.buffalo.edu/scic/sem-eds.html>>
  27. Stefánsson A, Gunnarsson I, Giroud N. "New methods for the direct determination of dissolved inorganic, organic and total carbon in natural waters by Reagent-Free Ion Chromatography and inductively coupled plasma atomic emission spectrometry." Analytica Chimica Acta 582 (2007): 69-74.
  28. Camner, P. and Anne Johansson. “Reaction of Alveolar Macrophages to Inhaled Metal Aerosols” Environmental Health Perspectives 97 (1992): 185-188.
  29. A.R. Murraya, et al “Oxidative stress and inflammatory response in dermal toxicity of single-walled carbon nanotubes.” Toxicology 257 (2009): 161–171.
  30. Weizhong Qian, Tang Liu, Zhanwen Wang, Hao Yu, Zhifei Li, Fei Wei and Guohua Luo. “Effect of adding nickel to iron–alumina catalysts on the morphology of as-grown carbon nanotubes.” Carbon 41 (2003): 2487-2493.
  31. Destree, Alexandra, Long Gary J., Vatoz Benjamin, Grandjean Fernande, Fonseca Antonio, Nagy Janos B, Fransolet A. M. “Synthesis and characterization of carbon nanotubes grown on montmorillonite clay catalysts.” Journal of Materials Science. 42 (2007): 8671-8689.
  32. Nagpal, N.K., Ministry of Environment, Lands and Parks Province of British Columbia. “Ambient Water Quality Criteria For Polycyclic Aromatic Hydrocarbons (PAHs).” February, 1993. <[\cdc.gov\private\M606\HKZ1\PAHs\Polycyclic Aromatic Hydrocarbons.mht](http://cdc.gov/private/M606/HKZ1/PAHs/Polycyclic Aromatic Hydrocarbons.mht)> Site visited: October, 2008.

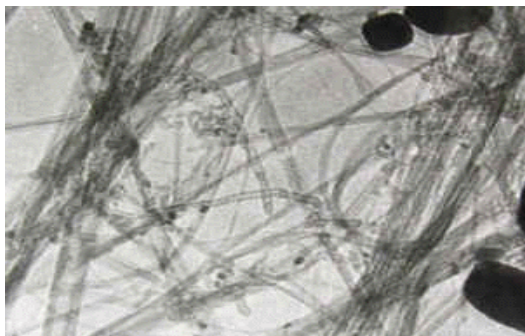
33. Agency for Toxic Substances and Disease Registry. "Polycyclic Aromatic Hydrocarbons." September 1996 <<http://www.atsdr.cdc.gov/tfacts69.pdf>> US Department of Health and Human Services, Agency for Toxic Substances and Disease Registry. "Polycyclic Aromatic Hydrocarbons (PAHs)." September 1996.
34. Bjerseth A. and Becher, G. (Editors) "PAH in Work Atmospheres: Occurrence and Determination." CRC Press, Boca Raton, Florida. (1986)
35. Kwabena A. Narh et al. "The Effect of Carbon Nanotube Agglomeration on the Thermal and Mechanical Properties of Polyethylene Oxide." Polymer Composites 29 (2008): 809-817.
36. Paradise, Melissa and Tarun Goswami. "Carbon nanotubes – Production and industrial applications." Materials and Design 28 (2007) 1477–1489.
37. Subramoney, Shekhar. "Novel Nanocarbons: Structure, Properties, and Potential Applications." Advanced Materials 10 (1998): 1157-1171.
38. Lam, Chiu-wing. "A Review of Carbon Nanotube Toxicity and Assessment of Potential Occupational and Environmental Health Risks." Critical Reviews in Toxicology 36 (2006): 189–217.
39. Bello, Dhimiter. et al. "Exposure to nanoscale particles and fibers during machining of hybrid advanced composites containing carbon nanotubes." J Nanoparticle Research 11 (2009):231–249.
40. Sharma, S. C., and T. S. Sheshadri. "Influence of Solvents on the MWCNT/Adhesive Grade Epoxy Nanocomposites Preparation." Journal of Reinforced Plastics and Composites (2008): 1-8.
41. Arepalli, S. et al. "Protocol for the characterization of single-wall carbon nanotube material quality." Carbon 42 (2004): 1783-1791.
42. Yang, Kun, and Baoshan Xing. "Desorption of polycyclic aromatic hydrocarbons from carbon nanomaterials in water." Critical Reviews in Toxicology. 36 (2006): 189–217.
43. Srogi, K. "Monitoring of environmental exposure to polycyclic aromatic hydrocarbons: a review." Environmental Chemistry Letters 5 (2007)
44. Tsai, Perng-Jy, Shieh, Hong-Yong, Lee, Wen-Jhy, and Lai, Soon-Onn. "Health-risk assessment for workers exposed to polycyclic aromatic hydrocarbons (PAHs) in a carbon black manufacturing industry." Sci Total Environ 278 (2001) 137-150.
45. Omar, Nasr Yousef M.J., Tan Chin Mon; Noorsaadah Rahman, A., and M. Abas Radzi. "Bin Distributions and health risks of polycyclic aromatic hydrocarbons (PAHs) in atmospheric aerosols of Kuala Lumpur." Malaysia 369 (2006): 76-81.
46. Kuo, C. Y., Hsu, Y. W., and Lee, H. S. "Study of Human Exposure to Particulate PAHs Using Personal Air Samplers" Archives of Environmental Contamination and Toxicology 44 (2003): 454-459.

Appendix A  
SWCNT and MWCNT Information from  
Cheap Tubes Inc.

# Single Walled Nanotubes-SWNTs

## Manufacturing Method: CCVD

### Single Walled Nanotubes-SWNTs 60wt% Specifications



*A TEM image of our Single Walled Nanotubes-SWNTs 60wt% 1-2nm OD*

**Outer Diameter: 1-2nm**

**Inside Diameter: 0.8-1.6nm**

**Ash: <3.0 wt%**

**Purity: >60 wt%**

**Additional MWNT content: >30wt%**

**Amorphous Carbon Content: <5wt%**

**Length: 5-30um**

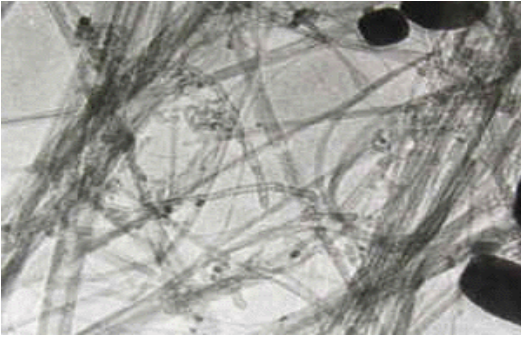
**Specific Surface Area: 407 m<sup>2</sup>/g**

**Electrical Conductivity: >100 S/cm**

**Bulk density: 0.14 g/cm<sup>3</sup>**

**True density: ~2.1 g/cm<sup>3</sup>**

## Short Single Walled Nanotubes-SWNTs 60wt% Specifications



*A TEM image of our Short Single Walled Nanotubes-SWNTs 60wt% 1-2nm OD*

**Outer Diameter: 1-2nm**

**Inside Diameter: 0.8-1.6nm**

**Ash: <3.0 wt%**

**Purity: >60 wt%**

**Additional MWNT content: >30wt%**

**Amorphous Carbon Content: <5wt%**

**Length: 5-30um**

**Specific Surface Area: 407 m<sup>2</sup>/g**

**Electrical Conductivity: >100 S/cm**

**Bulk density: 0.14 g/cm<sup>3</sup>**

**True density: ~2.1 g/cm<sup>3</sup>**

## Single Walled Nanotubes -SWNTs Elemental Analysis

Single-Walled Carbon Nanotubes-SWNTs, 90wt%	
Average outside diameter: 1.1 nm	
Length: 5-30 $\mu\text{m}$	
Components	Contents (%)
C	96.30
Al	0.08
Cl	0.41
Co	2.91
S	0.29
Analysis Method: Energy Dispersive X-ray Spectroscopy	

### Multi Walled Nanotubes-MWNTs 20-30nm Specifications



*A TEM image of our Multi Walled Nanotubes-MWNTs 95wt% 20-30nm OD*

**MWNTs Outer Diameter: 20-30nm**

**MWNTs Inside Diameter: 5-10nm**

**MWNTs Ash: <1.5 wt%**

**MWNTs Purity: >95 wt%**

**MWNTs Length: 10-30um**

**MWNTs Specific Surface Area: 110 m<sup>2</sup>/g**

**MWNTs Electrical Conductivity: >100 S/cm**

**MWNTs Bulk density: 0.28 g/cm<sup>3</sup>**

**MWNTs True density: ~2.1 g/cm<sup>3</sup>**

**Multi-Walled Nanotubes-MWNT, 95wt%**

**Outside diameter: 20-30nm**

**Inside diameter: 5-10 nm**

**Length: 10-30 mm**

Components	Contents (%)
C	98.35
Cl	0.45
Fe	0.26
Ni	0.94

Analysis Method: Energy Dispersive X-ray Spectroscopy

**Read more:**

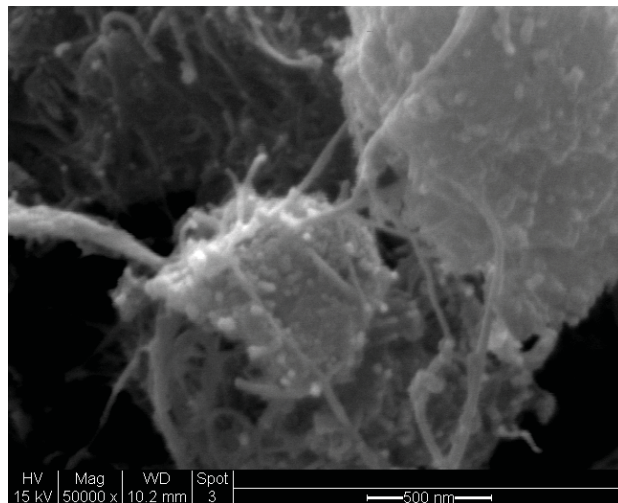
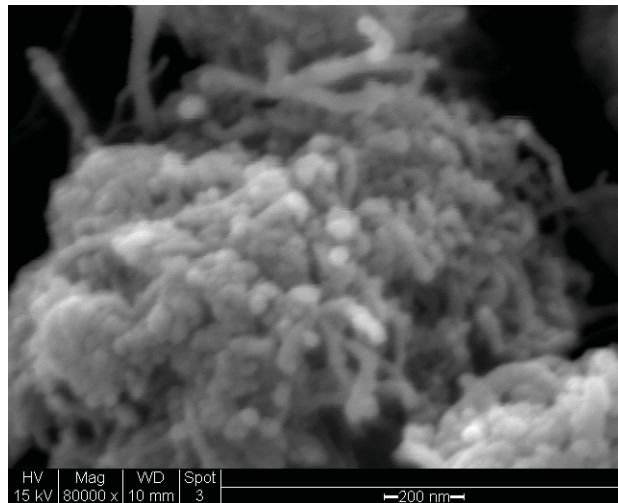
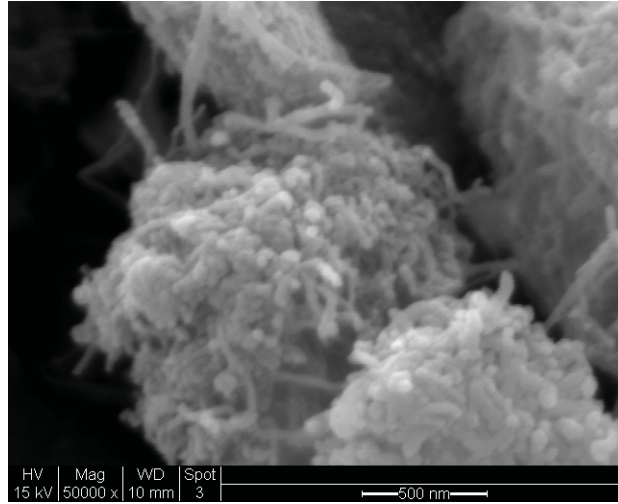
<http://www.cheaptubes.com/swnts>

<http://www.cheaptubes.com/mwnts>

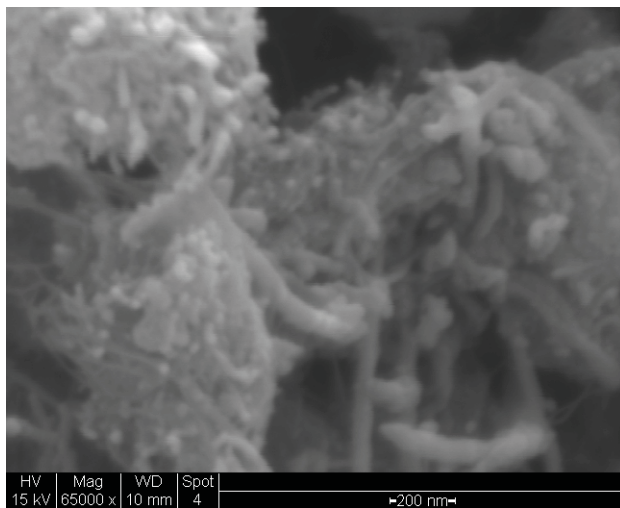
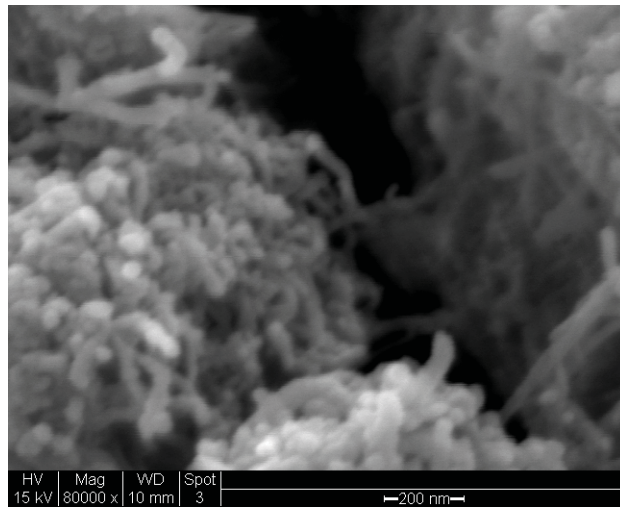
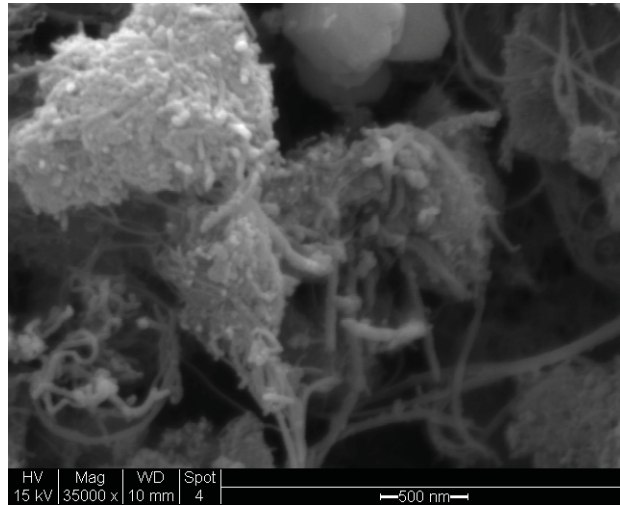
## Appendix B

SEM/EDS Results for Samples #21, #22,  
#28, #38, and the Final Product

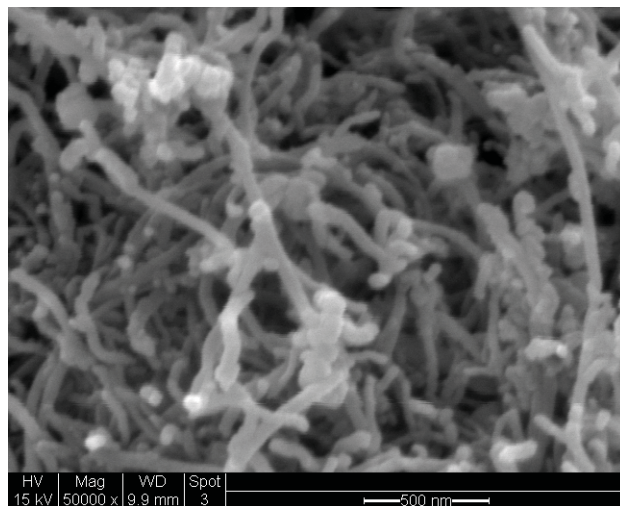
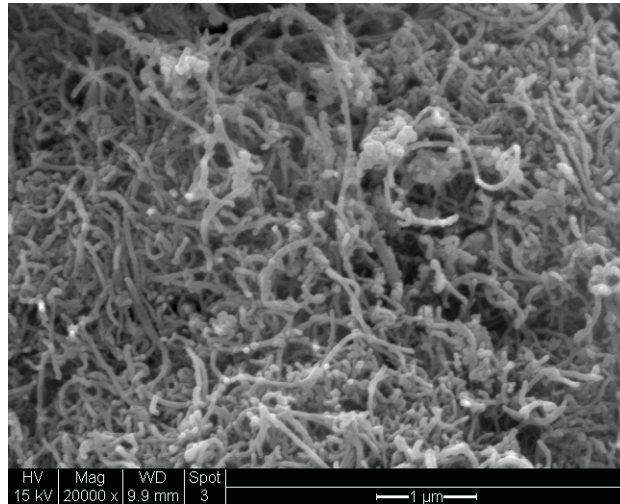
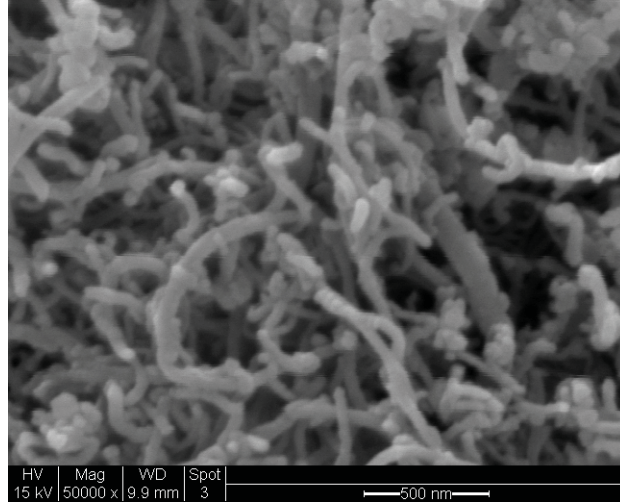
**Sample #28 Collected on Stage A**



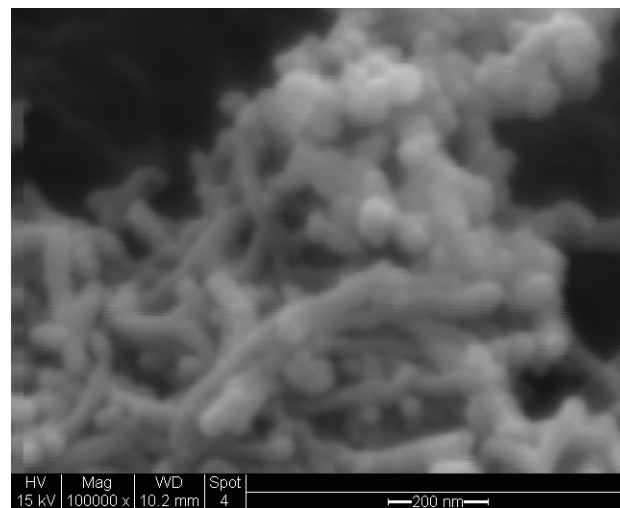
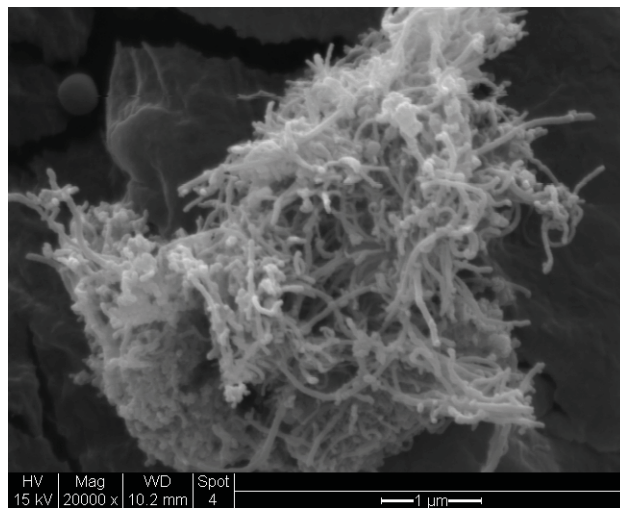
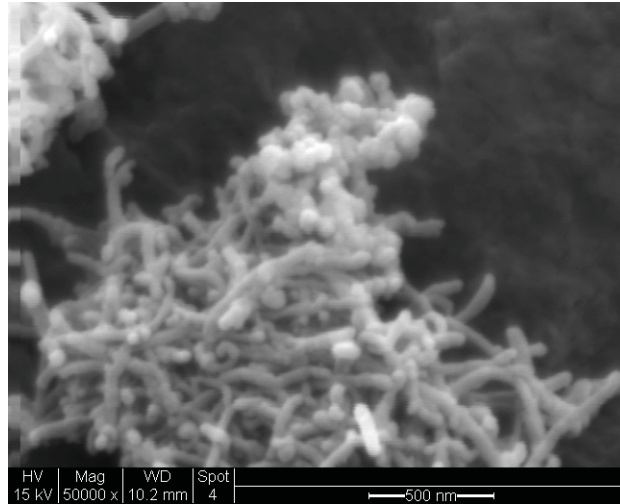
### Sample #28 Collected on Stage D



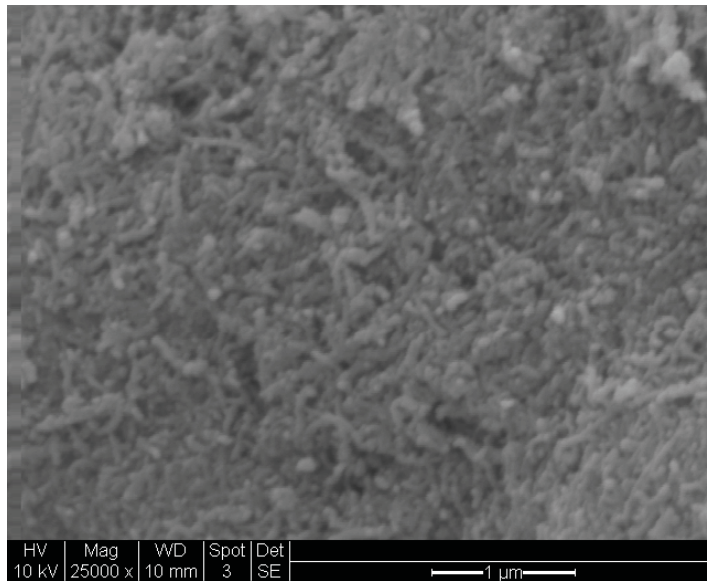
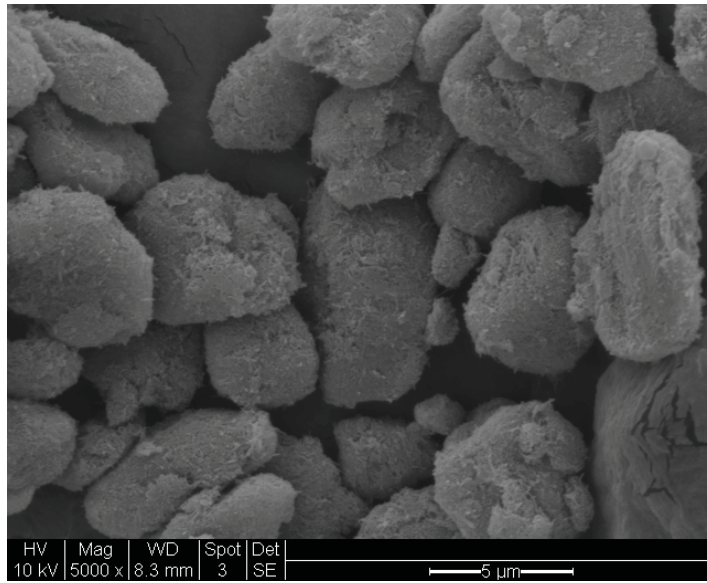
### Sample #38 Collected on Stage A



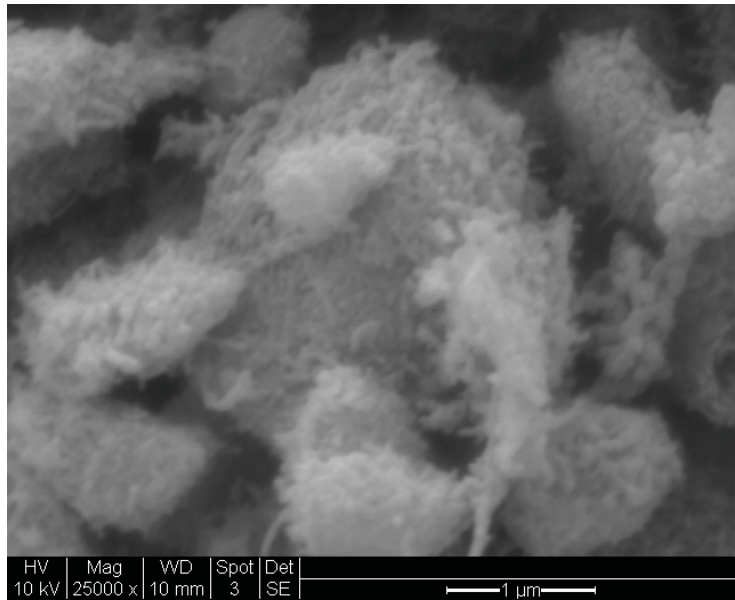
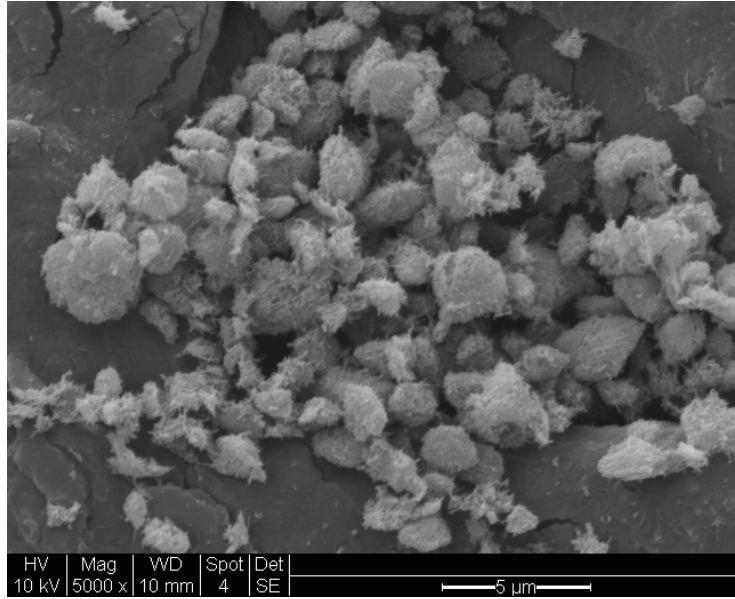
### Sample #38 Collected on Stage D



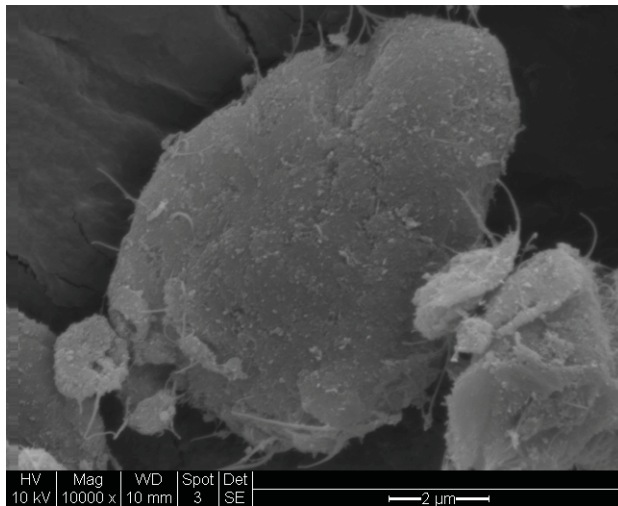
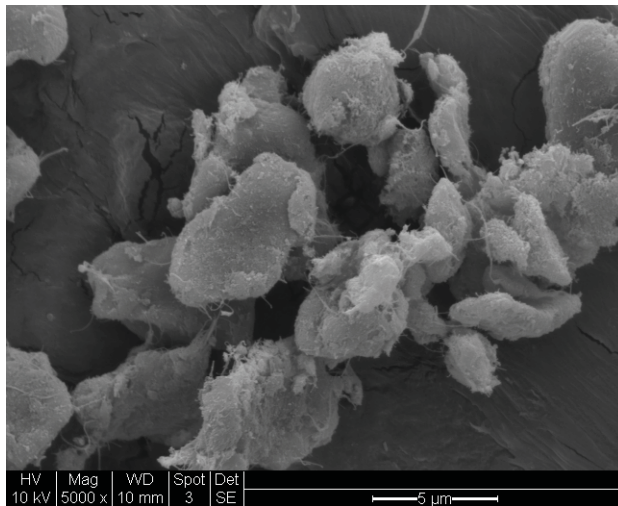
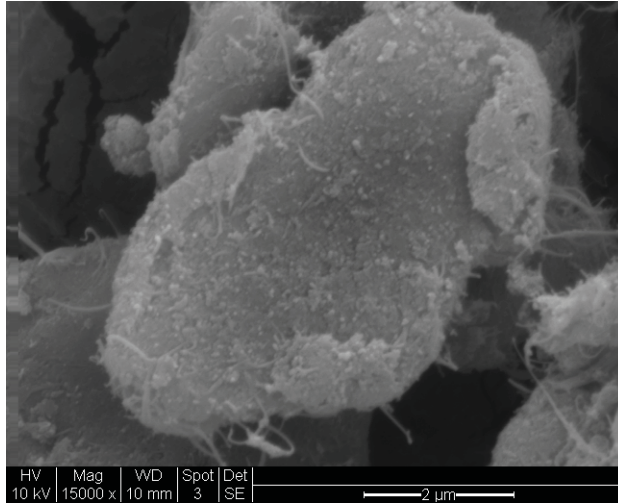
**Sample #21 Collected on Stage A (>2.5 $\mu$ m)**



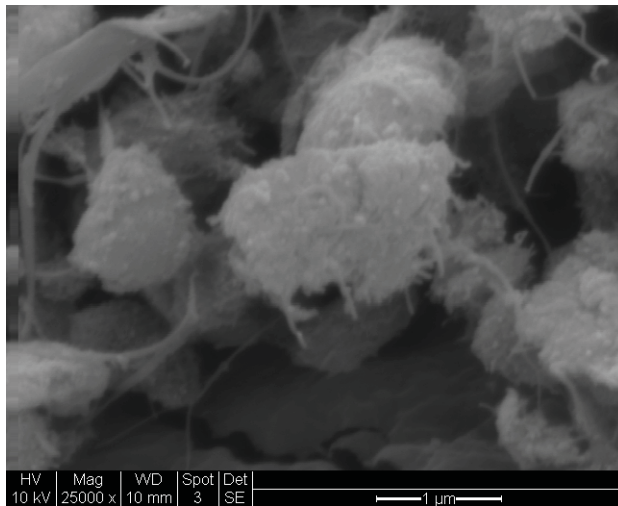
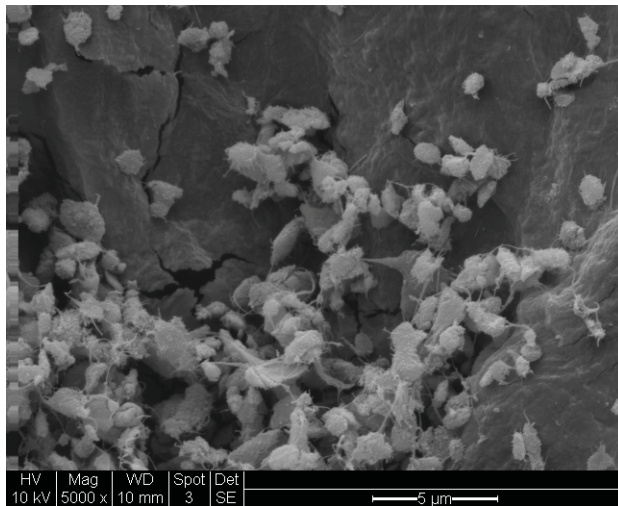
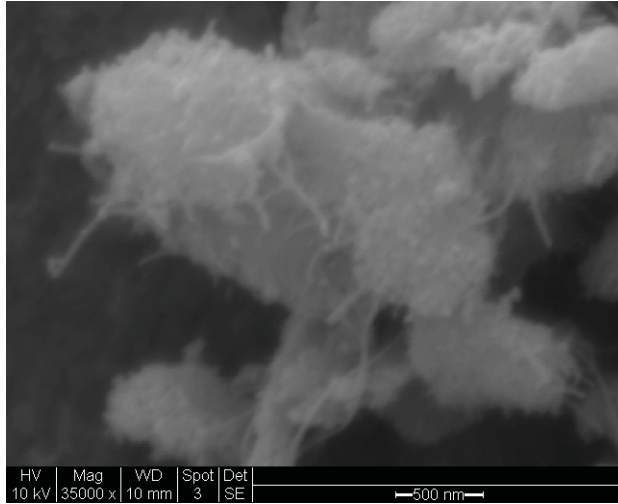
**Sample #21 Collected on Stage D (0.25-0.5 $\mu$ m)**



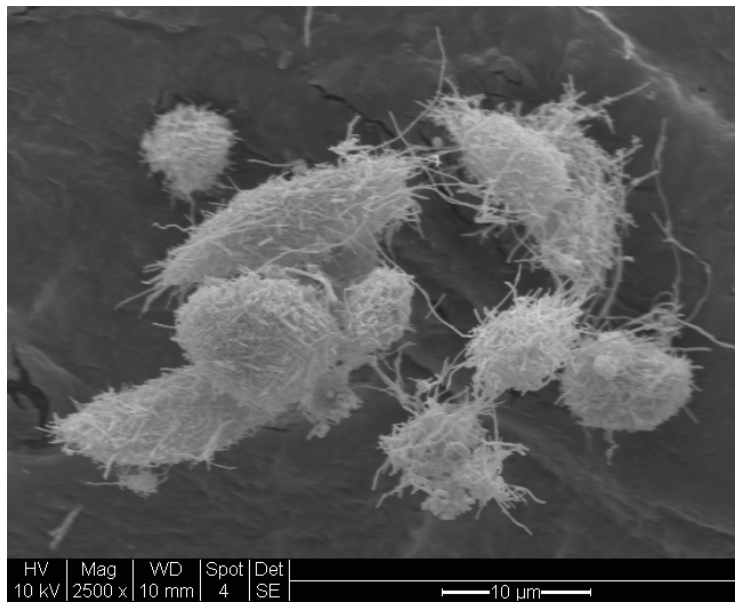
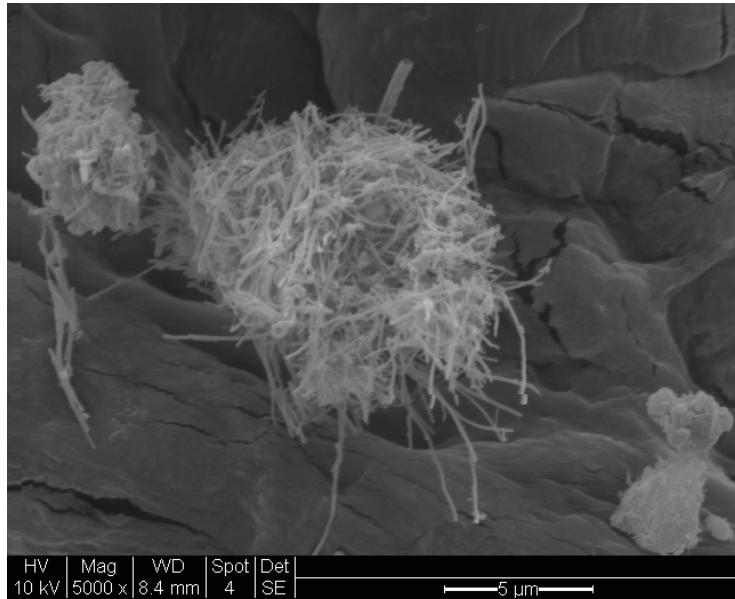
**Sample #22 Collected on Stage A**



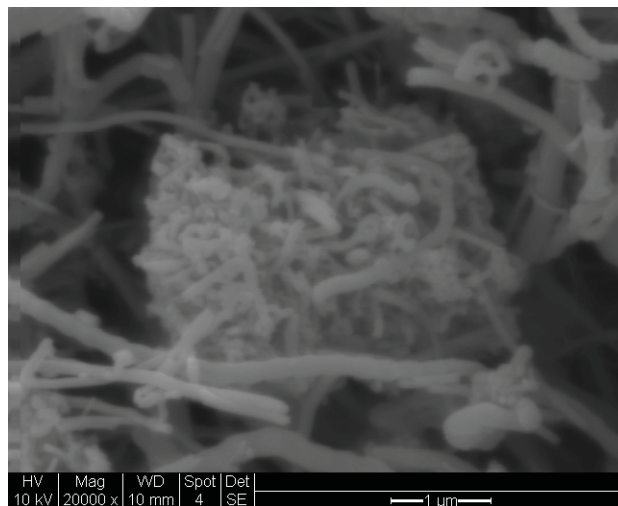
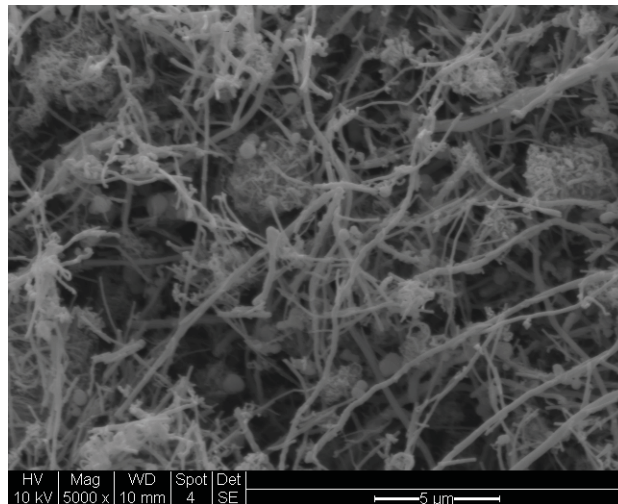
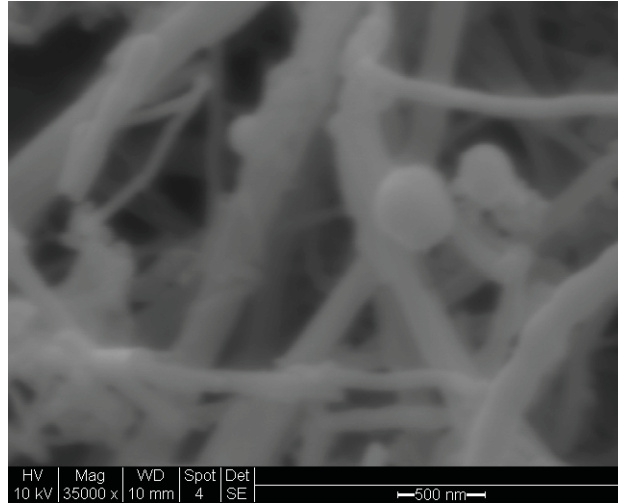
**Sample #22 Collected on Stage D**



## Final Product Collected on Stage A



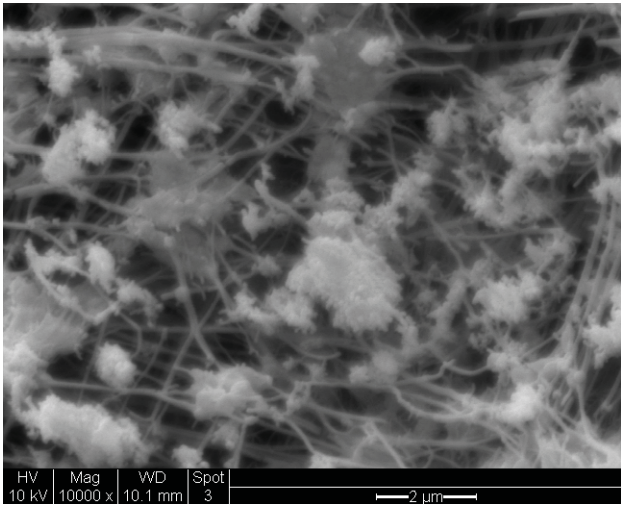
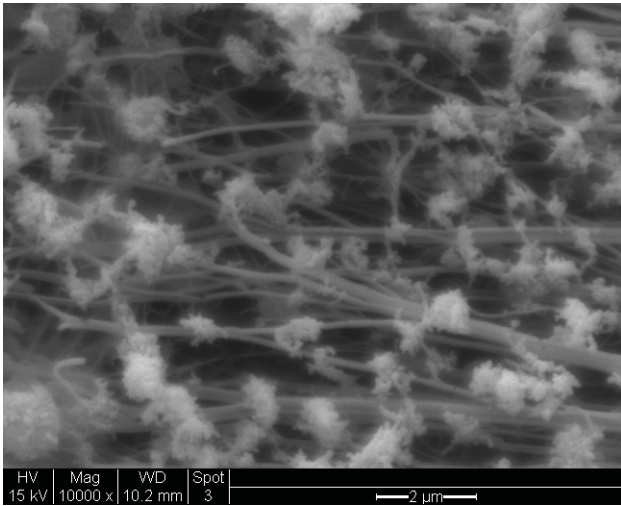
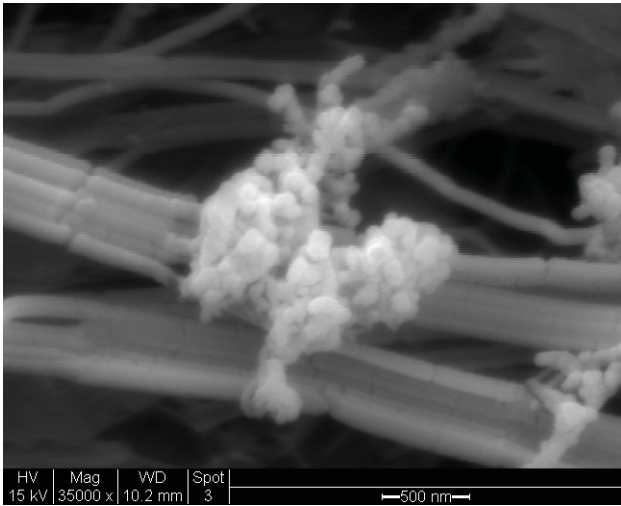
## Final Product Collected on Stage D



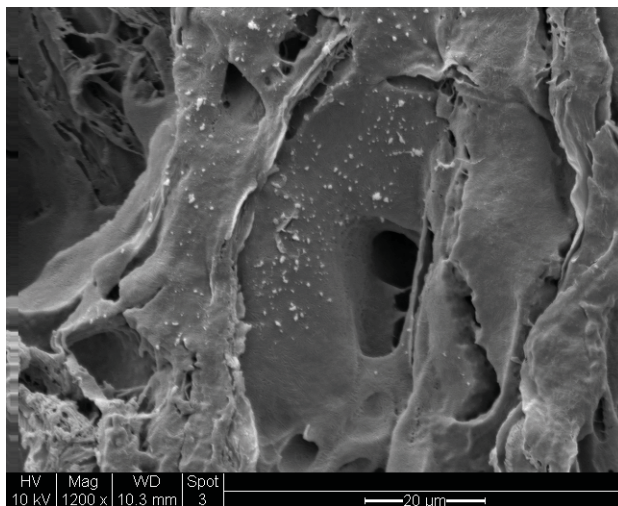
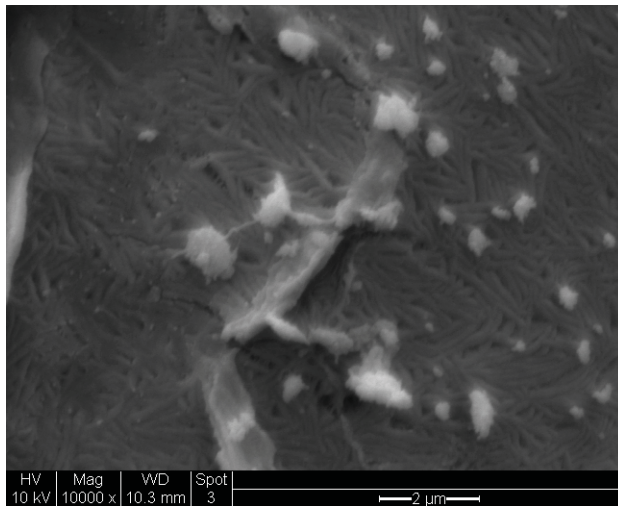
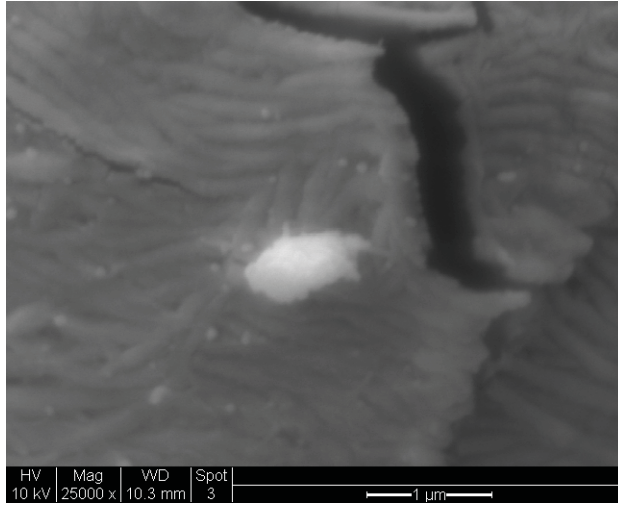
**Sample #28 Collected on the Final Filter (<0.25um)**



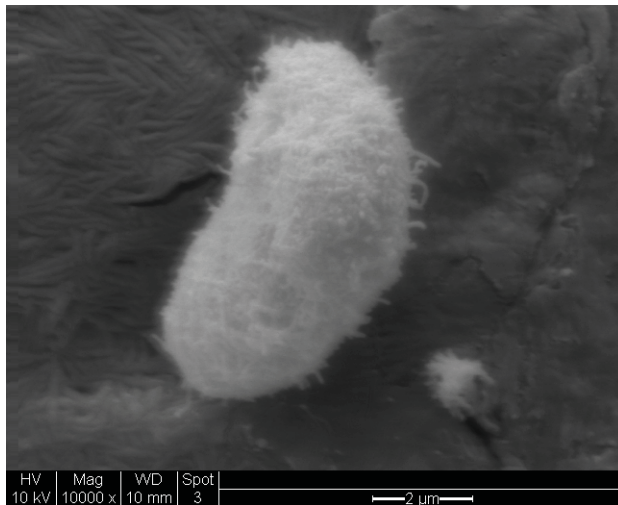
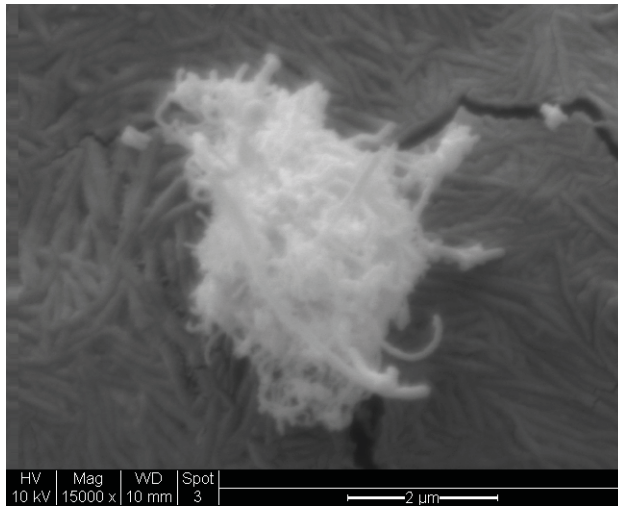
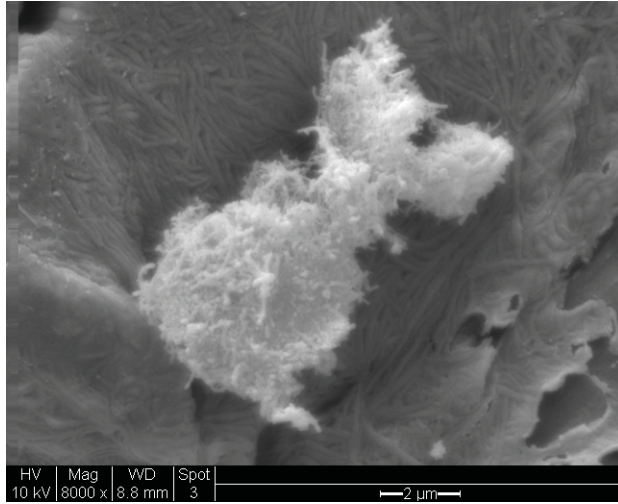
**Sample #21 Collected on the Final Filter (<0.25μm)**



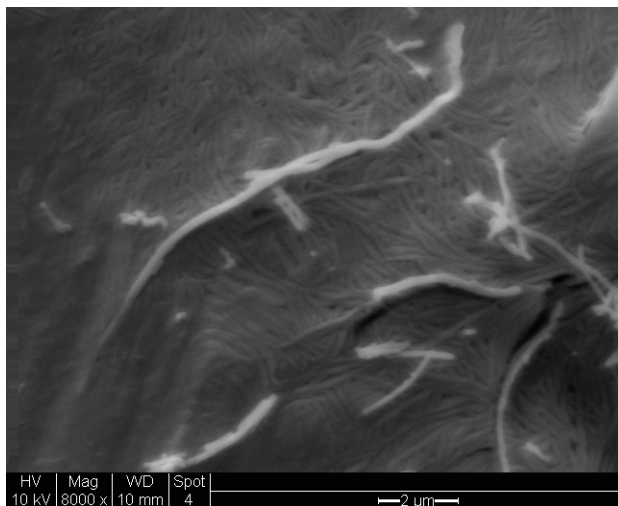
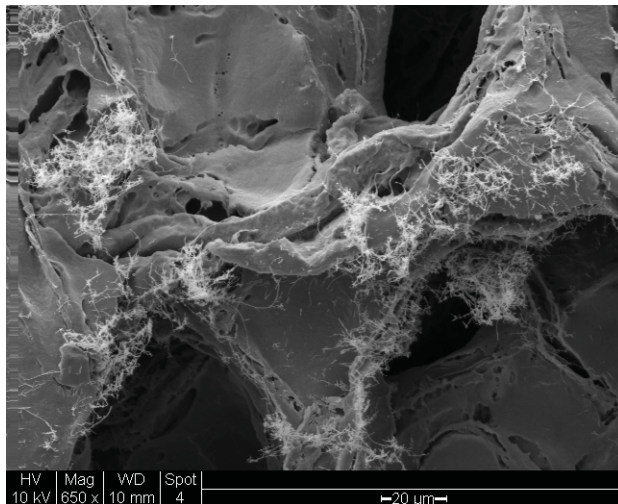
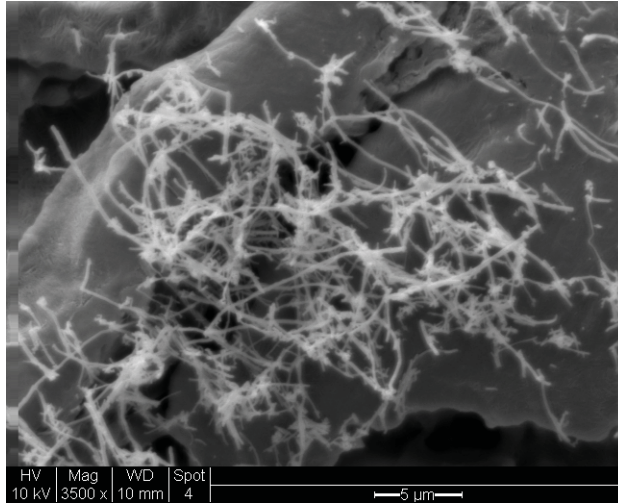
**Sample #22 Collected on the Final Filter**



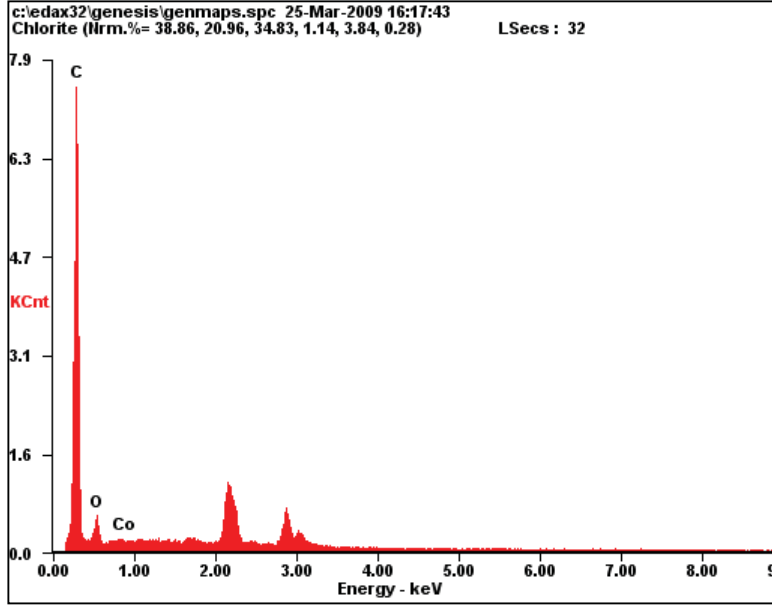
**Sample #38 Collected on the Final Filter**



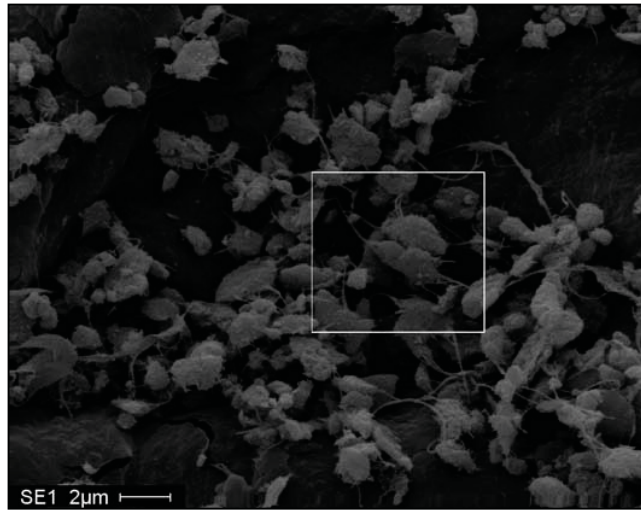
## Final Product Collected on the Final Filter



**SAMPLE #22 (SWCNT) STAGE A**

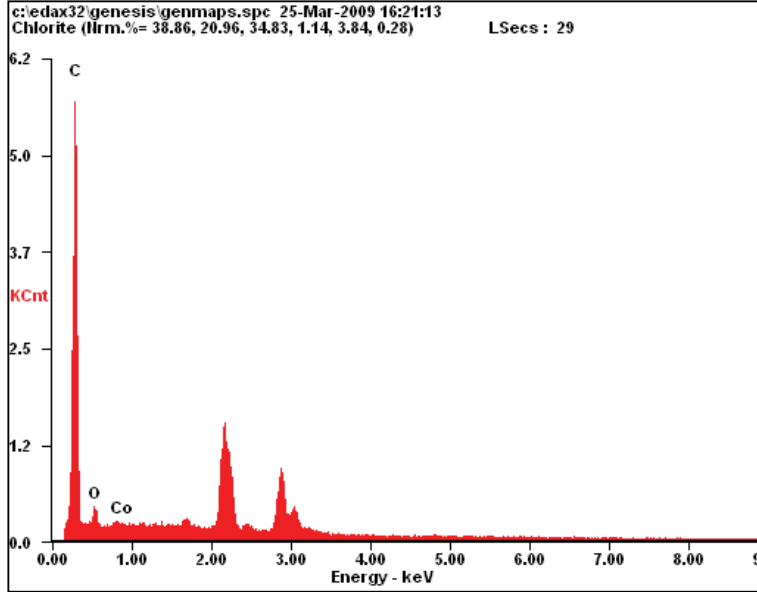


<i>Element</i>	<i>Wt%</i>	<i>At%</i>
<b>CK</b>	87.54	91.76
<b>OK</b>	09.74	07.66
<b>CoL</b>	02.72	00.58
<b>Matrix</b>	Correction	ZAF

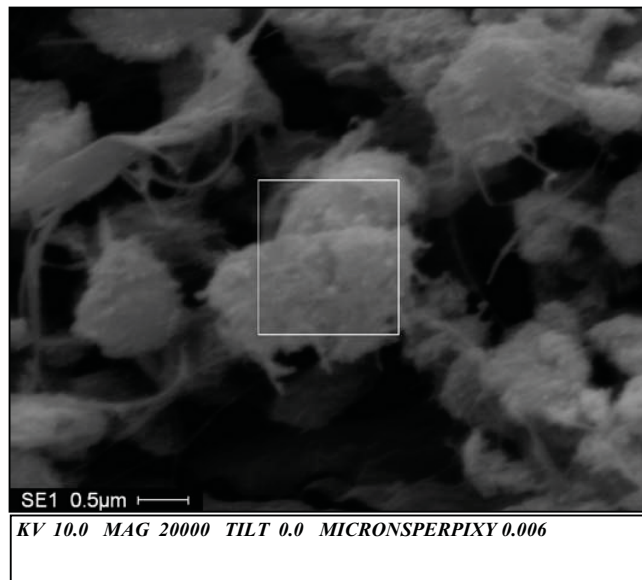


KV 10.0 MAG 5000 TILT 0.0 MICRONSPERPIXY 0.025

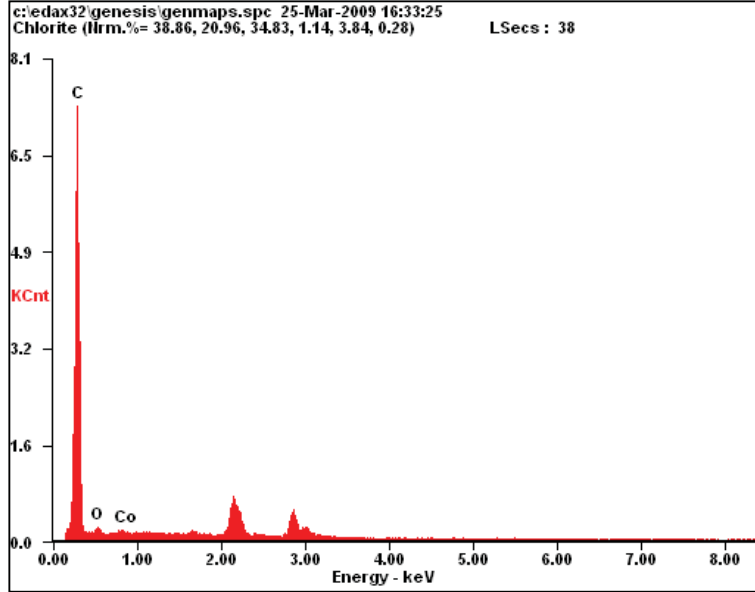
**SAMPLE #22 (SWCNT) STAGE D**



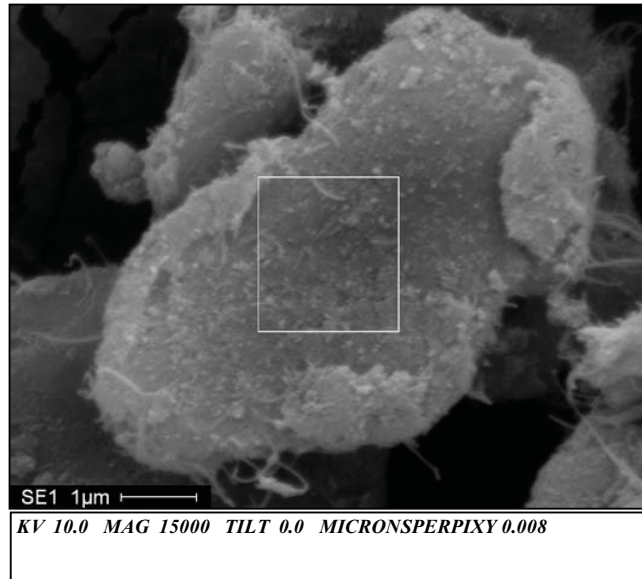
<i>Element</i>	<i>Wt%</i>	<i>At%</i>
<b>CK</b>	86.87	91.94
<b>OK</b>	09.03	07.17
<b>CoL</b>	04.10	00.88
<b>Matrix</b>	Correction	ZAF



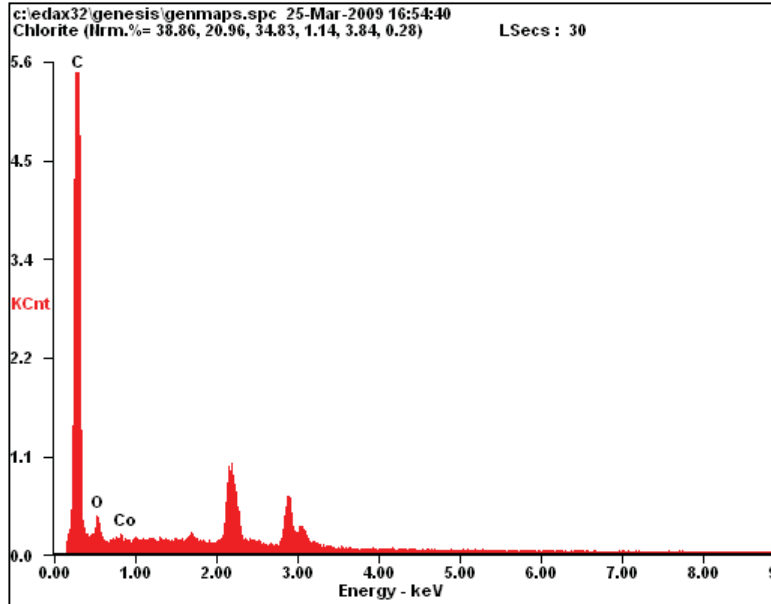
**SAMPLE #22 (SWCNT) STAGE A**  
 Area 2



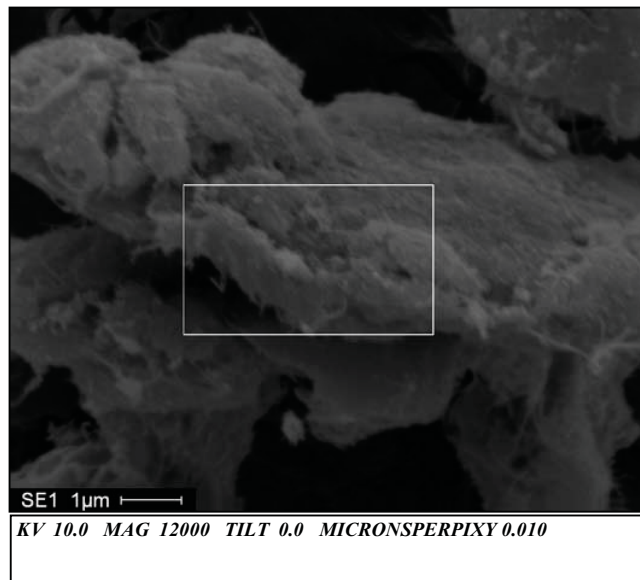
<i>Element</i>	<i>Wt%</i>	<i>At%</i>
<b>CK</b>	93.68	96.52
<b>OK</b>	03.83	02.96
<b>CoL</b>	02.49	00.52
<b>Matrix</b>	Correction	ZAF



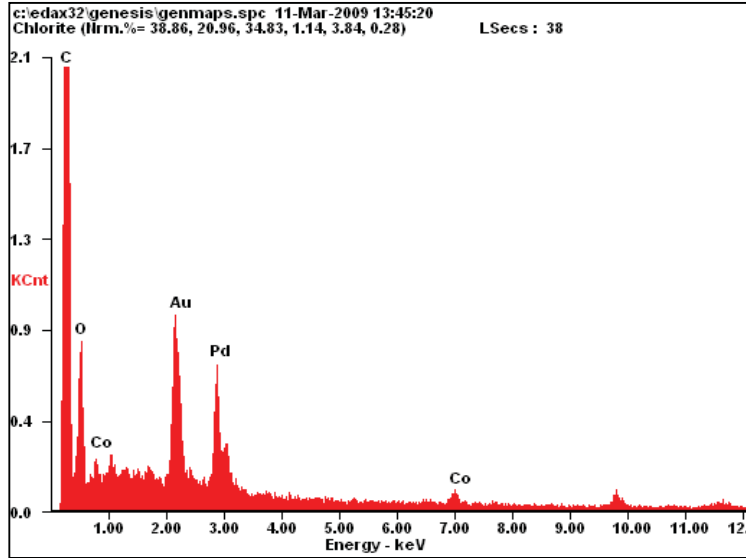
**SAMPLE #22 (SWCNT) STAGE A**  
 Area 3



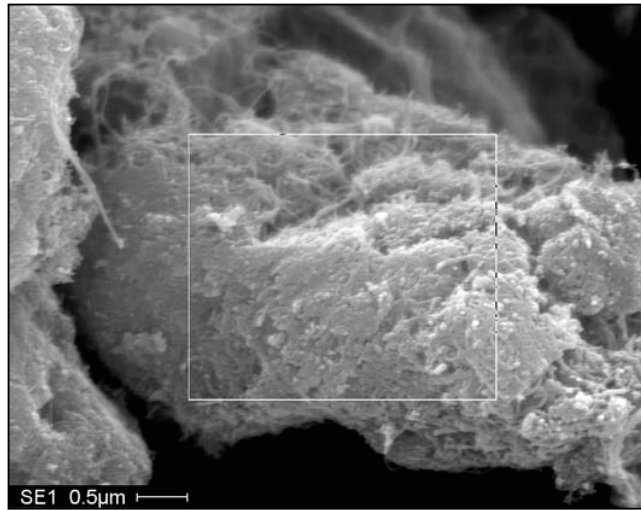
<i>Element</i>	<i>Wt%</i>	<i>At%</i>
<b>CK</b>	91.95	94.98
<b>OK</b>	05.89	04.57
<b>CoL</b>	02.16	00.45
<b>Matrix</b>	Correction	ZAF



**SAMPLE #28 (SWCNT) STAGE A**

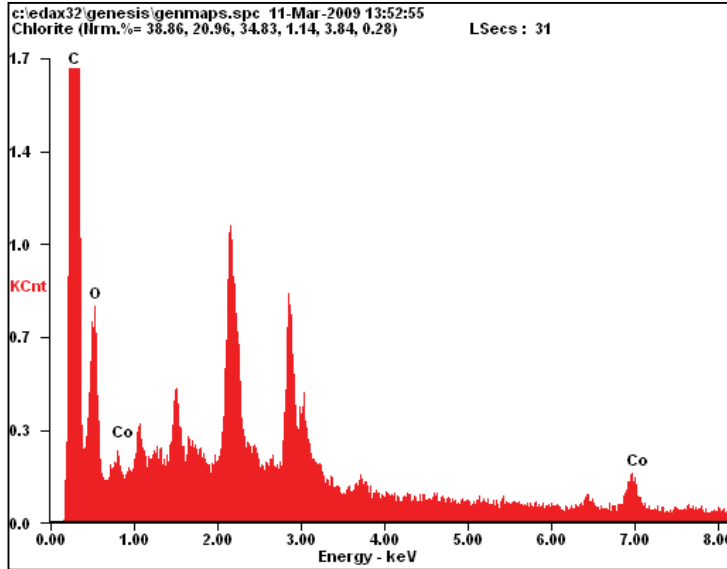


<i>Element</i>	<i>Wt%</i>	<i>At%</i>
<b>CK</b>	88.14	91.33
<b>OK</b>	10.88	08.47
<b>CoK</b>	00.98	00.21
<b>Matrix</b>	Correction	ZAF

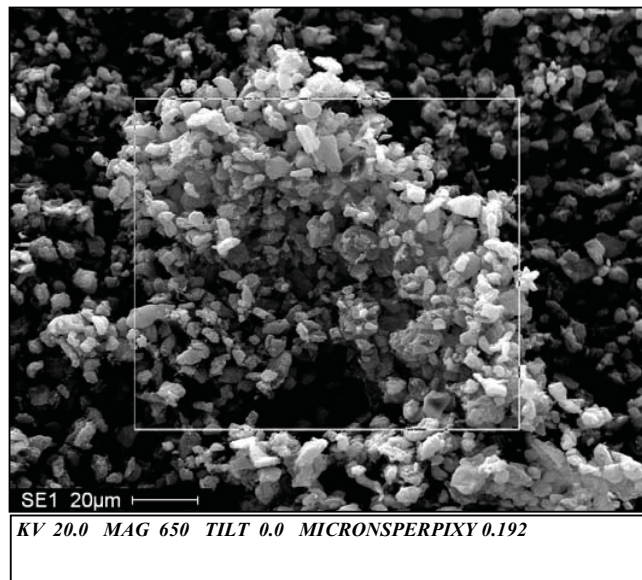


KV 20.0 MAG 20000 TILT 0.0 MICRONS PER PIX 0.006

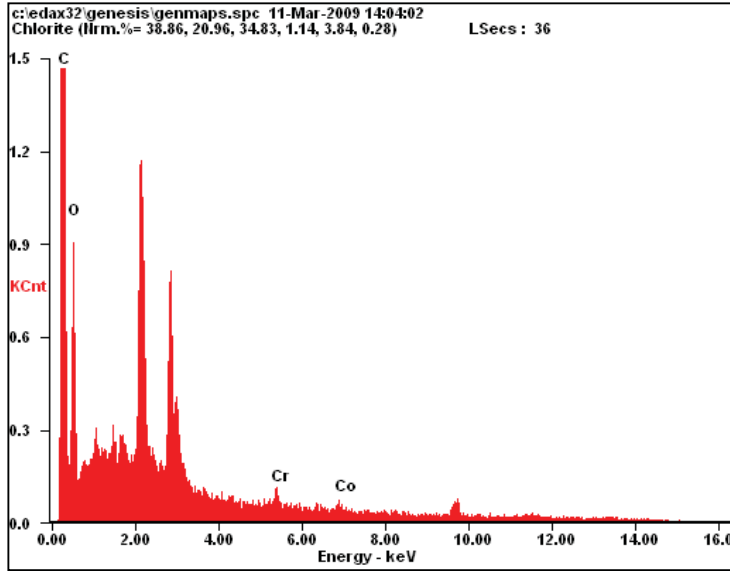
**SAMPLE #28 (SWCNT) STAGE A**  
 Area 2



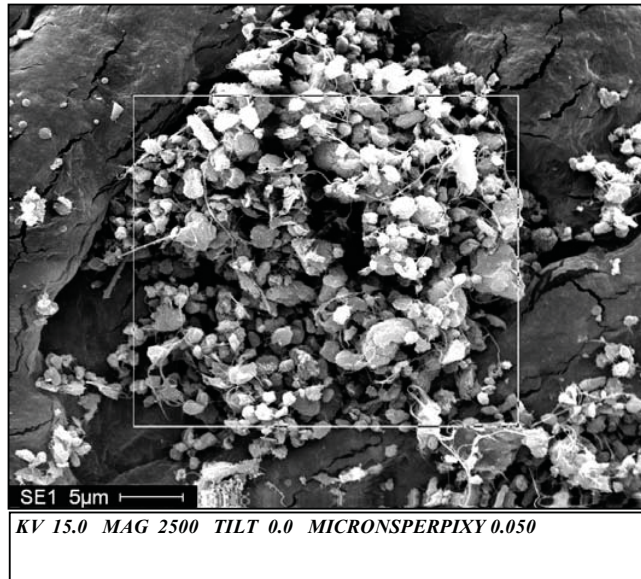
<i>Element</i>	<i>Wt%</i>	<i>At%</i>
<b>CK</b>	89.50	92.73
<b>OK</b>	08.92	06.94
<b>CoK</b>	01.59	00.33
<b>Matrix</b>	Correction	ZAF



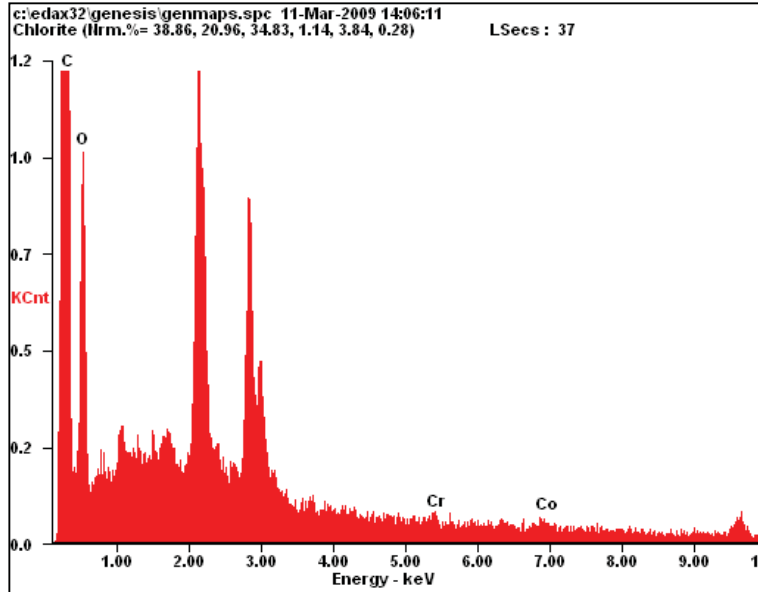
**SAMPLE #28 (SWCNT) STAGE D**



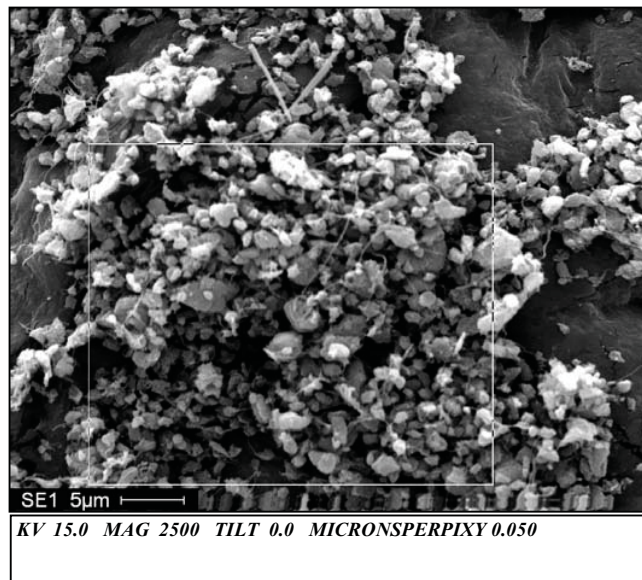
<i>Element</i>	<i>Wt%</i>	<i>At%</i>
<b>CK</b>	84.53	89.16
<b>OK</b>	12.98	10.28
<b>CrK</b>	00.92	00.22
<b>CoK</b>	01.57	00.34
<b>Matrix</b>	Correction	ZAF



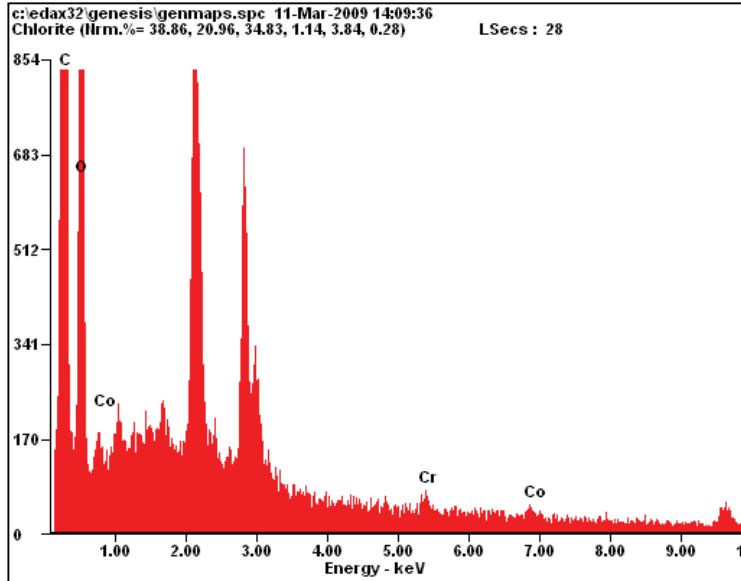
**SAMPLE #28 (SWCNT) STAGE D**  
 Area 2



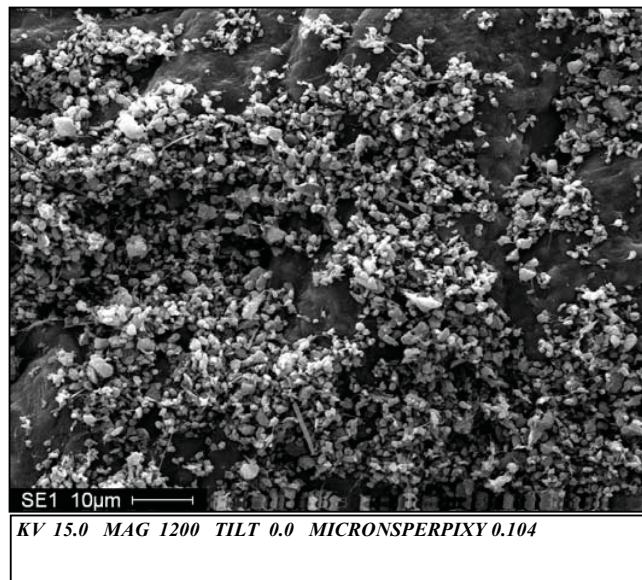
<i>Element</i>	<i>Wt%</i>	<i>At%</i>
<b>CK</b>	84.60	88.31
<b>OK</b>	14.73	11.55
<b>CrK</b>	00.00	00.00
<b>CoK</b>	00.66	00.14
<b>Matrix</b>	Correction	ZAF



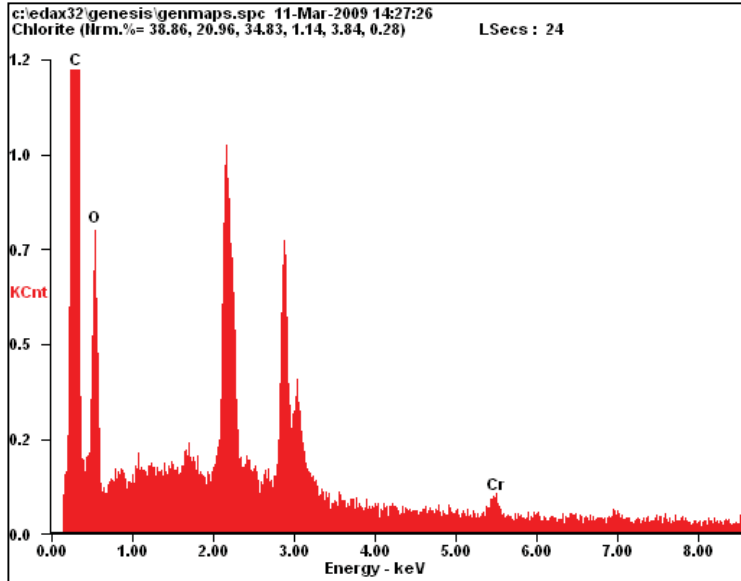
**SAMPLE #28 (SWCNT) STAGE D**  
 Area 3



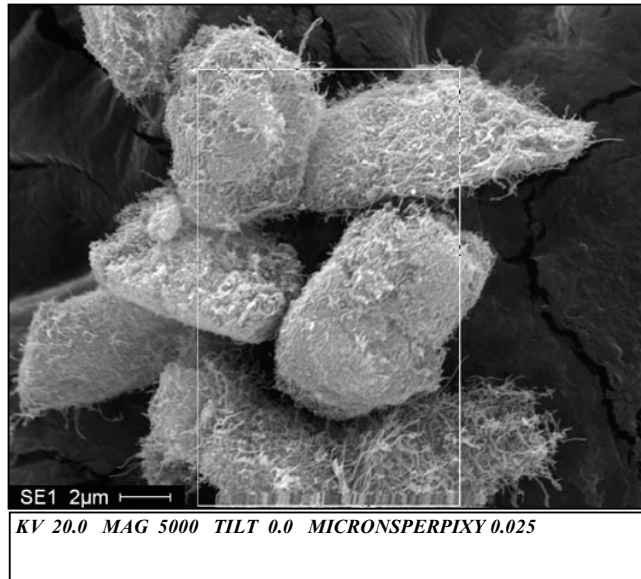
<i>Element</i>	<i>Wt%</i>	<i>At%</i>
<b>CK</b>	71.72	78.22
<b>OK</b>	25.95	21.24
<b>CrK</b>	00.85	00.21
<b>CoK</b>	01.48	00.33
<b>Matrix</b>	Correction	ZAF



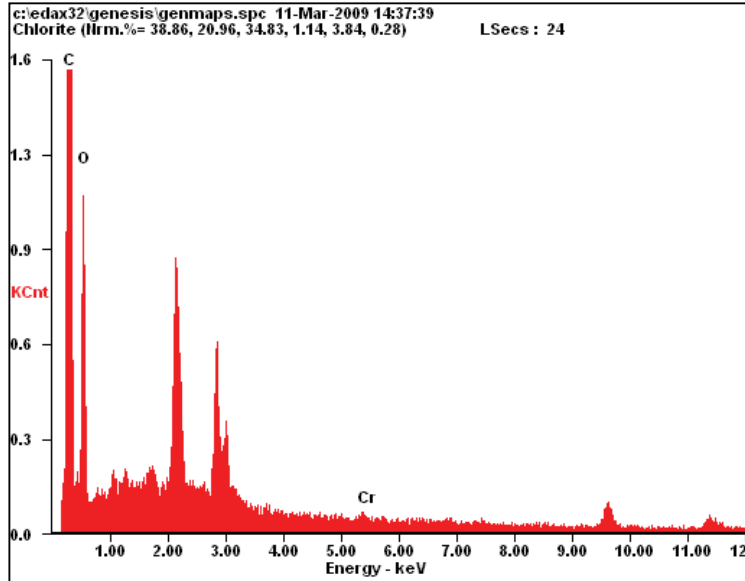
**SAMPLE #38 (MWCNT) STAGE A**



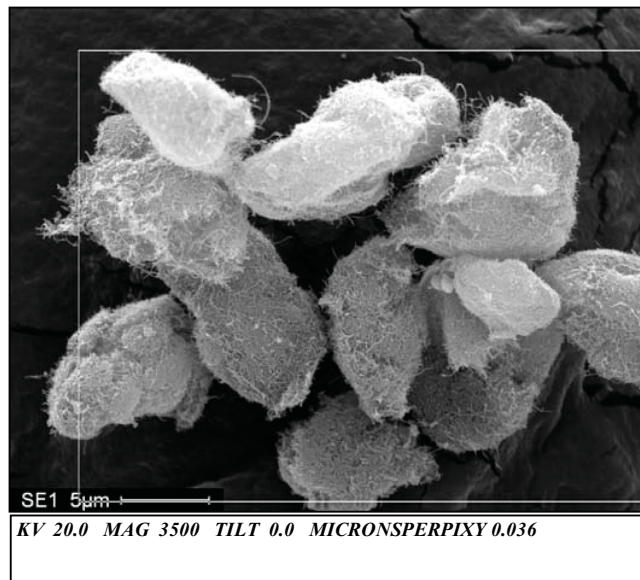
<i>Element</i>	<i>Wt%</i>	<i>At%</i>
<b>CK</b>	82.75	86.85
<b>OK</b>	16.45	12.96
<b>CrK</b>	00.79	00.19
<b>Matrix</b>	Correction	ZAF



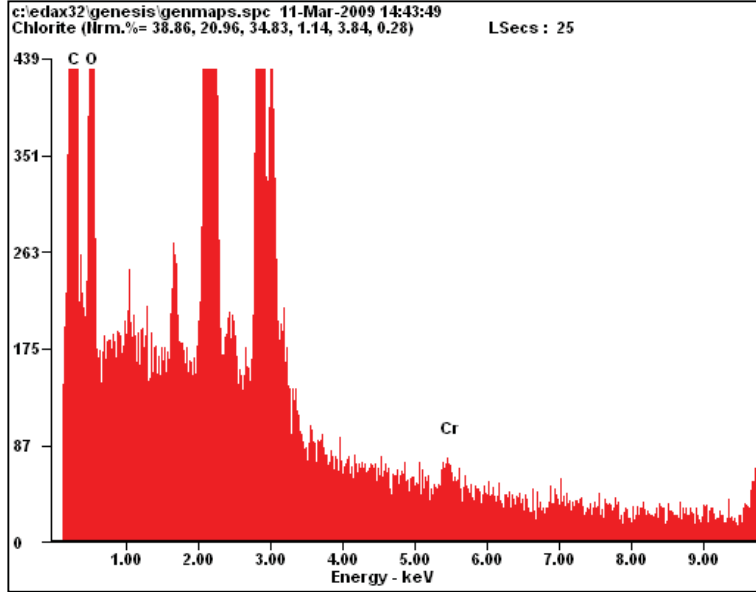
**SAMPLE #38 (MWCNT) STAGE A**  
 Area 2



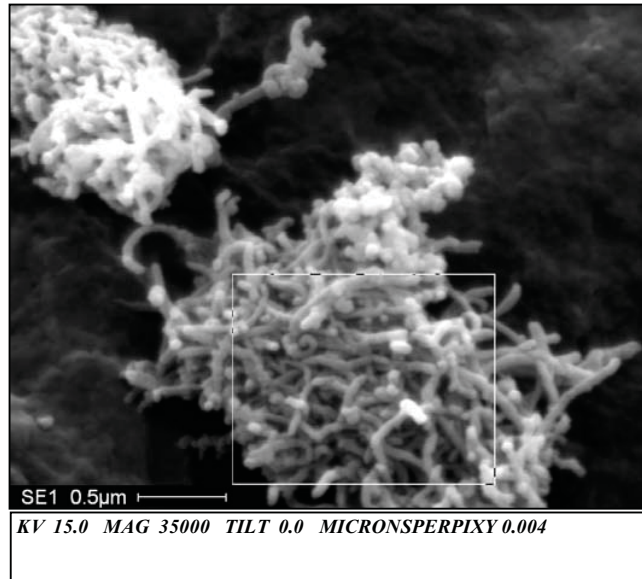
<i>Element</i>	<i>Wt%</i>	<i>At%</i>
<b>CK</b>	77.24	82.08
<b>OK</b>	22.33	17.81
<b>CrK</b>	00.44	00.11
<b>Matrix</b>	Correction	ZAF



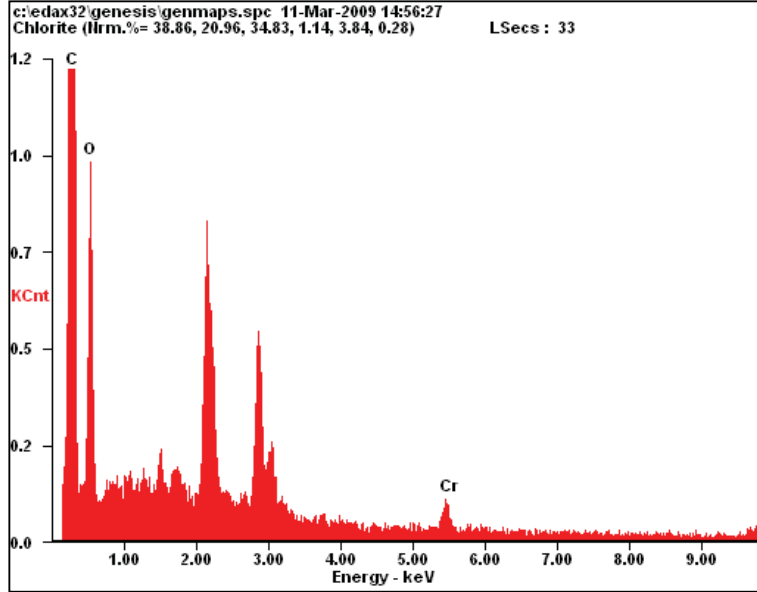
**SAMPLE #38 (MWCNT) STAGE D**



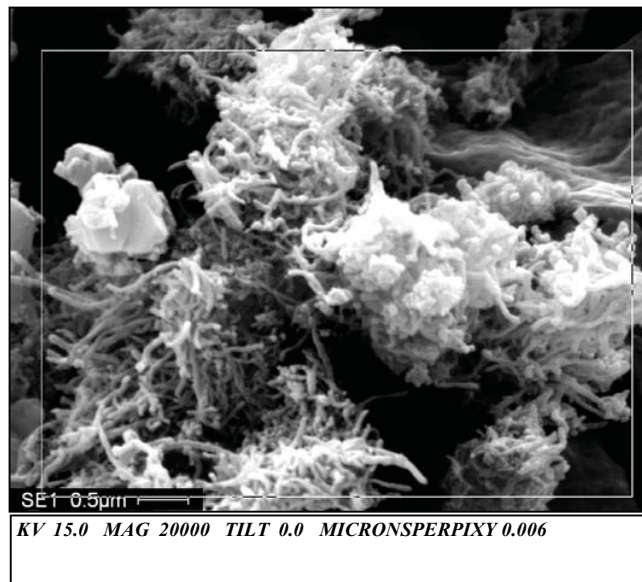
<i>Element</i>	<i>Wt%</i>	<i>At%</i>
<b>CK</b>	76.98	82.44
<b>OK</b>	21.32	17.14
<b>CrK</b>	01.69	00.42
<b>Matrix</b>	Correction	ZAF



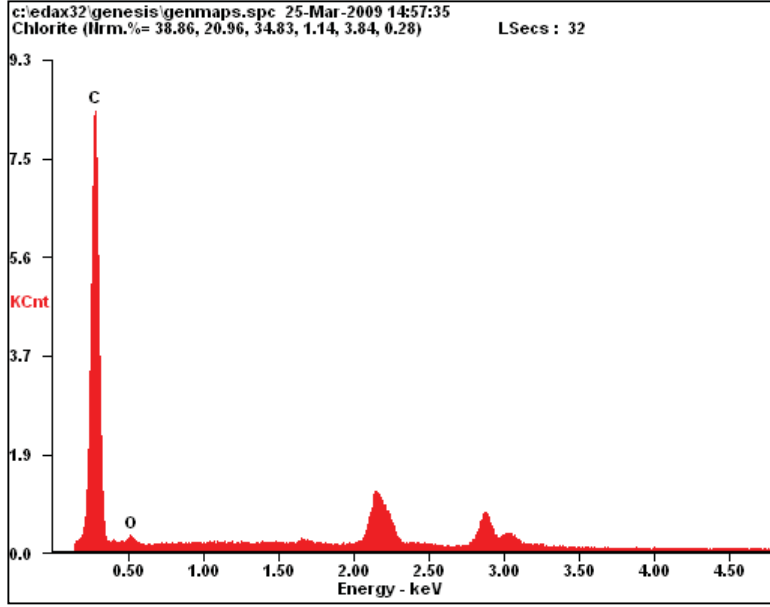
**SAMPLE #38 (MWCNT) STAGE D**  
 Area 2



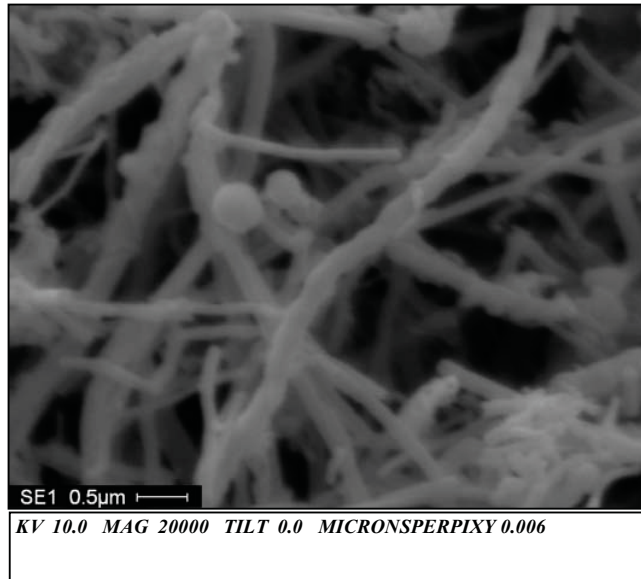
<i>Element</i>	<i>Wt%</i>	<i>At%</i>
<i>CK</i>	79.28	84.79
<i>OK</i>	18.15	14.57
<i>CrK</i>	02.57	00.64
<i>Matrix</i>	Correction	ZAF



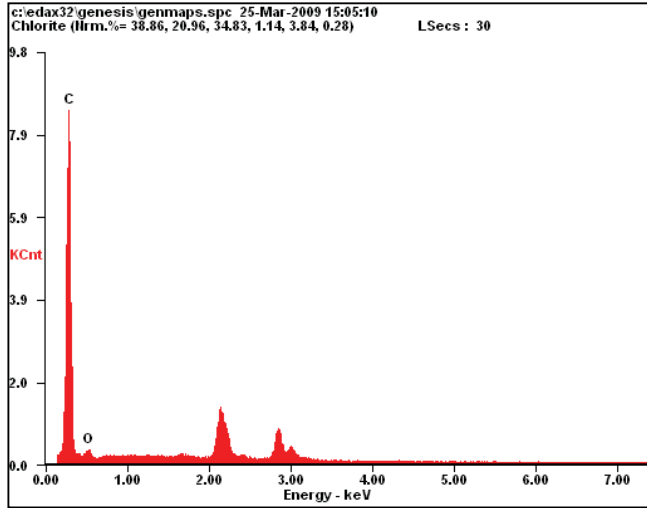
**FINAL PRODUCT STAGE D**



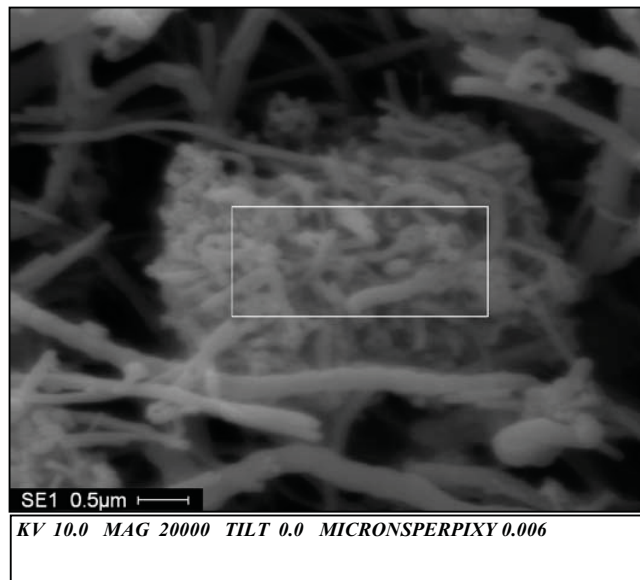
<i>Element</i>	<i>Wt%</i>	<i>At%</i>
<b>CK</b>	95.70	96.74
<b>OK</b>	04.30	03.26
<b>Matrix</b>	Correction	ZAF



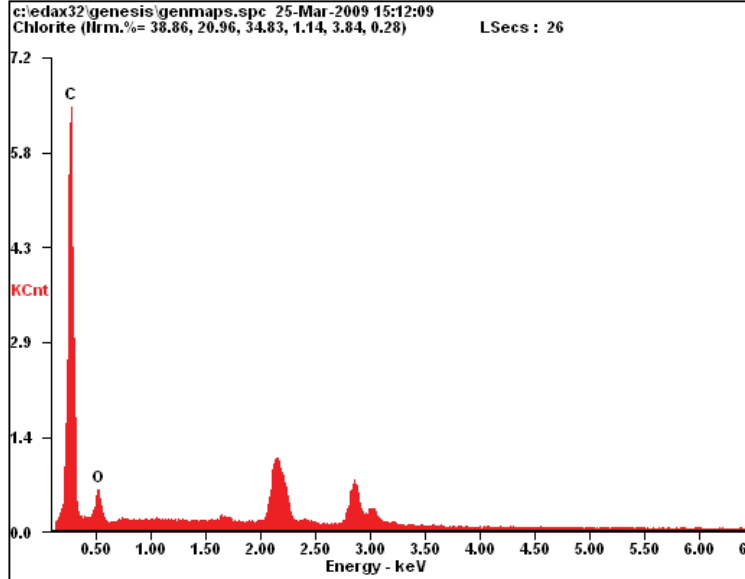
**FINAL PRODUCT STAGE D**  
**AREA 2**



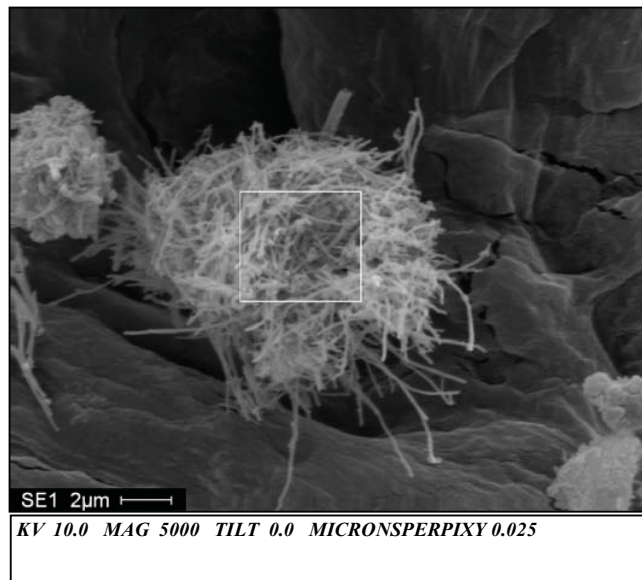
<i>Element</i>	<i>Wt%</i>	<i>At%</i>
<b>CK</b>	94.51	95.82
<b>OK</b>	05.49	04.18
<b>Matrix</b>	Correction	ZAF



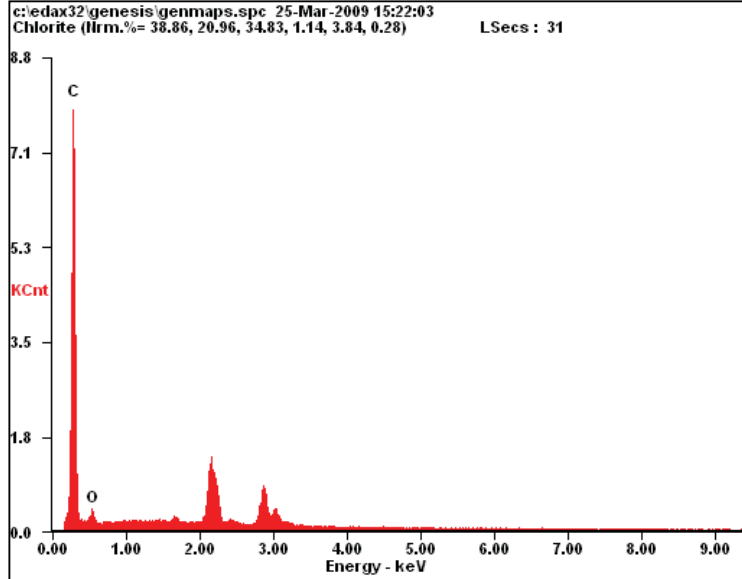
**FINAL PRODUCT STAGE A**



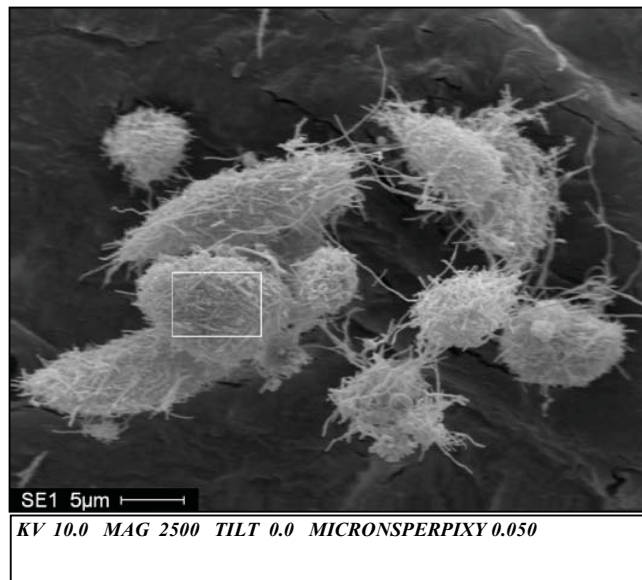
<i>Element</i>	<i>Wt%</i>	<i>At%</i>
<b>CK</b>	86.99	89.90
<b>OK</b>	13.01	10.10
<b>Matrix</b>	Correction	ZAF



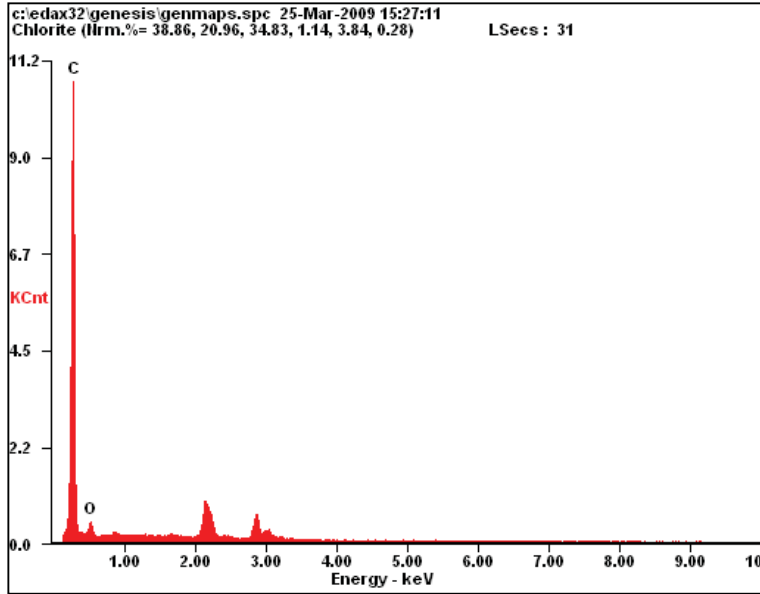
**FINAL PRODUCT STAGE A**  
**AREA 2**



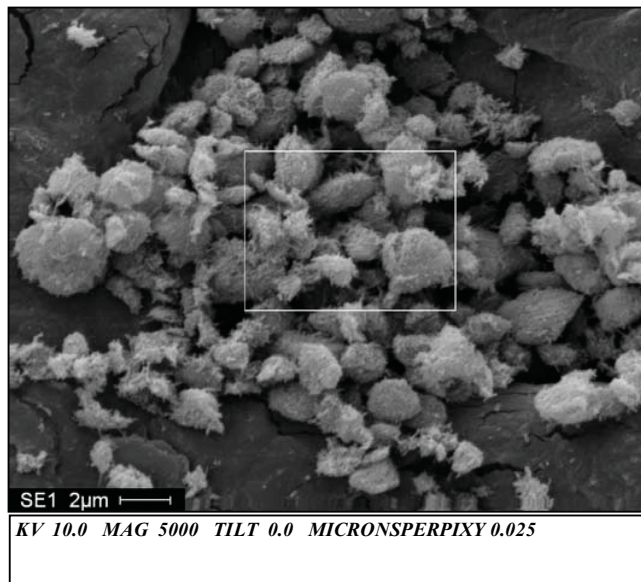
<i>Element</i>	<i>Wt%</i>	<i>At%</i>
<b>CK</b>	93.12	94.74
<b>OK</b>	06.88	05.26
<b>Matrix</b>	Correction	ZAF



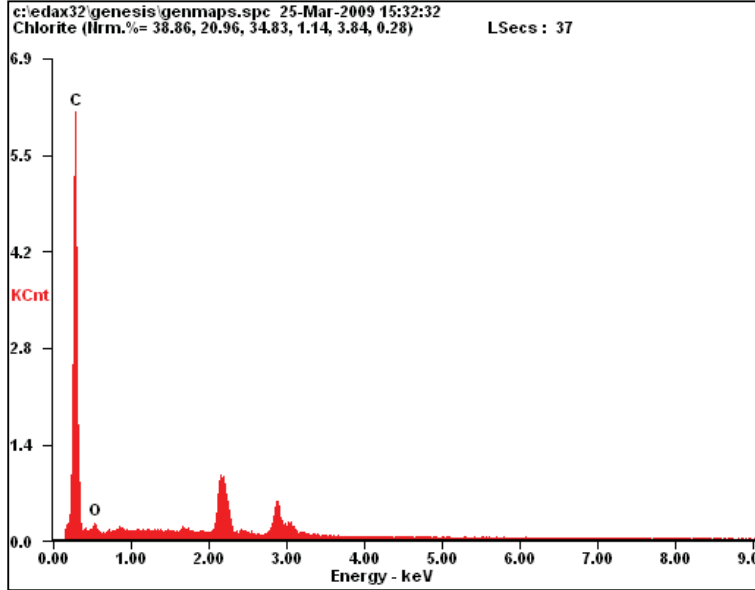
**SAMPLE #21 (MWCNT) STAGE D**



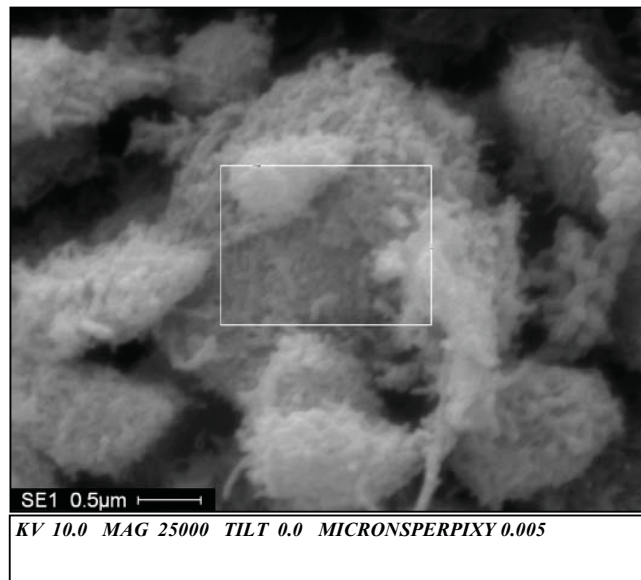
<i>Element</i>	<i>Wt%</i>	<i>At%</i>
<b>CK</b>	93.00	94.65
<b>OK</b>	07.00	05.35
<b>Matrix</b>	Correction	ZAF



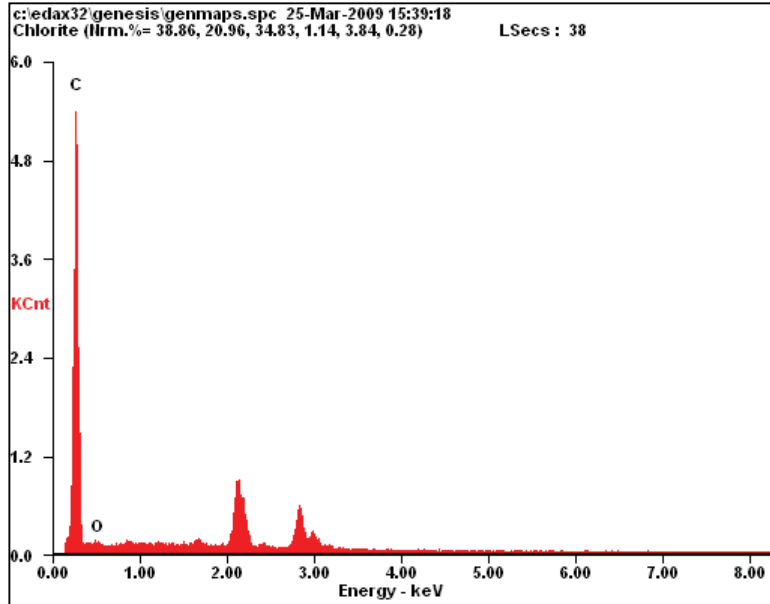
**SAMPLE #21 (MWCNT) STAGE D**  
**AREA 2**



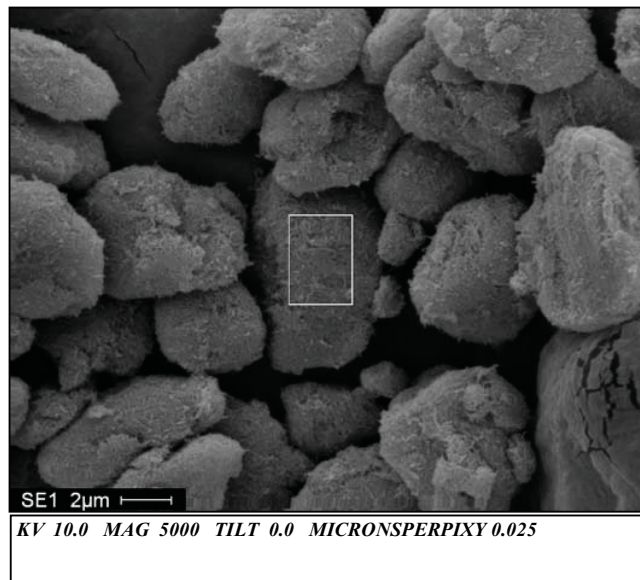
<i>Element</i>	<i>Wt%</i>	<i>At%</i>
<b>CK</b>	95.34	96.46
<b>OK</b>	04.66	03.54
<b>Matrix</b>	Correction	ZAF



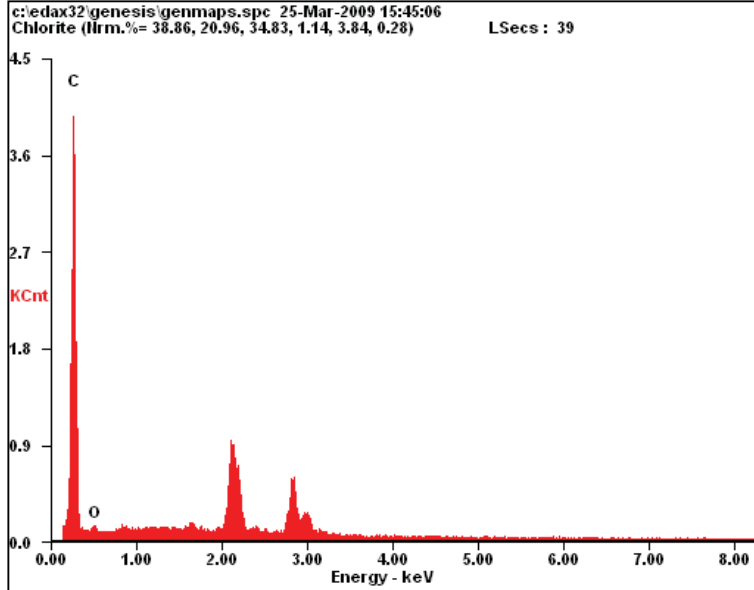
**SAMPLE #21 (MWCNT) STAGE A**



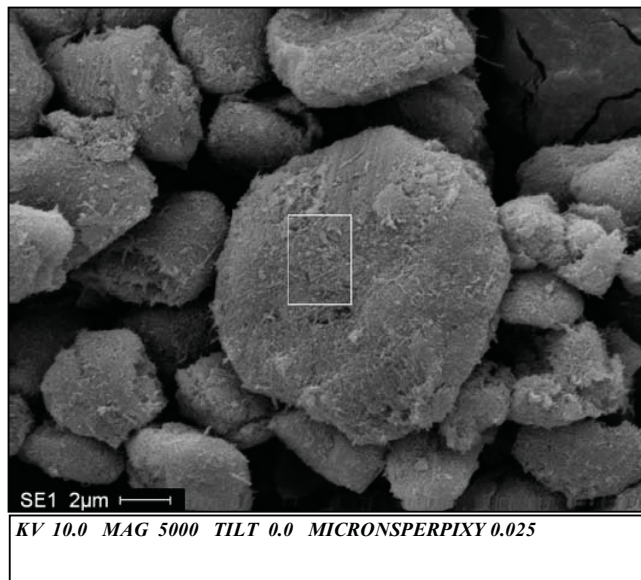
<i>Element</i>	<i>Wt%</i>	<i>At%</i>
<b>CK</b>	96.68	97.49
<b>OK</b>	03.32	02.51
<b>Matrix</b>	Correction	ZAF



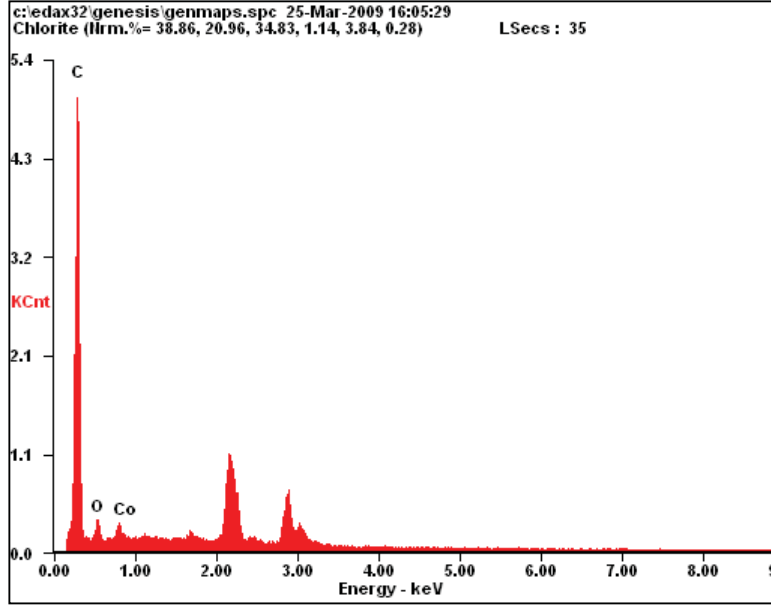
**SAMPLE #21 (MWCNT) STAGE A**  
**AREA 2**



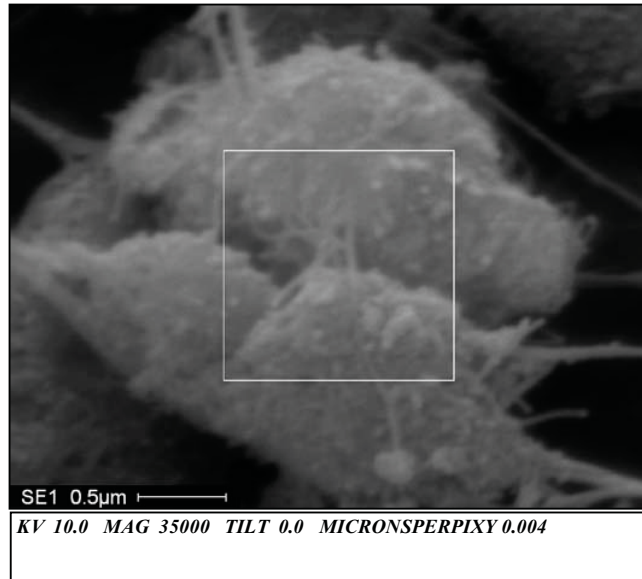
<i>Element</i>	<i>Wt%</i>	<i>At%</i>
<b>CK</b>	96.23	97.14
<b>OK</b>	03.77	02.86
<b>Matrix</b>	Correction	ZAF



**SAMPLE #22 (SWCNT) STAGE D  
 AREA 2**



<i>Element</i>	<i>Wt%</i>	<i>At%</i>
<b>CK</b>	84.19	92.24
<b>OK</b>	07.06	05.81
<b>CoL</b>	08.75	01.95
<b>Matrix</b>	Correction	ZAF



Appendix C  
TEM Images for Sample #28

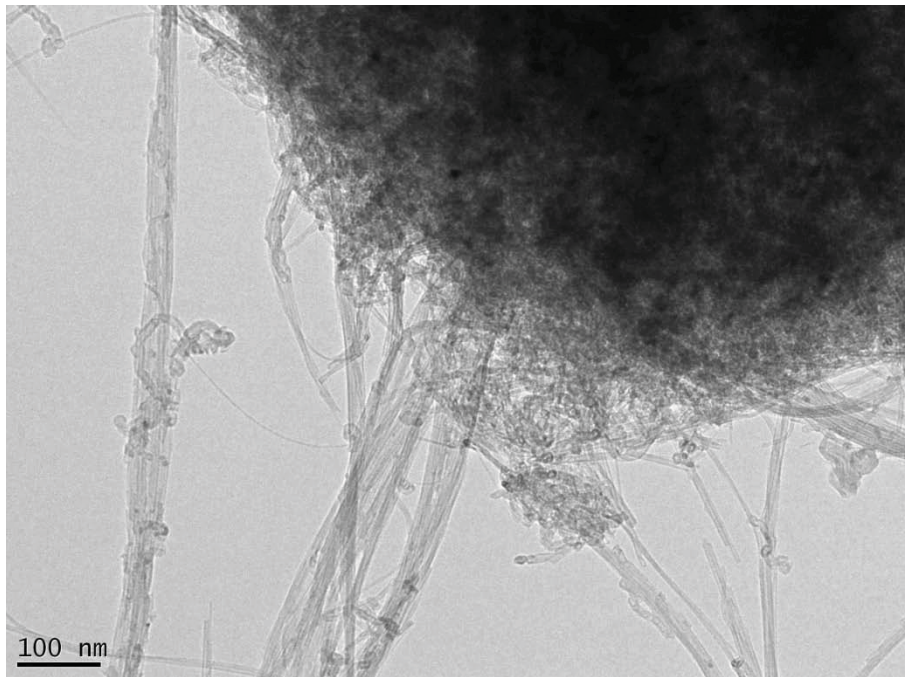


Figure 1: TEM Image of Sample #28



Figure 2: TEM Image of Sample #28

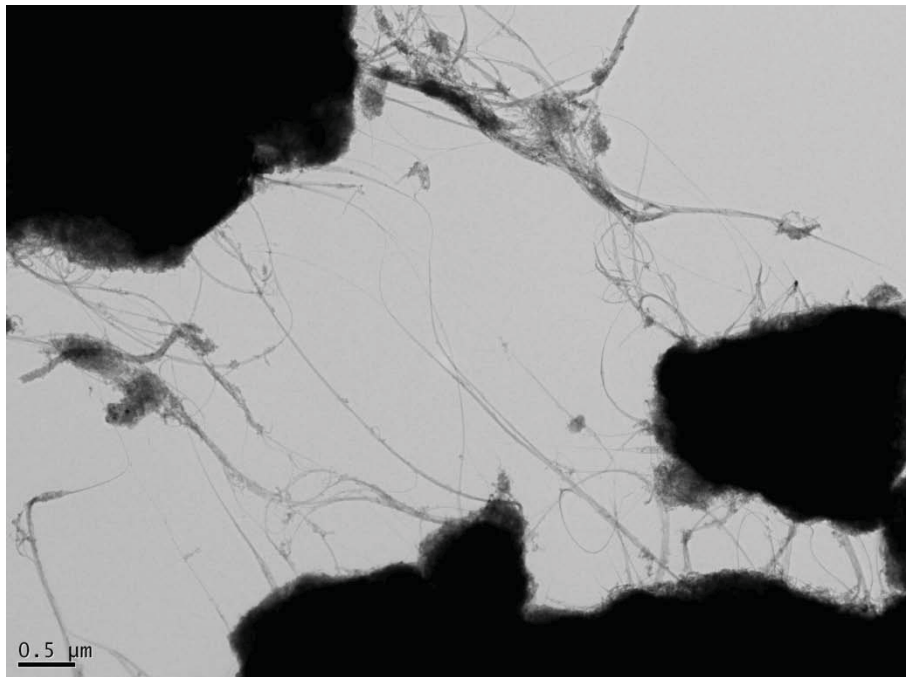


Figure 3: TEM Image of Sample #28



Figure 4: TEM Image of Sample #28